J. Fluid Mech. (2014), *vol.* 741, *pp* 404–460. © Cambridge University Press 2014
doi:10.1017/jfm.2013.666

Linearized oscillations of a vortex column: the singular eigenfunctions

Anubhab Roy‡ and Ganesh Subramanian†

Engineering Mechanics Unit, Jawaharlal Nehru Centre for Advanced Scientific Research, Jakkur, Bangalore, 560 064, India

(Received 18 November 2012; revised 23 August 2013; accepted 13 December 2013; first published online 20 February 2014)

In 1880 Lord Kelvin analysed the linearized inviscid oscillations of a Rankine vortex as part of a theory of vortex atoms. These eponymously named neutrally stable modes are, however, exceptional regular oscillations that make up the discrete spectrum of the Rankine vortex. In this paper, we examine the singular oscillations that make up the continuous spectrum (CS) and span the entire base state range of frequencies. In two dimensions, the CS eigenfunctions have a twin-vortex-sheet structure similar to that known from earlier investigations of parallel flows with piecewise linear velocity profiles. The vortex sheets are cylindrical, being threaded by axial lines, with one sheet at the edge of the core and the other at the critical radius in the irrotational exterior; the latter refers to the radial location at which the fluid co-rotates with the eigenmode. In three dimensions, the CS eigenfunctions have core vorticity and may be classified into two families based on the singularity at the critical radius. For the first family, the singularity is a cylindrical vortex sheet threaded by helical vortex lines, while for the second family it has a localized dipole structure with radial vorticity. The presence of perturbation vorticity in the otherwise irrotational exterior implies that the CS modes, unlike the Kelvin modes, offer a modal interpretation for the (linearized) interaction of the Rankine vortex with an external vortical disturbance. It is shown that an arbitrary initial distribution of perturbation vorticity, both in two and three dimensions, may be evolved as a superposition over the discrete and CS modes; this modal representation being equivalent to a solution of the corresponding initial value problem. For the restricted case of an initial axial vorticity distribution in two dimensions, the modal representation may be generalized to a smooth vortex. Finally, for the three-dimensional case, the analogy between rotational flows and stratified shear flows, and the known analytical solution for stratified Couette flow, are used to clarify the singular manner in which the modal superposition for a smooth vortex approaches the Rankine limit.

Key words: vortex dynamics, vortex instability, waves in rotating fluids

†Email address for correspondence: sganesh@jncasr.ac.in

‡Present address: School of Chemical and Biomolecular Engineering, Cornell University, Ithaca, 14853, NY, USA.

https://doi.org/10.1017/jfm.2013.666 Published online by Cambridge University Press

1. Introduction

Helmholtz's demonstration of the permanence of vortical structures in an inviscid fluid, and the resulting implications for a theory of vortex atoms, motivated Lord Kelvin to carry out exhaustive investigations on inviscid vortex motion and stability in the late nineteenth century. Of particular importance is his 1880 paper wherein he characterized the spectrum of waves supported on a central core of rigidly rotating liquid surrounded by an irrotational flow (Kelvin 1880). This top-hat vorticity profile, commonly referred to as the Rankine vortex, was shown to support a countable infinity of neutrally stable oscillations now known as the Kelvin modes. A schematic of the resulting dispersion curves are shown in figure 1 where the modal frequency (ω) is plotted as a function of the axial wavenumber (k) for a fixed non-zero azimuthal wavenumber (m). For any non-zero k, one may evidently classify the modes into two groups: the co-grade modes ($\omega > m\Omega$, Ω being the core angular velocity) that travel faster than the fluid in the undisturbed core and the retrograde modes ($\omega < m\Omega$) that travel slower (Saffman 1992). An underlying feature of the Kelvin modes is that the perturbation vorticity arises due to the oscillating column, and is evidently restricted to the region within the core and its edge; there is no perturbation vorticity outside the core. The analysis here shows that the Kelvin modes constitute the discrete spectrum of a Rankine vortex. There is an additional continuous spectrum (CS) consisting of singular non-axisymmetric modes that make up the frequency intervals between the neighbouring retrograde dispersion curves in figure 1 (see, for instance, figure 3 in § 2.2), thereby spanning the entire base state range of frequencies ($\omega \epsilon (0, m\Omega)$). These singular eigenfunctions have perturbation vorticity outside the vortex core. While the Kelvin modes are sufficient to determine the linearized inviscid evolution of an initially deformed vortex column (Arendt, Fritts & Andreassen 1997), the inclusion of additional singular modes is necessary to similarly characterize the interactions of such a column with external vortical disturbances (ambient turbulence).

Apart from its fundamental significance, the interaction of a vortex column with ambient turbulence is relevant to the stability of aircraft trailing vortices (Widnall 1975; Spalart 1998), and to the dynamics of coherent structures in quasi-geostrophic turbulence (McWilliams 1984). Motivated by such applications, there have been several studies of vortex column dynamics from both modal and non-modal perspectives. Modal analyses include those of Le Dizès and co-workers who have examined, using a WKBJ formalism, the characteristics of Kelvin modes for a wide class of homogeneous swirling flows with or without an axial flow component in appropriate asymptotic limits (Le Dizès & Lacaze 2005; Fabre, Sipp & Jacquin 2006; Heaton 2007*a*; Le Dizès & Fabre 2007; Fabre & Le Dizès 2008). Recent investigations along these lines have included the effects of a stable stratification along the rotation axis (Le Dizès & Billant 2009). Fabre *et al.* (2006) have conducted a detailed numerical study of the viscous eigenspectrum of a Lamb–Oseen profile. The authors show that, in contrast to the neutral retrograde modes of the Rankine vortex, one obtains instead multiple families of singular (inviscidly) damped modes in the base state range of frequencies, the damping arising from a viscous critical layer. Further, there arises a new family of modes that owes its origin entirely to viscosity. These results, although substantially more complicated, are similar in a sense to the non-trivial differences originally identified between the eigenspectra of the Rayleigh and the Orr–Sommerfeld equations in the context of parallel shearing flows (Lin 1955). Complementing such modal investigations are the studies of Hussain and co-workers (Melander & Hussain 1993; Pradeep & Hussain 2006, 2010) and others (Antkowiak & Brancher 2004; Heaton 2007*b*) who have examined the transient growth

https://doi.org/10.1017/jfm.2013.666 Published online by Cambridge University Press

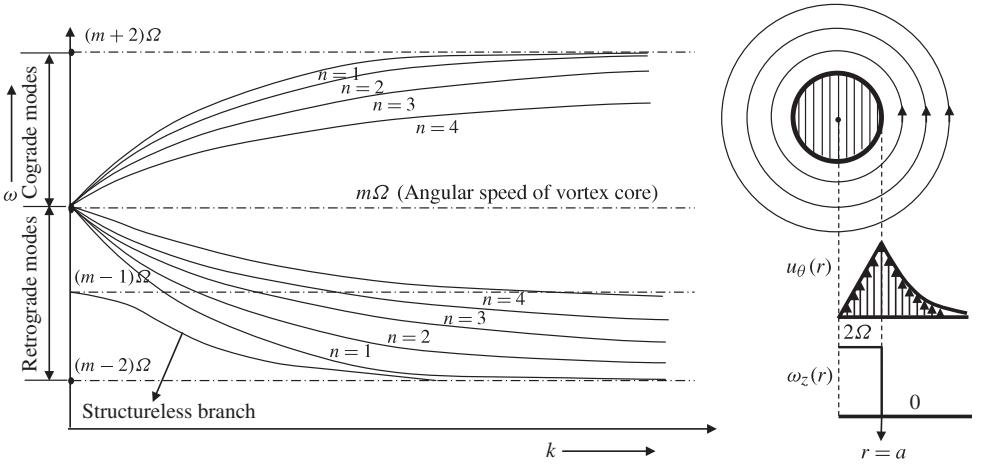

FIGURE 1. A sketch of the dispersion curves for the non-axisymmetric ($m \neq 0$) modes associated with a Rankine vortex. Here m and k are the azimuthal and axial wavenumbers, respectively.

of a vortex column via both linear and nonlinear direct numerical simulations. This short-time algebraic growth of column perturbations owes its origin to the non-normal evolution operator and the physics of the transient growth, in the linear regime, has been elucidated in detail (Pradeep & Hussain 2006). However, quantitative results for the growth amplitude, and the nature of optimal perturbations, are restricted to a Lamb–Oseen profile, and to Reynolds numbers (Re) up to $O(10^4)$.

The formidable difficulty of the eigenvalue problem for a general swirling flow implies that the above modal investigations are typically restricted to a fraction of the full eigenspectrum. The complexity of the latter is particularly evident with the inclusion of an axial flow which leads to an intricate array of instabilities of both inviscid (Lessen, Singh & Paillet 1974; Mayer & Powell 1992; Heaton & Peake 2006, 2007) and viscous origins (Khorrami 1991; Fabre & Le Dizès 2008). The instabilities typically occur as nearly convected centre modes, in the vicinity of the CS, with the eigenfunction concentrated in a region asymptotically close to the critical radius: the spatial location corresponding to the singularity of the inviscid equations, and that arises from co-rotation of the fluid in the base state with the eigenmode. Such modes have been shown to determine the inviscid stability characteristics of the Batchelor vortex (Heaton 2007*b*). However, even for a linearly stable base state with purely azimuthal flow and monotonically decreasing (axial) vorticity profile, a sensible comparison of the results (Fabre 2002; Fabre *et al.* 2006) with those of a Rankine vortex is impeded by the unavailability of the complete eigenspectrum in the latter case. The Rankine vortex may be regarded as the equivalent of Couette flow for swirling flows, since both correspond to (piecewise) constant vorticity profiles, leading to analytically soluble eigenvalue problems. It was originally shown by Case (1960*a*) that the singular modes comprising the inviscid CS of Couette flow are flow-aligned vortex sheets in two dimensions. For a nonlinear base state, these eigenfunctions possess a principal-value (PV) singularity in addition to the vortex-sheet contribution (Case 1959; Balmforth & Morrison 1995). While the Rankine vortex eigenfunctions in two dimensions consist of cylindrical vortex sheets, similar to Couette flow, the three-dimensional spectrum exhibits interesting differences. In contrast to Couette

https://doi.org/10.1017/jfm.2013.666 Published online by Cambridge University Press

flow (a purely continuous inviscid spectrum (Fadeev 1971)) or piecewise variants of the same (discrete neutral modes arise solely due to kinks in the base state profile (Sazonov 1989)), as already mentioned, the restoring action of Coriolis forces implies that the Rankine vortex supports a denumerable infinity of discrete modes. Only one of these, the so-called structureless or isolated mode, (the dispersion curve in figure 1 with $\omega \to (m-1)\Omega$ for $k \to 0$), arises from the discontinuity in the top-hat vorticity profile. Even for the CS modes, the singularity in the vorticity eigenfunctions at the critical radius, in three dimensions, differs from that known for parallel flows (Sazonov 1996). The analysis for the Rankine vortex here, while similar in spirit to that of Case (1960*a*), accounts for these crucial differences in characterizing the CS. The discrete (Kelvin) modes emerge as an exceptional instance when the amplitude of the singular vortical structure goes to zero. Indeed, the requirement that this amplitude equal zero yields the Kelvin-mode dispersion relation (Saffman 1992). The Rankine analysis may thus be regarded as a 'baseline' scenario for more general vorticity profiles, at least as far as the singular modes are concerned. It should also serve as a starting point towards unravelling the more complicated continuous spectra that would emerge with the incorporation of stratification or viscoelasticity. In the latter case, for instance, the structure of the singular eigenfunctions has largely been examined in the inertialess limit (Graham 1998; Kupferman 2005), and little is known for the case where inertial effects are dominant (Rallison & Hinch 1995). To this end, we first extend the results for the Rankine spectrum in two dimensions to a smooth vorticity profile, and then, for the three-dimensional case, we present a local analysis, based on Frobenius expansions, that examines the non-trivial effect of a small but finite base state vorticity (present for a smooth vorticity profile) on the nature of the singularity in the CS eigenfunctions. By way of an analogy with stratified flows, the approach to the Rankine limit is then elucidated.

The initial value problem (IVP) for a Rankine vortex that extends the analysis of Arendt *et al.* (1997) to include exterior vortical disturbances, and its equivalence to the modal representation given here, will be reported separately (Roy 2013). It is nevertheless worth noting here the relation between the modal and non-modal (IVP) perspectives. Studies of parallel shearing flows show that the transient growth phenomenon is intimately related to an underlying inviscid CS. While the original IVP analyses for Couette flow were in terms of Fourier modes with time-dependent wave vectors (see Farrell (1984), also known as Kelvin modes), an equivalent description exists in terms of a convected superposition of flow-aligned vortex sheets (the CS modes). The work of Farrell and co-workers (Farrell 1984, 1989; Farrell & Ioannou 1993*b*) has shown that one of the mechanisms leading to transient growth, the Orr mechanism (Orr 1907), involves the progressive phase alignment of an initially staggered superposition of singular vortex-sheet eigenfunctions. The second mechanism, the lift-up effect (Landahl 1980), responsible for the growth of spanwise perturbations, may also be interpreted in terms of the asymptotic de-phasing of a superposition of vortex-sheet eigenfunctions, and the corresponding ensemble of singular Squire-jet modes (Roy & Subramanian 2012). In general, for problems where the CS alone governs the temporal evolution, the dynamics may be divided into three regimes: an initial phase characterized by the aforementioned algebraic growth, a terminal phase with an algebraic decay in integral measures such as the perturbation kinetic energy due to the eventual de-phasing of the CS modes by the ambient shear (Bassom & Gilbert 1998), and an intermediate phase with an exponential decay (the presence of additional discrete modes would lead to a long-time saturated response rather than a terminal algebraic decay). In the aforementioned

https://doi.org/10.1017/jfm.2013.666 Published online by Cambridge University Press

intermediate phase, appropriate superpositions of the CS modes behave as decaying discrete (quasi-)modes, a phenomenon known as Landau damping in the plasma physics context (Briggs, Daugherty & Levy 1970; Schecter *et al.* 2000; Schecter & Montgomery 2003). Both Couette flow and the Rankine vortex constitute important and singular limiting scenarios in that although neither exhibits the aforementioned intermediate asymptotics, the addition of a small curvature or a small vorticity gradient/vorticity does lead to quasi-modes (Balmforth, Smith & Young 2001; Shrira & Sazonov 2001, 2003). For instance the solution of the two-dimensional IVP shows that a 'near-Rankine' profile exhibits an exponential decay phase with the damping rate being proportional to the (small) vorticity gradient at the critical radius (Le Dizès 2000; Schecter *et al.* 2000). The analogous scenario for three dimensions is not known. However, numerical results for a Lamb–Oseen profile indicate a denumerable infinite of quasi-modes (Fabre 2002). Although we discuss the Rankine vortex and 'near-Rankine' profiles from the normal-mode perspective in this paper, the above discussion highlights the relevance of these limiting scenarios from the IVP perspective.

The paper is organized as follows. In § 2, we examine the inviscid CS of a Rankine vortex. Section 2.1 analyses the two-dimensional singular modes for which the perturbation vorticity is confined to a pair of cylindrical vortex sheets: one at the edge of the core and the other at the critical radius, the radial location where the base state angular velocity equals the modal frequency. A physical interpretation of the twin-vortex-sheet structure is given. A second family of singular eigenfunctions, in two dimensions, takes the form of (infinitely) localized axial jets. The localization of the axial velocity perturbation implies that these jets remain valid eigenfunctions for an arbitrary base-state vorticity profile. It is then shown that an arbitrary distribution of axial vorticity may be evolved as a superposition of the two-dimensional CS modes. In § 2.2, the analysis is extended to three-dimensional modes, all of which also possess vorticity in the interior of the core. The CS eigenfunctions that arise, in addition to the denumerably infinite number of Kelvin modes, may be conveniently classified based on the nature of the singularity in the perturbation vorticity at the critical radius. The first family (§ 2.2.1) resembles the two-dimensional singular modes in that the singularity is again a cylindrical vortex sheet, one threaded by helical vortex lines, in the otherwise irrotational exterior. For the second family (§ 2.2.2), the singular structure includes radial vorticity and has a dipole singularity at the critical radius. Members of this latter family asymptote to the aforementioned axial-jet eigenfunctions in the limit of a vanishing axial wavenumber. In § 2.2.3, it is shown that an arbitrary initial distribution of vorticity may be evolved as a superposition of the discrete and CS modes, this modal representation being equivalent to the solution of the corresponding IVP for the Rankine vortex (Roy 2013). In § 3, the Rankine modal representation in § 2.1, for an initial distribution of axial vorticity, is extended to a smooth vorticity profile. Next, the three-dimensional singular eigenfunctions of a smooth vorticity profile are analysed using Frobenius expansions, valid in the vicinity of the critical radius, the perturbation vorticity field then being obtained by drawing on an analogy with the eigenfunctions known for a stratified shear flow. The approach towards the singular forms obtained for the Rankine vortex in earlier sections, is then examined. In § 4, we discuss the existence of inviscid centre-modes for smooth vortices and their disappearance in the Rankine limit. Finally in § 5, we present a summary of the main results.

https://doi.org/10.1017/jfm.2013.666 Published online by Cambridge University Press

2. Inviscid normal mode analysis for a Rankine vortex

If a and Ω_0 be the core radius and angular velocity, respectively, the Rankine velocity profile is given by $u_\theta^{(0)} = r\Omega(r)$, with $\Omega(r) = \Omega_0$ for $r < a$ and $\Omega(r) = \Omega_0(a/r)^2$ for $r \geqslant a$; the base-state (axial) vorticity (Z) and vorticity gradient are $Z(r) = 2\Omega_0\mathcal{H}(a-r)$ and $\mathrm{D}Z(r) = -2\Omega_0\delta(r-a)$, $\mathcal{H}(z)$ and $\delta(z)$ being the Heaviside and delta functions. The Rankine vortex corresponds to a stable stratification of angular momentum, and supports neutrally stable axisymmetric oscillations in the absence of viscosity (Chandrasekhar 1961). Further, Z being a monotonically decreasing (generalized) function of r, the analogue of Rayleigh's inflection point theorem in a cylindrical geometry implies (modal) stability to non-axisymmetric perturbations (Michalke & Timme 1967; Drazin & Reid 1981). The governing equation for the linearized evolution of inviscid perturbations is, however, singular at the point (the critical radius) where the modal frequency equals the base state angular velocity, and this leads to an inviscid CS. The normal mode analysis in the following subsections is carried out with an emphasis on the CS modes. Two-dimensional perturbations are examined in § 2.1, and the analysis is extended to perturbations with a finite axial wavenumber (k) in § 2.2.

2.1. *The two-dimensional CS modes*

Assuming small-amplitude perturbations of the form $(u_r', u_\theta') = (\hat{u}_r(r), \hat{u}_\theta(r))\mathrm{e}^{\mathrm{i}(m\theta-\omega t)}$, where m is the azimuthal wavenumber and ω is the (real) angular frequency, the inviscid stability equation governing the radial velocity eigenfunction, $\hat{u}_r(r)$, may be derived along lines similar to that for the Rayleigh equation for parallel shear flows (Drazin & Reid 1981), and is given by

$$[(\omega - m\Omega)\{r^2\mathrm{D}^2 + 3r\mathrm{D} - (m^2-1)\} + mr\mathrm{D}Z]\hat{u}_r = 0, \tag{2.1}$$

where $\mathrm{D} \equiv \mathrm{d}/\mathrm{d}r$. As one can see that $\omega(m) = -\omega(-m)$, $\hat{u}_r(r;\, m) = \hat{u}_r(r;\, -m)$, it is sufficient to restrict the analysis to positive values of m. Since Z is constant within the core and zero outside it, equation (2.1) simplifies to

$$(\omega - m\Omega)\{r^2\mathrm{D}^2 + 3r\mathrm{D} - (m^2-1)\}\hat{u}_r = 0 \tag{2.2}$$

for $r \neq a$, and thereby allows for two possibilities. The first rather obvious one is the homogeneous solution,

$$\{r^2\mathrm{D}^2 + 3r\mathrm{D} - (m^2-1)\}\hat{u}_r = 0. \tag{2.3}$$

Physically, this corresponds to an irrotational velocity perturbation both within and outside the core. The perturbation vorticity resides in a cylindrical vortex sheet at $r = a$, and is the linearized representation of a small-amplitude wavy deformation. The eigenvalue problem involving (2.3), with the required continuity of radial and (total) tangential velocity components at $r = a$, was originally solved by Lord Kelvin (see Kelvin 1880), and yields a single neutral mode for each m with $\omega_d = (m-1)\Omega_0$. The mode lags behind the fluid motion in the core since the velocity perturbation acts to deform the core in a retrograde sense. These Kelvin modes make up the two-dimensional discrete spectrum (see Saffman 1992). They are interpreted here as (regular) discrete modes despite the singular vorticity eigenfunction ($\propto \delta(r-a)$), since the singularity arises solely due to the discontinuity in the base state vorticity profile. If the Rankine profile were to be smoothed such that Z decreases from $2\Omega_0$ to 0 in a small but finite interval, then the vorticity eigenfunction would no longer be singular. On the other hand, the CS modes, to be discussed below, continue to be

https://doi.org/10.1017/jfm.2013.666 Published online by Cambridge University Press

singular even with this smoothing, since they owe their origin to the singular point in the governing equation (2.2).

The second possibility, leading to the CS, was recognized by Case (1960*a*) (among others; see Dikii 1960), in the context of Couette flow; that equation (2.2) also allows for

$$\{r^2\mathrm{D}^2 + 3r\mathrm{D} - (m^2 - 1)\}\hat{u}_r \propto \delta(\omega - m\Omega), \tag{2.4}$$

since $x\delta(x) = 0$ is an equality in the generalized sense (Lighthill 1958). Physically, equation (2.4) implies the existence of a cylindrical vortex sheet, threaded by axial vortex lines, and coincident with the streamsurface at the critical radius, r_f, satisfying $\omega = m\Omega(r_f)$. The sheet is convected with the base-state velocity at $r = r_f$, while its infinitesimal thickness prevents smearing out by the shear. One therefore has a singular normal mode. The Rankine core is degenerate in the sense that an arbitrary distribution of axial vorticity is convected unchanged in this region. It is therefore sufficient to consider the case where the vortex sheet is located outside the core. The equality $\omega = m\Omega(r_f)$ implies $r_f = (m\Omega_0/\omega)^{1/2}a$, and for r_f ranging from a^+ to infinity, one obtains the two-dimensional CS with ω decreasing from $m\Omega_0$ to 0. There remains the one exceptional value of r_f where the vortex sheet amplitude goes to zero, corresponding to the Kelvin mode above. To see this, one may rewrite (2.4) as

$$\{r^2\mathrm{D}^2 + 3r\mathrm{D} - (m^2 - 1)\}\hat{u}_r = \mathrm{i}mr_fA(r_f)\delta(r - r_f), \tag{2.5}$$

where $-A(r_f)$ denotes the (unknown) vortex sheet strength. The solution of (2.5) is readily obtained by separate consideration of the regions: $r < a$, $a < r < r_f$ and $r_f < r < \infty$. The solutions in these regions, consistent with the absence of singularities at the origin and at infinity, are ($m > 0$)

$$\hat{u}_r^1 = d\left(\frac{r}{a}\right)^{m-1}, \quad (0 < r < a), \tag{2.6}$$

$$\hat{u}_r^2 = c_1\left(\frac{r}{a}\right)^{m-1} + c_2\left(\frac{a}{r}\right)^{m+1}, \quad (a < r < r_f), \tag{2.7}$$

$$\hat{u}_r^3 = \Omega_0\frac{a^2}{r_f}\left(\frac{a}{r}\right)^{m+1}, \quad (r > r_f), \tag{2.8}$$

where the constant in (2.8) is chosen as $(\Omega_0 a^2/r_f)$ for convenience. The constants c_1 and c_2 may be determined following the standard procedure for the determination of the Green's function of a second-order differential equation (Friedman 1990). Thus, integrating (2.5) over an infinitesimal interval including $r = r_f$, one obtains the following matching conditions:

$$\hat{u}_r^2 = \hat{u}_r^3 \quad \text{at } r = r_f, \tag{2.9}$$

$$\mathrm{D}\hat{u}_r^3 - \mathrm{D}\hat{u}_r^2 = \frac{\mathrm{i}mA(r_f)}{r_f} \quad \text{at } r = r_f, \tag{2.10}$$

with the latter denoting the jump in the tangential velocity component across the vortex sheet at $r = r_f$. From (2.7) to (2.10),

$$c_1 = -\frac{\mathrm{i}A(r_f)}{2}\left(\frac{a}{r_f}\right)^{m-1}, \tag{2.11}$$

$$c_2 = \frac{\Omega_0 a^2}{r_f} + \frac{\mathrm{i}A(r_f)}{2}\left(\frac{r_f}{a}\right)^{m+1}. \tag{2.12}$$

https://doi.org/10.1017/jfm.2013.666 Published online by Cambridge University Press

The constant d in (2.6) is determined from the continuity of the radial velocity at $r=a$:

$$d=\frac{\Omega_0 a^2}{r_f}+\frac{\mathrm{i}A(r_f)}{2}\left[\left(\frac{r_f}{a}\right)^{m+1}-\left(\frac{a}{r_f}\right)^{m-1}\right]. \tag{2.13}$$

Finally, the vortex sheet amplitude, $A(r_f)$, is determined by the jump in tangential velocity across $r=a$. The latter is obtained by integrating (2.5), with $\mathrm{D}Z=-2\Omega_0\delta(r-a)$ included, over an infinitesimal interval including $r=a$:

$$(\omega-m\Omega_0)\left[\mathrm{D}\hat{u}_r^2-\mathrm{D}\hat{u}_r^1\right]=2m\frac{\Omega_0}{a}\hat{u}_r \quad \text{at } r=a. \tag{2.14}$$

Using $\omega=m\Omega_0(a/r_f)^2$, and after some algebra,

$$A=\frac{2\mathrm{i}\Omega_0\left(a^2/r_f\right)(\omega_d-\omega)}{\Omega_0\left(a/r_f\right)^{m-1}+(\omega_d-\omega)\left(r_f/a\right)^{m+1}} \tag{2.15}$$

where $\omega_d=(m-1)\Omega_0$ is the frequency of the two-dimensional Kelvin mode. The denominator in (2.15) may be written in the form

$$\begin{aligned}&(m-1)\left(\frac{r_f}{a}\right)^m-m\left(\frac{r_f}{a}\right)^{m-2}+\left(\frac{a}{r_f}\right)^m\\&\quad=\frac{\left[\left(r_f/a\right)^2-1\right]}{\left(r_f/a\right)^m}\left[\left[\left(\frac{r_f}{a}\right)^{2m-2}-1\right]+\left[\left(\frac{r_f}{a}\right)^{2m-2}-\left(\frac{r_f}{a}\right)^2\right]+\cdots\right.\\&\qquad\left.+\left[\left(\frac{r_f}{a}\right)^{2m-2}-\left(\frac{r_f}{a}\right)^{2m-4}\right]\right],\end{aligned} \tag{2.16}$$

and is always positive when $r_f>a$. The sign of $\mathrm{Re}(A(r_f))$ is therefore determined by the numerator in (2.15); in particular, the vortex sheet disappears when $\omega=\omega_d$ or $r_{fk}=(m/(m-1))^{1/2}\,a$. Thus, the generic eigenmodes comprising the two-dimensional CS have a twin-vortex-sheet structure, and for the chosen normalization, the vorticity eigenfunction is given by

$$\hat{w}_z^{CSM}(r;r_f)=\left[\frac{2\mathrm{i}\Omega_0 d}{\omega-m\Omega_0}\delta(r-a)-A(r_f)\delta(r-r_f)\right]. \tag{2.17}$$

The jumps in tangential velocity across the two vortex sheets have the same sign for $r>r_{fk}(\mathrm{Re}(A)<0)$, and having opposite signs when $a<r_f<r_{fk}$ $(\mathrm{Re}(A)>0)$; see figure 2. The amplitude of the second vortex sheet vanishes for $r_f=r_{fk}$, leading to the Kelvin-mode eigenfunction:

$$\hat{w}_z^{Kelvin}(r)=-\frac{2\mathrm{i}\Omega_0 a^2}{r_{fk}}\delta(r-a), \tag{2.18}$$

with a single vortex sheet at $r=a$. In contrast to Case's original analysis of the two-dimensional CS in Couette flow, for which the normal component of the velocity perturbation in Couette flow is required to vanish at each boundary (or at infinity for an unbounded domain), the radial velocity field induced by the vortex sheet at $r=r_f$ will not, in general, vanish at $r=a$. Instead, it acts to deform the core, leading to the additional edge vortex sheet. Although the strength, $A(r_f)$, of the vortex sheet at $r=r_f$ is still arbitrary, as in Couette flow, the ratio of the strengths of the two vortex

https://doi.org/10.1017/jfm.2013.666 Published online by Cambridge University Press

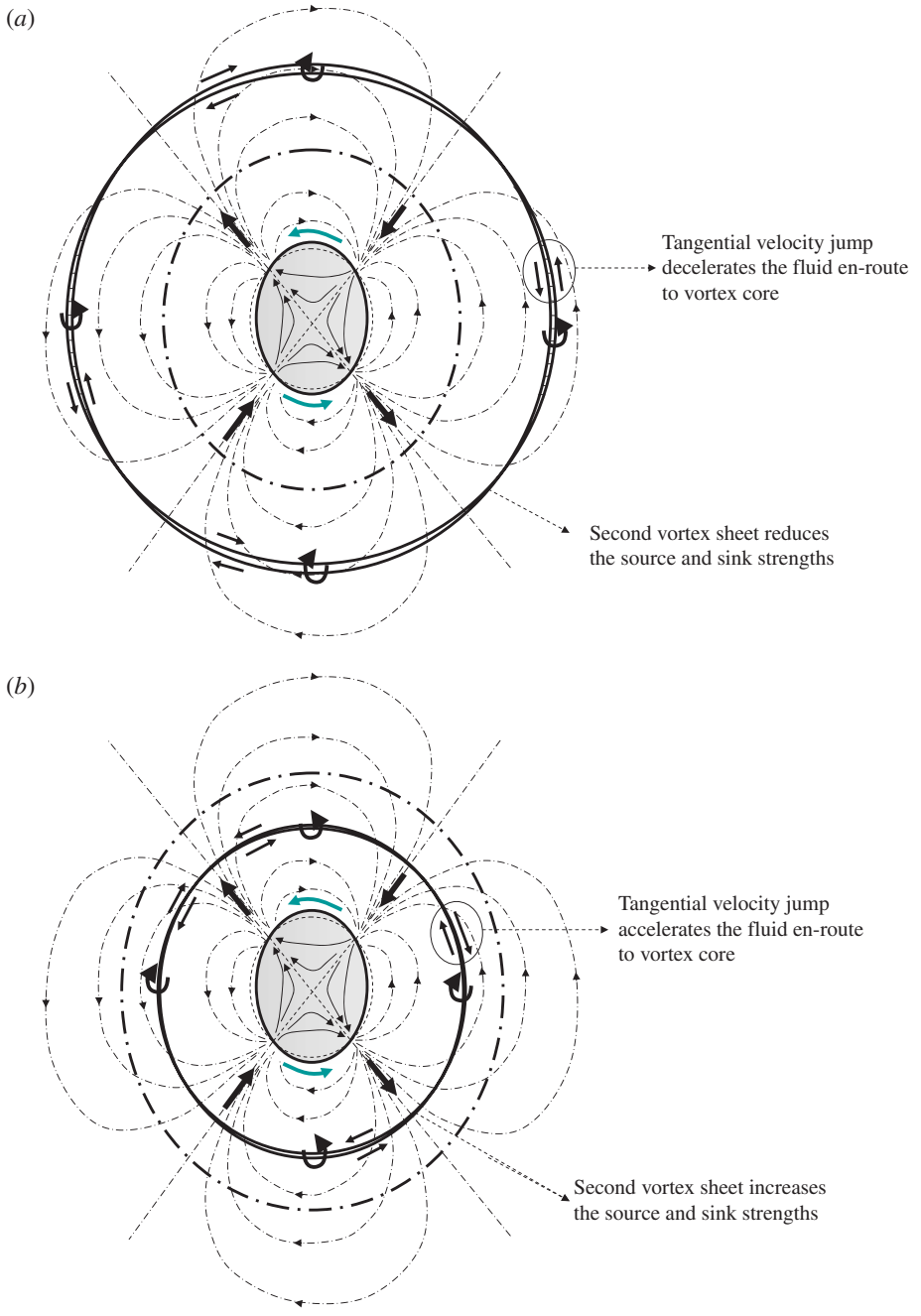

FIGURE 2. (Colour online) (*a*) The disturbance velocity field when the vortex sheet at $r = r_f$ co-rotates with the elliptically deformed vortex core at a frequency lower than the $m = 2$ Kelvin mode; (*b*) the disturbance velocity field when the vortex sheet at $r = r_f$ co-rotates with the elliptically deformed vortex core at a frequency higher than the $m = 2$ Kelvin mode. The dash–dot circle denotes the ring of fluid rotating at the Kelvin-mode frequency.

https://doi.org/10.1017/jfm.2013.666 Published online by Cambridge University Press

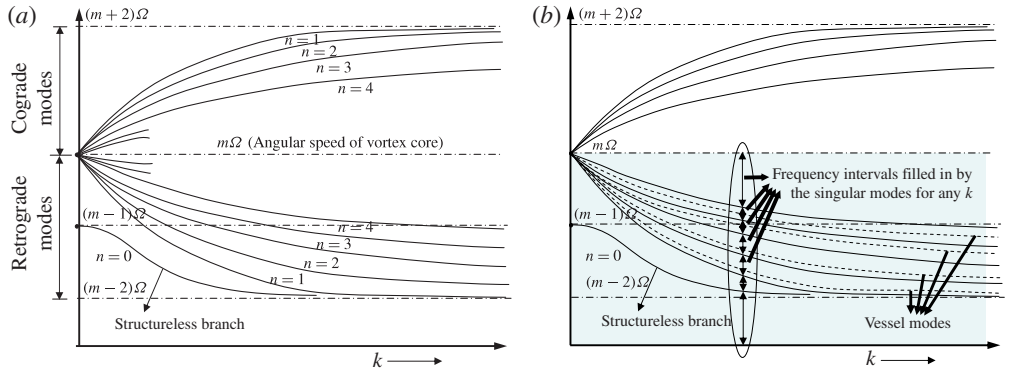

FIGURE 3. (Colour online) The sketch on the left is of dispersion curves that result from (2.35) for a given m. The sketch on the right includes the CS depicted by the shaded region; the additional dashed curves in the retrograde frequency range denote the three-dimensional vessel modes defined by (A 10). For each k, the singular eigenmodes that make up the CS fill up the frequency intervals between the retrograde dispersion curves.

sheets is not, and a discrete mode arises when this ratio is zero. The exact analogue of Couette flow would be a point vortex that results for $\Omega_0 \to \infty$, $a \to 0$ with $\Omega_0 a^2$ fixed. In this limit, $r_{fk} \to 0$, and a purely CS remains. On the other hand, the parallel flow analogue of the Rankine vortex is the piecewise linear profile, with a single jump in the velocity gradient, analysed by Sazonov (1989).

The existence of singular modes becomes evident on considering the underlying physical mechanism. Without loss of generality, one may look at $m = 2$, in which case the Kelvin mode is the small-amplitude limit of the well-known Kirchoff vortex (Lamb 1932). The exterior velocity field associated with the Kelvin mode may be regarded as the result of a distribution of sources and sinks along the edge of the unperturbed core, the strength of the source or sink being proportional to the local slope of the wavy core perturbation. The source and sink strengths are greatest midway between the principal axes of the elliptical core, and the regions of outflow and inflow are centred around these directions. The core rotation may be slowed down or accelerated, and the modal frequency altered, by an appropriate change of the strength of these radial flows. A co-rotating vortex sheet in the otherwise irrotational region, via tangential velocity jumps, provides for just such a mechanism, and leads to the two-dimensional CS modes. Figure 2 shows the velocity field associated with CS modes with frequencies both lower and higher than the corresponding Kelvin mode. In each case, the perturbation velocity field for $r > r_f$ remains identical to the Kelvin mode (2.8), but the jumps in tangential velocity across $r = r_f$ alter the velocity field in the region $r < r_f$.

The discussion above applies to $m \geqslant 2$. The case $m = 1$, in two dimensions, corresponds to a mere displacement of the vortex core. Translational invariance for an unbounded domain implies the absence of any restoring force, and the two-dimensional Kelvin modes are therefore restricted to $m \geqslant 2$ ($r_{fk} \to \infty$ for $m = 1$). The CS modes continue to exist for $m = 1$ since the outer vortex sheet breaks the invariance. However, naively setting $m = 1$ in (2.15) leads to a divergence of the vortex sheet amplitude for any r_f. This is because the analysis above proceeds by normalizing the velocity field for $r > r_f$, while for $m = 1$, the second vortex sheet 'screens' the disturbance velocity field induced by the displaced core, and the velocity perturbation

https://doi.org/10.1017/jfm.2013.666 Published online by Cambridge University Press

is confined to the region $r < r_f$. Physically, the $m = 1$ CS modes correspond to the small-amplitude orbiting motion of the displaced (but undeformed) vortex core around the centre of a cylindrical vessel with radius r_f. The image vorticity needed to satisfy the impenetrability condition at the vessel wall is, to linear order, a vortex sheet coincident with the vessel wall. The ratio of the vortex sheet strengths, predicted by the analysis above, is unaffected by the velocity field normalization, and equals $-(a/r_f)$. The trivial translatory (discrete) mode thus corresponds to a vessel with an infinitely large radius ($r_f \to \infty$). In § 2.2, we encounter modes of a similar nature for a finite axial wavenumber. Unlike the two-dimensional case, where an $m = 1$ CS mode may be interpreted as a vessel mode for any $r_f > a$, the analogy, for a non-zero axial wavenumber, remains true only for a denumerably infinite sequence of r_f (see appendix A). A subtle point related to the analysis for $m = 1$ above (and later in § 2.2 for a finite k) is the dependence of $A(r_f)$ of the order of the limits $m \to 1$ and $a \to 0$. The vessel mode results when m is taken as unity to begin with. The opposite order leads to a non-trivial exterior velocity field corresponding to a translating potential dipole. It may, however, be shown that the modal superpositions that appear below remain insensitive to the order of the limiting processes.

The discussion of the CS modes has thus far been for cases where the perturbation vorticity is restricted to the region $r \geqslant a$. As pointed out earlier, modes with core axial vorticity are expected to have a degenerate character, since rigid-body rotation allows for an arbitrary axial vorticity distribution to evolve with its structure unchanged. From a normal-mode perspective, there is still a mild restriction, however, since an arbitrary core vorticity distribution would deform the core, thereby also exciting a Kelvin mode. This would lead to a pair of frequencies that characterize the evolution for a given azimuthal wavenumber: the first being the core angular frequency ($m\Omega_0$) corresponding to the interior vorticity and the second being the Kelvin-mode frequency ($(m-1)\Omega_0$) corresponding to the edge vorticity. Thus, any normal mode with core vorticity must have, in addition, a projection at the edge of the core that cancels out the Kelvin-mode contribution. Assuming the core vorticity distribution to be given by $g\,(r/a)$ (with $g\,(r/a) = 0$ for $r \geqslant a$), it may be shown that the (axial) vorticity eigenfunction of a two-dimensional core eigenmode is given by

$$\hat{w}_z^{core}(r) = g\left(\frac{r}{a}\right) - \delta(r-a)\int_0^a g\left(\frac{r'}{a}\right)\left(\frac{r'}{a}\right)^{m+1} \mathrm{d}r', \tag{2.19}$$

where the delta function denotes the additional edge-vorticity component. That $g\,(r/a)$ is arbitrary is consistent with the aforementioned degeneracy. The velocity eigenfunction is restricted to $r < a$, so the exterior irrotational region remains quiescent. These two-dimensional core eigenmodes find a mention in Kopiev & Chernyshev (1997) in the context of vortex ring oscillations. Note that $g\,(r/a)$ may be expanded in terms of any of the standard orthogonal families, and each of these expansions will lead to a particular, denumerably infinite, representation of the core eigenmodes. One such representation, in terms of Bessel functions, arises naturally as the limiting form of the three-dimensional structured modes in § 2.2.

Interestingly, the degeneracy associated with the core-eigenmodes, and the resulting arbitrariness in their functional form, disappears on considering the analogous modes for a vortex ring. This is because the base-state circumferential vorticity is required to increase in proportion to the distance from the axis of symmetry in order satisfy the Euler equations that now include an additional vortex-stretching term. The resulting differential shear in a meridional plane, within the vortex ring core, ensures that the

https://doi.org/10.1017/jfm.2013.666 Published online by Cambridge University Press

CS modes have a uniquely determined structure. The analogue of the two-dimensional column disturbances are the axisymmetrical ring modes that do not depend on the coordinate along the ring perimeter. For the isochronous ring, where the ratio of the azimuthal vorticity to the transverse radial distance is a constant (in the limit of small-cored rings, this is only one of an infinite set of vorticity distributions that allow for a steadily propagating distribution of vorticity (Fraenkel 1970)), the axisymmetric CS modes have indeed been shown to exhibit a twin-vortex-sheet structure, the vortex sheets being in the form of hollow tori (Kopiev & Chernyshev 1997). Although the original analysis was for rings with a small cross-section, and restricted to the CS modes within the ring cores, similar conclusions would apply to the CS modes that govern the evolution of vortical disturbances in the much larger envelope of irrotational fluid that is entrained by the propagating ring.

The evolution of an initial axial vorticity distribution of the form $w_{z0}(r)\mathrm{e}^{\mathrm{i}m\theta}$, as an integral superposition of the two-dimensional Kelvin and CS modes, is given by

$$w_z(r,\theta,t) = w_z^{core}\mathrm{e}^{\mathrm{i}m(\theta-\Omega_0 t)} + \int_{a^+}^{\infty} B_1(r_f)\hat{w}_z^{CSM}(r;r_f)\mathrm{e}^{\mathrm{i}m(\theta-\Omega(r_f)t)}\,\mathrm{d}r_f + \int_0^{\infty} B_2(r_f)\hat{w}_z^{Kelvin}(r)\mathrm{e}^{\mathrm{i}(m\theta-\omega_d t)}\,\mathrm{d}r_f, \tag{2.20}$$

where $\hat{w}_z^{CSM}$ and $\hat{w}_r^{Kelvin}$ are given by (2.17) and (2.18), and the respective eigenfunction amplitudes are given by $B_1(r_f) = -w_{z0}(r_f)/A(r_f)$, $B_2(r_f) = -(\mathrm{i}/2)(w_{z0}(r_f)r_{fk}/a^2(\omega_d - m\Omega))\left(a/r_f\right)^{qm-1}$ and $q = \mathrm{sgn}(r_f - a)$. On substituting the expressions for B_1, B_2 and $A(r_f)$, equation (2.20) can be simplified to

$$w_z(r,\theta,t) = w_{z0}(r)\mathrm{e}^{\mathrm{i}[m(\theta-\Omega(r)t)]}\mathcal{H}(r-a) + \hat{w}_z^{core}\mathrm{e}^{\mathrm{i}m[\theta-\Omega_0 t]} + \delta(r-a)\left[\mathrm{e}^{-\mathrm{i}\omega_d t}\int_0^a w_{z0}(r_f)\left(\frac{r_f}{a}\right)^{m+1}\mathrm{d}r_f + \int_{a^+}^{\infty}\Omega_0\left(\frac{a}{r_f}\right)^{m-1} w_{z0}(r_f)\frac{\mathrm{e}^{-\mathrm{i}m\Omega(r_f)t} - \mathrm{e}^{-\mathrm{i}\omega_d t}}{(\omega_d - m\Omega(r_f))}\,\mathrm{d}r_f\right]\mathrm{e}^{\mathrm{i}m\theta}. \tag{2.21}$$

In (2.20), the second term accounts for the distribution of CS modes required to represent a specified axial vorticity distribution outside the core. The edge-vorticity contribution that arises from this superposition is then projected onto the Kelvin mode which appears as the third term in (2.20); the lower limit a^+ instead of a ensures that an initial condition consisting solely of edge vorticity evolves as a Kelvin mode. The equivalence of (2.20) to a solution of the two-dimensional IVP is readily established (Roy 2013). The coefficients B_1 and B_2 are singular at $r_f = r_{fk}$, when $A(r_f) = 0$, and this is a signature of the secular growth for an initial condition localized at the Kelvin critical radius. The growth is linear in time for the velocity field, and with reference to the plasma physics literature (Hirota, Tatsuno & Yoshida 2003), the secular growth may be interpreted as a resonance between the discrete (point) and continuous spectra.

For a point vortex, as pointed out earlier, the inviscid spectrum is purely continuous, and an initial axial vorticity distribution evolves as a superposition of the CS modes alone. Thus, (2.20) reduces to the much simpler form:

$$w_z(r,\theta,t) = \int_0^{\infty} w_{z0}(r_f)\hat{w}_z^{CSM}(r;r_f)\mathrm{e}^{\mathrm{i}m(\theta-\Omega(r_f)t)}\,\mathrm{d}r_f \tag{2.22}$$

with $\hat{w}_z^{CSM}(r;r_f) = \delta(r-r_f)$.

https://doi.org/10.1017/jfm.2013.666 Published online by Cambridge University Press

Finally, there are certain exceptional eigenmodes, those that do not involve a radial velocity perturbation, and are therefore not covered by the above analysis. The simplest among these is the trivial case of an axisymmetric hollow vortex sheet at $r = a$. The resulting perturbation velocity field corresponds to a quiescent core, and is identical to the base state ($u'_\theta \sim 1/r$) outside it. This mode is, in fact, included in (2.19). In enforcing a quiescent exterior for all m, (2.19), for $m = 0$, requires an axisymmetric vortex sheet at the edge of the core with a strength equal and opposite to the core circulation. A second class of eigenmodes neglected by the analysis are those wherein the axial velocity component itself has a delta-function singularity. Physically, this corresponds to a concentrated jet-like profile and the localization of the velocity field ensures that these jet-like modes remain eigenfunctions of an arbitrary smooth vorticity profile. Although not relevant to an IVP involving only an axial vorticity component as given by (2.20) above, these modes rise as limiting forms of the three-dimensional CS modes (the Λ_2 family) that include radial vorticity. Sazonov (1996) has identified similar modes for inviscid Couette flow which, together with the three-dimensional generalization of the Case vortex sheets, complete the three-dimensional CS for the specific flow profile.

2.2. *The three-dimensional CS modes*

In this section we analyse the CS modes with a non-zero axial wavenumber. The equations governing the inviscid evolution of three-dimensional disturbances have been written down in various forms by different authors. Howard & Gupta (1962) reduce the set of stability equations to a single one governing the radial velocity eigenfunction (the Howard–Gupta equation) as in § 2.1. On the other hand, Saffman (1992) derives an equation governing the disturbance pressure field that has since been generalized to a base state with axial flow (Le Dizès 2004). Here, following Arendt *et al.* (1997), we write down the stability equation in terms of the axial velocity eigenfunction $\hat{u}_z(r)$ which is best suited for the Rankine vortex. For small-amplitude perturbations of the form $(u'_r, u'_\theta, u'_z) = [\hat{u}_r(r), \hat{u}_\theta(r), \hat{u}_z(r)]\mathrm{e}^{\mathrm{i}(kz+m\theta-\omega t)}$, one obtains

$$\begin{aligned}&[(\omega - m\Omega)^2\{r^2\mathrm{D}^2 + r\mathrm{D} - m^2 - k^2r^2\} - r(\omega - m\Omega)\{m(2r\Omega'\mathrm{D} + \mathrm{D}Z)\\ &\quad + Q'Q^{-1}\{(\omega - m\Omega)r\mathrm{D} - mZ\}\} + 2k^2r^2\Omega Z]\hat{u}_z = 0,\end{aligned} \tag{2.23}$$

for a general vorticity profile where $Q \equiv \{(\omega - m\Omega)^2 - 2\Omega Z\}$. Here, $2\Omega Z$ is proportional to the Rayleigh discriminant governing centrifugal stability (see Chandrasekhar 1961), and equals $4\Omega_0^2 H(a - r)$ for a Rankine vortex. The radial and azimuthal components of the perturbation velocity field are given by

$$Q\hat{u}_r = -\frac{\mathrm{i}}{rk}(\omega - m\Omega)[(\omega - m\Omega)r\mathrm{D} - mZ]\hat{u}_z, \tag{2.24}$$

$$Q\hat{u}_\theta = -\frac{1}{rk}[Z(\omega - m\Omega)r\mathrm{D} - m\{(\omega - m\Omega)^2 + r\Omega' Z\}]\hat{u}_z. \tag{2.25}$$

Owing to the symmetry $\omega(m, k) = \omega(m, -k) = -\omega(-m, k)$ (Fabre *et al.* 2006) with $\hat{u}_z(r, m, k) = \hat{u}_z(r, -m, k) = \hat{u}_z(r, m, -k) = \hat{u}_z(r, -m, -k)$, valid for real-valued ω, it is sufficient to restrict the analysis to positive values of m and k.

For a Rankine vortex, equation (2.23) may be solved, separately, inside the core ($r \leqslant a$) and in the irrotational exterior ($r > a$). Note that (2.23) involves the base state vorticity itself in addition to its radial gradient, and equations inside the core therefore differ in form from those outside. This is a reflection of Coriolis forces coming into play within the core in three dimensions. Inviscid axisymmetric oscillations (the 'sausaging' modes) of a vortex column result from Coriolis forces

https://doi.org/10.1017/jfm.2013.666 Published online by Cambridge University Press

driving the alternate expansion and contraction of closed material curves, within the core, in a plane transverse to the rotation axis (Batchelor 1967); there exists an equivalent interpretation in terms of the periodic twisting and untwisting of vortex lines (Melander & Hussain 1994). Since $\Omega = \Omega_0$, $Z = 2\Omega_0$ and $Q' = 0$ inside the core, equations (2.23)–(2.25) reduce to

$$[(\omega - m\Omega_0)^2\{r^2\mathrm{D}^2 + r\mathrm{D} - m^2 - k^2r^2\} + 4k^2r^2\Omega_0^2]\hat{u}_z^i = 0, \tag{2.26}$$

$$\{(\omega - m\Omega_0)^2 - 4\Omega_0^2\}\hat{u}_r^i = -\frac{\mathrm{i}}{rk}(\omega - m\Omega_0)[(\omega - m\Omega_0)r\mathrm{D} - 2m\Omega_0]\hat{u}_z^i, \tag{2.27}$$

$$\{(\omega - m\Omega_0)^2 - 4\Omega_0^2\}\hat{u}_\theta^i = -\frac{1}{rk}(\omega - m\Omega_0)[2\Omega_0 r\mathrm{D} - m(\omega - m\Omega_0)]\hat{u}_z^i. \tag{2.28}$$

In the outer irrotational region, $Z = 0$ and (2.23)–(2.25) simplify to

$$(\omega - m\Omega)^2[r^2\mathrm{D}^2 + r\mathrm{D} - m^2 - k^2r^2]\hat{u}_z^o = 0, \tag{2.29}$$

$$\hat{u}_r^o = -\frac{\mathrm{i}}{k}\mathrm{D}\hat{u}_z^o, \tag{2.30}$$

$$\hat{u}_\theta^o = \frac{m}{rk}\hat{u}_z^o, \tag{2.31}$$

where the superscripts i and o denote the core and exterior regions, respectively.

The equation for $\hat{u}_z^i$ may be rewritten as a Bessel equation, and analyticity at the origin implies

$$\hat{u}_z^i \propto d\mathrm{J}_m(\beta r). \tag{2.32}$$

In (2.32), $\beta^2 \equiv k^2(4\Omega_0^2 - g^2)/g^2$ with $g = (m\Omega_0 - \omega)$ may be regarded as a radial wavenumber. The equation for $\hat{u}_z^o$ is the modified Bessel equation, and similar to the two-dimensional scenario, allows for two possibilities. The first is the homogeneous solution of (2.29) consistent with a decaying far-field:

$$\hat{u}_z^o \propto \mathrm{K}_m(kr), \tag{2.33}$$

$\mathrm{K}_m(z)$ being the modified Bessel function of the second kind, and leads to an irrotational velocity field outside the core. Continuity of u_z at $r = a$ gives

$$\hat{u}_z^i = \frac{\mathrm{J}_m(\beta r)}{\mathrm{J}_m(\beta a)}, \quad \hat{u}_z^o = \frac{\mathrm{K}_m(kr)}{\mathrm{K}_m(ka)}, \tag{2.34}$$

and, further, enforcing continuity of u_r at $r = a$ gives the familiar dispersion relation for the three-dimensional Kelvin modes (see Saffman 1992):

$$\frac{g^2}{(4\Omega_0^2 - g^2)}\left[\frac{\beta a\mathrm{J}_m'(\beta a)}{\mathrm{J}_m(\beta a)} + \frac{2m\Omega_0}{g}\right] = -\frac{ka\mathrm{K}_m'(ka)}{\mathrm{K}_m(ka)}. \tag{2.35}$$

The relation (2.35) yields a denumerable infinity of modes for a fixed k and m. For a given non-zero m, the dispersion curves (see the left-hand side of figure 3) span the interval $\omega \equiv [(m-2)\Omega_0, (m+2)\Omega_0]$. The modes may be classified based on the sign of the Doppler frequency; $g < 0$ corresponds to the co-grade modes and $g > 0$ to the retrograde modes. The co-grade and retrograde families are not symmetric (about $m\Omega_0$) for non-zero m. Apart from numerical differences in the ω values for a given k, the retrograde family includes an additional (structureless)

https://doi.org/10.1017/jfm.2013.666 Published online by Cambridge University Press

branch that reduces to the two-dimensional Kelvin mode with $\omega \to (m-1)\Omega_0$ for $k \to 0$. It is convenient to use a modal index, n, to enumerate the solutions $(\beta_{n,b})$ of (2.35) where $\beta_{n,+1}$ and $\beta_{n,-1}$, with n being a positive integer, correspond to the retrograde and co-grade families, respectively. Here $\beta_{1,1}$ corresponds to the structureless mode, while the remainder of the dispersion curves, both co-grade and retrograde, correspond to the 'structured' modes, a measure of this structure being the number of zero crossings of the axial vorticity ($w_z \propto \mathrm{J}_m(\beta_{n,b}r)$) which increases with increasing n. Further, $\beta_{n,b} \to \infty$, $\omega_n^b \to m\Omega_0$ for $n \to \infty$, so the structured modes become nearly-convected modes, concentrated in the vicinity of the symmetry axis, for large n. The Kelvin-mode vorticity eigenfunctions are given by

$$\hat{w}_{z,nb}^{Kelvin}(r) = -\frac{2g_{n,b}\Omega_0\beta_{n,b}^2}{k\{g_{n,b}^2 - 4\Omega_0^2\}}\frac{\mathrm{J}_m(\beta_{n,b}r)}{\mathrm{J}_m(\beta_{n,b}a)}\mathcal{H}(a-r) + \left[\hat{u}_\theta\right]_{r=a^-}^{r=a^+}\delta(r-a), \tag{2.36}$$

$$\hat{w}_{r,nb}^{Kelvin}(r) = -\frac{2\mathrm{i}\Omega_0}{r\{g_{n,b}^2 - 4\Omega_0^2\}}\left[g_{n,b}\frac{\beta_{n,b}r\mathrm{J}_m'(\beta_{n,b}r)}{\mathrm{J}_m(\beta_{n,b}a)} + 2m\Omega_0\frac{\mathrm{J}_m(\beta_{n,b}r)}{\mathrm{J}_m(\beta_{n,b}a)}\right]\mathcal{H}(a-r), \tag{2.37}$$

$$\hat{w}_{\theta,nb}^{Kelvin}(r) = \frac{2\Omega_0}{r\{g_{n,b}^2 - 4\Omega_0^2\}}\left[2\Omega_0\frac{\beta_{n,b}r\mathrm{J}_m'(\beta_{n,b}r)}{\mathrm{J}_m(\beta_{n,b}a)} + mg_{n,b}\frac{\mathrm{J}_m(\beta_{n,b}r)}{\mathrm{J}_m(\beta_{n,b}a)}\right]\mathcal{H}(a-r), \tag{2.38}$$

where

$$\left[\hat{u}_\theta\right]_{r=a^-}^{r=a^+} = -\frac{2\Omega_0}{ka(g_{n,b}^2 - 4\Omega_0^2)}\left\{g_{n,b}\frac{\beta_{n,b}a\mathrm{J}_m'(\beta_{n,b}a)}{\mathrm{J}_m(\beta_{n,b}a)} + 2m\Omega_0\right\}, \tag{2.39}$$

with $g_{n,b} = (m\Omega_0 - \omega_n^b)$ and $\beta_{n,b}^2 = k^2(4\Omega_0^2 - g_{n,b}^2)/g_{n,b}^2$; the subscript $b = \pm 1$ in (2.36)–(2.38) discriminates between retrograde and co-grade modes.

The inclusion of viscosity in the linearized stability equations should lead to a weak $O(Re^{-1})$ damping of the Rankine Kelvin modes. Self-consistency requires, however, that the effect of viscosity also be included in the base state which must then lead to a smooth non-compact vorticity profile. As mentioned in the introduction, the two-dimensional Kelvin mode transforms into a damped singular mode for a general smooth vorticity profile with $\mathrm{D}Z(r_f) \neq 0$ (Le Dizès 2000). Importantly, the damping rate is independent of Re for $Re \gg 1$, arising due to an increasingly fine-scaled structure (the radial scale being $O(Re^{-1/2})$) inside a viscous critical layer with a thickness of $O(\mathrm{D}Z)$ around r_f (Lin 1955). Both computations for large Re, and estimates based on a contour deformation calculation show that for a Lamb–Oseen profile the three-dimensional retrograde modes of a Rankine vortex are again replaced by inviscidly damped critical-layer modes (Fabre 2002; Fabre *et al.* 2006). There appear to exist a countable infinity of such modes with the damping rate possibly dependent on the values of both Z and $\mathrm{D}Z$ at r_f. The singular effect of viscosity is especially important for the retrograde structured modes. In sharp contrast to the predictions of (2.35), the relevant dispersion curves for the Lamb–Oseen profile do not asymptote to the core angular frequency in the limit $k \to 0$. Bending modes ($m = 1$) are particularly important in this regard, since (2.35) for $m = 1$ allows for modes with a negative ω (counter-grade) that then lie outside the base state range of frequencies. Every retrograde bending mode invariably becomes counter-grade for large enough k and, correspondingly, the critical radius moves off to infinity and onto the complex plane. Counter-grade modes for a smooth vorticity profile are therefore expected to remain qualitatively unaltered for a general vorticity profile and with the inclusion of viscosity, as is confirmed by numerical calculations (Fabre *et al.* 2006).

The dispersion curves for axisymmetric column oscillations, as given by (2.35) with $m = 0$, are symmetric about $\omega = 0$, and denote sausaging modes that travel

https://doi.org/10.1017/jfm.2013.666 Published online by Cambridge University Press

in opposite directions along the core. The dynamics involves the alternate twisting and untwisting of the vortex lines on surfaces approximately concentric with the cylindrical core boundary. The associated radial displacements are smaller for larger n, and the weaker (Coriolis) restoring forces imply that $\omega_n^b \to 0$ for $n \to \infty$. The absence of a critical layer singularity also implies that the dispersion curves for the sausaging modes remain qualitatively unaltered for a smooth vorticity profile and for large but finite Re (Fabre 2002). Importantly, equation (2.23), for $m = 0$, defines a regular Sturm–Liouville problem for an arbitrary axial vorticity profile and the completeness of the denumerably infinite family of axisymmetric modes follows (Ince 1956; Chandrasekhar 1961). Thus, for a general non-compact vorticity profile, an arbitrary small-amplitude axisymmetric disturbance may still be represented as a superposition of evolving axisymmetric Kelvin modes. For a Rankine vortex, however, the complete separation of the regions of strain ($r > a$) and vorticity ($r < a$) implies that one must distinguish between vortical perturbations related to an axisymmetric column deformation and similar disturbances present in the irrotational exterior. The standard Sturm–Liouville arguments allow one to infer the completeness of the axisymmetric Kelvin modes, with frequencies obtained from (2.35), for the former class of disturbances (column deformations). The question regarding the response of the Rankine vortex to exterior vortical perturbations remains. Since any perturbation with $m = 0$ evolves unchanged even in the presence of differential shear, there is evidently a degeneracy as regards a modal decomposition for exterior perturbations. We return to this point, and the related implications for the transient growth observed in recent simulations, even for $m = 0$ (Pradeep & Hussain 2006), after the analysis for the non-axisymmetric CS modes in §§ 2.2.1 and 2.2.2.

Since the Kelvin modes above arise from the homogeneous solution of (2.29), they have vorticity within the core and an axial vortex sheet at its edge. A natural question is whether these modes can therefore represent an arbitrary vortical initial condition restricted to the region $r \leqslant a$, that is to say, an arbitrary small-amplitude deformation of the vortex column. The discussion in the preceding paragraph shows that this is certainly true for $m = 0$. For non-zero m, however, equation (2.23) has singular coefficients, and the standard Sturm–Liouville arguments do not apply. Thus, the completeness of the Kelvin modes alone, in the absence of additional singular eigenmodes (constituting the CS), is not obvious. This question has been recently answered in the affirmative by Arendt *et al.* (1997), and our primary focus here is on the complementary situation: the additional modes required for the evolution of an arbitrary vortical initial condition outside the core, a situation of particular relevance to the transient growth recently observed for single vortices (see Antkowiak & Brancher 2004; Pradeep & Hussain 2006). In what follows, we show that there are two retrograde families of singular eigenmodes needed to evolve an arbitrary initial condition (an arbitrary solenoidal distribution of vorticity). With the inclusion of these singular eigenmodes, every retrograde frequency except for that corresponding to the Kelvin modes, is doubly degenerate. There is some leeway as to how the aforementioned partition of the CS into two families may be made, and we choose a division based on the presence or absence of radial vorticity in the singular part of the eigenfunction. For the eigenfunctions in the first family, the singular structure is a cylindrical vortex sheet at the critical radius, threaded by helical lines, and thereby devoid of radial vorticity. For the eigenfunctions in the second family, the singular structure is again localized at the critical radius, but possesses radial vorticity; the vortex lines in this case form cells of an infinitesimal thickness in the plane transverse to the rotation axis.

https://doi.org/10.1017/jfm.2013.666 Published online by Cambridge University Press

2.2.1. *Three-dimensional CS modes: the Λ_1 family (zero radial vorticity)*

The Λ_1 eigenmodes are the natural generalization of the two-dimensional CS modes analysed in § 2.1. Equation (2.29) allows for a vortex sheet, threaded by helical lines, in the outer irrotational region. Thus,

$$[r^2\mathrm{D}^2 + r\mathrm{D} - m^2 - r^2k^2]\hat{u}_z^o = a_1\delta(\omega - m\Omega) + a_2\delta'(\omega - m\Omega), \tag{2.40}$$

so that, as in (2.4), there is again an inhomogeneity proportional to a generalized function. Here, we have used the identity $x^2\{a_1\delta(x) + a_2\delta'(x)\} = 0$. One may rewrite (2.40) as

$$[r^2\mathrm{D}^2 + r\mathrm{D} - m^2 - r^2k^2]\hat{u}_z^o = A_1(r_f)\delta(r - r_f) + A_2(r_f)\delta'(r - r_f), \tag{2.41}$$

with $r_f = (m\Omega_0/\omega)^{1/2}a$ denoting the location of the exterior vortex sheet. For the vortex sheet to lie in the physical domain, r_f must be real, and ω must therefore lie in the base state range of angular frequencies. The analysis that follows is thus restricted to the retrograde frequency range $(0, m\Omega_0]$. Using $\boldsymbol{w} = \boldsymbol{\nabla} \wedge \boldsymbol{u}$, and in the absence of radial vorticity ($\hat{w}_r = 0$), the following relation between $\hat{u}_z$ and the vorticity field holds for $r \geqslant a$:

$$[r^2\mathrm{D}^2 + r\mathrm{D} - m^2 - r^2k^2]\hat{u}_z = -r\mathrm{D}(r\hat{w}_\theta). \tag{2.42}$$

Note that $\hat{w}_\theta$ for the Λ_1 family is proportional to $\delta(r - r_f)$. One may now equate (2.41) and (2.42) which leads to the relation between A_1 and A_2 such that the singular forcing in (2.41) represents a cylindrical vortex sheet. One obtains $A_2(r_f) = -r_fA_1(r_f)$. The azimuthal and axial components of the (helical) vortex sheet strength (A_{Λ_1}) are $A_{\theta\Lambda_1} = A_1(r_f)/r_f$ and $A_{z\Lambda_1} = -mA_1(r_f)/(kr_f^2)$, respectively, the pitch of a helical vortex line being $|2\pi r_f(A_{z\Lambda_1}/A_{\theta\Lambda_1})| = (2\pi m)/k$.

The solution of (2.41) is obtained by separate consideration of three ($r < a$, $a < r < r_f$ and $r > r_f$) rather than two regions (as was the case for the regular Kelvin modes). The solutions in these regions, consistent with regularity both at the origin and at infinity, are

$$\hat{u}_z^{i1} = d\mathrm{J}_m(\beta r), \quad (0 < r < a), \tag{2.43}$$

$$\hat{u}_z^{o2} = c_1\mathrm{I}_m(kr) + c_2\mathrm{K}_m(kr), \quad (a < r < r_f), \tag{2.44}$$

$$\hat{u}_z^{o3} = f(ka)\frac{\Omega_0a^2}{r_f}\mathrm{K}_m(kr), \quad (r > r_f), \tag{2.45}$$

where the normalization, as in § 2.1, is applied to the region outside the vortex sheet at $r = r_f$. As will be seen later, the normalizing factor, $f(ka) = -\mathrm{i}/[mka\mathrm{K}_m(ka)]$, enforces agreement between the limiting forms of the three-dimensional modes, for $k \to 0$, and the two-dimensional modes found earlier. The constants c_1 and c_2 are now determined from the following matching conditions obtained by integrating (2.41) over an infinitesimal interval including $r = r_f$:

$$A_2(r_f) = -r_fA_1(r_f), \tag{2.46}$$

$$\hat{u}_z^{o2} - \hat{u}_z^{o3} = -\frac{A_2(r_f)}{r_f^2} = \frac{A_1(r_f)}{r_f} \quad \text{at } r = r_f, \tag{2.47}$$

$$\mathrm{D}\hat{u}_z^{o2} = \mathrm{D}\hat{u}_z^{o3} \quad \text{at } r = r_f. \tag{2.48}$$

The condition (2.46) has already been obtained above, and shows that the jumps in the axial and azimuthal components of the velocity perturbation are not independent,

https://doi.org/10.1017/jfm.2013.666 Published online by Cambridge University Press

being related by the fact that the pitch of the helical vortex lines at $r = r_f$ is entirely determined by m and k. Equation (2.48) enforces continuity of the radial velocity perturbation, thereby excluding a singular jet-like profile riding on the vortex sheet, while (2.47) characterizes the jump in the axial velocity across the helical vortex sheet at $r = r_f$. From (2.44), (2.45), (2.47) and (2.48), one obtains

$$c_1 = -k\mathrm{K}'_m(kr_f)A_1(r_f), \tag{2.49}$$

$$c_2 = f(ka)\frac{\Omega_0 a^2}{r_f} + k\mathrm{I}'_m(kr_f)A_1(r_f), \tag{2.50}$$

the simplified expressions arising from use of the Wronskian for the modified Bessel equation. The constant d in (2.43) is determined from the continuity of the axial velocity at $r = a$, and given by

$$d = \frac{(f(ka)\Omega_0 a^2/r_f)\mathrm{K}_m(ka) + kA_1(r_f)\{\mathrm{I}'_m(kr_f)\mathrm{K}_m(ka) - \mathrm{K}'_m(kr_f)\mathrm{I}_m(ka)\}}{\mathrm{J}_m(\beta a)}. \tag{2.51}$$

From (2.27) and (2.30) we have the following expressions for radial velocity at $r = a$,

$$\hat{u}_r^{i1}|_{r=a} = -\frac{\mathrm{i}dg}{ka(g^2 - 4\Omega_0^2)}\{g\beta a\mathrm{J}'_m(\beta a) + 2m\Omega_0\mathrm{J}_m(\beta a)\}, \tag{2.52}$$

$$\hat{u}_r^{o2}|_{r=a} = -\frac{\mathrm{i}}{\mathrm{I}'_m(kr_f)}[c_2\{\mathrm{I}'_m(kr_f)\mathrm{K}'_m(ka) - \mathrm{K}'_m(kr_f)\mathrm{I}'_m(ka)\} + \mathrm{K}'_m(kr_f)\mathrm{I}'_m(ka)]. \tag{2.53}$$

Equating (2.52) and (2.53), to enforce continuity of the radial velocity at $r = a$, one obtains, after some algebra, the following expression for the vortex-sheet amplitude:

$$A_1(r_f) = f(ka)\frac{\Omega_0 a^2}{r_f}\frac{M(r_f; ka, \beta a)}{k\{\mathrm{K}'_m(kr_f)N(r_f; ka, \beta a) - \mathrm{I}'_m(kr_f)M(r_f; ka, \beta a)\}}, \tag{2.54}$$

where

$$\begin{aligned} M(r_f; ka, \beta a) = {} & g^2\beta a\mathrm{J}'_m(\beta a)\mathrm{K}_m(ka) + 2m\Omega_0 g\mathrm{J}_m(\beta a)\mathrm{K}_m(ka) \\ & + (4\Omega_0^2 - g^2)\mathrm{J}_m(\beta a)ka\mathrm{K}'_m(ka), \end{aligned} \tag{2.55}$$

$$\begin{aligned} N(r_f; ka, \beta a) = {} & g^2\beta a\mathrm{J}'_m(\beta a)\mathrm{I}_m(ka) + 2m\Omega_0 g\mathrm{J}_m(\beta a)\mathrm{I}_m(ka) \\ & + (4\Omega_0^2 - g^2)\mathrm{J}_m(\beta a)ka\mathrm{I}'_m(ka). \end{aligned} \tag{2.56}$$

As in § 2.1, the retrograde Kelvin modes naturally emerge as those for which $A_1(r_f) = 0$. The functions M and N remain finite for any finite r_f, and so do the modified Bessel functions. Further, since the zeros of M and N interlace each other, the condition of a vanishing vortex-sheet amplitude implies $M = 0$; this is precisely the dispersion relation for the Kelvin modes (see (2.35)). In contrast to the two-dimensional case, where a vanishing vortex-sheet amplitude led to a single value of r_f (the structureless mode) for a fixed m ($r_{fk} = (m/(m-1))^{1/2}a$), in three-dimensional one has a countable infinity of critical radii for a given m and k. The vorticity field associated with a Λ_1 eigenmode is given by

$$\hat{w}_z^{\Lambda_1}(r; r_f) = -\frac{2dg\Omega_0\beta^2\mathrm{J}_m(\beta r)}{k\{g^2 - 4\Omega_0^2\}}\mathcal{H}(a - r) + \left[\hat{u}_\theta\right]_{r=a^-}^{r=a^+}\delta(r - a) - \frac{mA_1(r_f)}{kr_f^2}\delta(r - r_f), \tag{2.57}$$

https://doi.org/10.1017/jfm.2013.666 Published online by Cambridge University Press

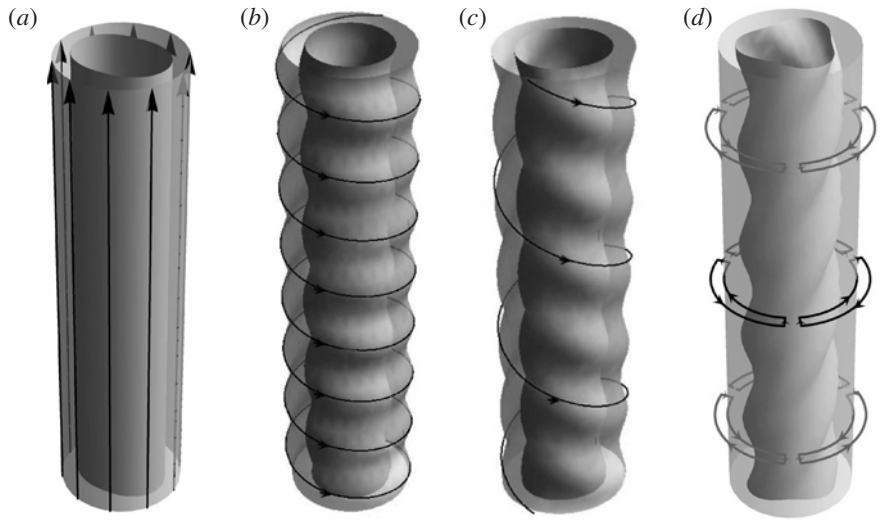

FIGURE 4. (*a*) Schematic of a two-dimensional CS mode for $m=2$ with an elliptically deformed core and with axial vortex lines threading the cylindrical sheet in the irrotational exterior. Here $w_z \neq 0$. (*b,c*) Schematics of the three-dimensional Λ_1-modes for $m=1$ (a single helical phase contour is shown) and $m=2$ (only one of two helical phase contours is shown), respectively, with helical lines that thread the cylindrical sheet. Here $w_z \neq 0$, $w_\theta \neq 0$. (*d*) Schematic of the $\Lambda-2$ modes for $m=3$ with the core deformed into a three-lobed structure, and the vortex lines within the infinitesimal cylindrical sheet now corresponding to a singular dipole structure. Here $w_r \neq 0$, $w_\theta \neq 0$.

$$\hat{w}_r^{\Lambda_1}(r;\, r_f) = -\frac{2\mathrm{i}d\Omega_0}{r\{g^2-4\Omega_0^2\}}\left[g\beta r\mathrm{J}'_m(\beta r)+2m\Omega_0\mathrm{J}_m(\beta r)\right]\mathcal{H}(a-r), \tag{2.58}$$

$$\hat{w}_\theta^{\Lambda_1}(r;\, r_f) = \frac{2d\Omega_0}{r\{g^2-4\Omega_0^2\}}\left[2\Omega_0\beta r\mathrm{J}'_m(\beta r)+mg\mathrm{J}_m(\beta r)\right]\mathcal{H}(a-r)+\frac{A_1(r_f)}{r_f}\delta(r-r_f), \tag{2.59}$$

where

$$\left[\hat{u}_\theta\right]_{r=a^-}^{r=a^+} = \frac{m}{ka}\left[c_1\mathrm{I}_m(ka)+c_2\mathrm{K}_m(ka)\right]-\frac{dg}{ka\{g^2-4\Omega_0^2\}}\left[2\Omega_0\beta a\mathrm{J}'_m(\beta a)+mg\mathrm{J}_m(\beta a)\right], \tag{2.60}$$

with the radial vorticity field, expectedly, being confined to the core region. Here, c_1, c_2 and d are given by (2.49)–(2.51). Typical Λ_1 eigenmodes are shown in figure 4.

Figure 5 plots $A_1(r_f)$ as a function of r_f for $m=2$ and $k=3$; the essential features remain unchanged for other values of m and k. Interestingly, in addition to the values of r_f corresponding to the Kelvin-mode frequencies, for which $A_1(r_f)=0$, there are values at which $A_1(r_f)$ diverges. Since M and N have zeros interlacing each other as a function of r_f, the zeros and singularities of $A_1(r_f)$ also interlace each other, and the latter again form a countably infinite set. The divergences are an artifact of the normalization used in (2.43)–(2.45), and physically, at these r_f, the vortex sheet entirely screens the perturbation velocity field induced by the oscillating column (that is, $\hat{u}_z^{o3}=0$). In doing so, the sheet acts as an impenetrable wall, and,

https://doi.org/10.1017/jfm.2013.666 Published online by Cambridge University Press

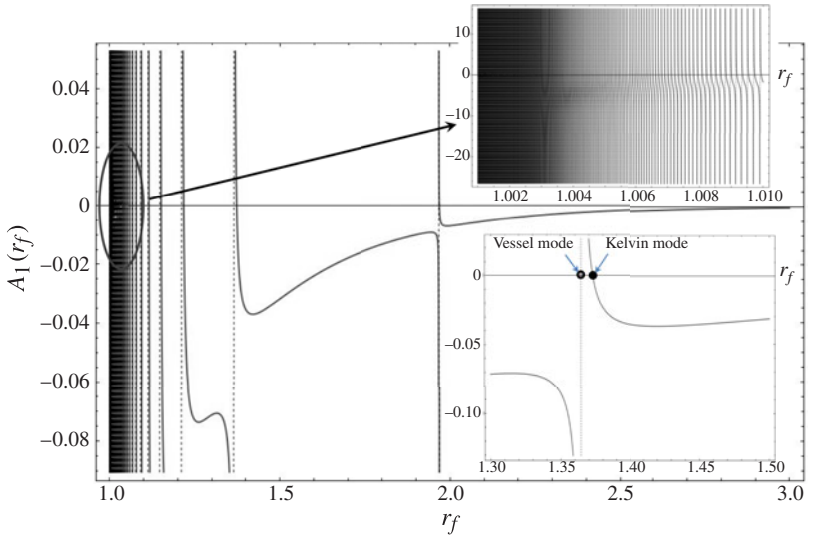

FIGURE 5. (Colour online) The vortex-sheet amplitude, $A_1(r_f)$, for $m = 2$ and $k = 3$. The vertical dashed lines, defined by $1/A_1 = 0$, correspond to the vessel mode loci (that interlace the Kelvin-mode frequencies). The amplitude changes sign at an increasingly rapid rate as $r_f \to 1$, and the inset offers a magnified view of the variation near the core.

for the given m and k, the corresponding frequency must therefore be a solution of the dispersion relation for a Rankine vortex in a cylindrical vessel of size r_f. From (2.54), the locations at which $A_1(r_f) \to \infty$ must satisfy $\mathrm{K}'_m(kr_f)N - \mathrm{I}'_m(kr_f)M = 0$; in appendix A, it is shown that this is indeed the relation governing the normal modes of a Rankine vortex with a core of radius a embedded in a vessel of radius r_f. For a fixed r_f, and thence, a fixed $\omega(= m\Omega_0(a/r_f)^2)$ in the range $[(m-2)\Omega_0, m\Omega_0]$, the singular eigenmodes are coincident with vessel modes, in the region $0 < r < r_f$, at a denumerable infinity of axial wavenumbers (the limit point being infinity). Clearly, not all vessel modes will be recovered from the present analysis since, for a vessel unbounded in the vertical direction, one expects the regular modes to span a continuum of axial wavenumbers. This is because, in the bounded problem, while the vessel wall may be regarded as a vortex sheet, it is required to convect at the modal angular velocity. On the other hand, in the present context, the vortex sheet must convect with the base-state angular velocity at $r = r_f$. Thus, only those vessel modes are recovered for which these two angular velocities are coincident.

A sketch of the frequency intervals spanned by the CS modes, including the vessel mode loci, appears on the right-hand side in figure 3. (Note that this is a schematic depiction. As shown in figure 5, the locations corresponding to the divergences of the singular structure amplitude are very close to the zeros, implying that, in reality, a given vessel mode curve is much closer to one of the neighbouring Kelvin-mode curves than the other.) The CS modes occupy the intervals between the discrete retrograde frequencies, and with their inclusion, the Rankine spectrum, for fixed m and k, consists of the denumerable infinity of co-grade frequencies together with the entire retrograde frequency interval $(0, m\Omega_0)$. The case $m = 1$ is an exception, since the counter-grade mode frequencies remain unaffected, and the spectrum therefore remains discrete in the interval $[-\Omega_0, 0]$. The analysis for the Λ_1 eigenmodes above, although more involved algebraically, is still analogous to that in two dimensions,

https://doi.org/10.1017/jfm.2013.666 Published online by Cambridge University Press

in the sense that the difference between the regular (retrograde Kelvin) and singular eigenmodes is the existence, in the latter case, of an additional vortex sheet at the critical radius. This may be seen from comparing the vorticity eigenfunctions for a Λ_1 eigenmode, given by (2.57)–(2.59), with those of a Kelvin mode given by (2.36)–(2.38).

The singularity of the Λ_2 eigenmodes analysed below, although not a vortex sheet, is again localized at the critical radius. This localization of the vorticity is possible due to the complete spatial separation of the regions of (base state) vorticity and shear for a Rankine vortex. For a parallel flow, on the other hand, both the vorticity and shear are proportional to U', and the impossibility of a spatial separation between the two, makes the three-dimensional singular eigenmodes quite different from the two-dimensional ones. As shown in Sazonov (1996), for unbounded Couette flow, the singular modes with wave vectors inclined to the plane of shear are no longer localized vortex sheets coincident with streamlines of the base state flow like those originally found by Case (1960*a*) in two dimensions. Instead, the spanwise variation of the perturbation velocity field acts to stretch and tilt the ambient vorticity, leading to additional non-local contributions (with a PV singularity) to the perturbation vorticity field. As will be seen in § 2.2.3, this makes the solution of the three-dimensional IVP for the Rankine vortex, via a modal superposition, (conceptually) easier than that for Couette flow (Roy & Subramanian 2012).

2.2.2. *Three-dimensional CS modes: the Λ_2 family (with radial vorticity)*

Unlike the Λ_1 family, the Λ_2 eigenmodes possess radial vorticity localized in the singular vortical structure at the critical radius (see figure 4*d*). It is convenient to analyse this case starting from (2.42) now generalized to a non-zero $\hat{w}_r$:

$$[r^2\mathrm{D}^2 + r\mathrm{D} - m^2 - r^2k^2]\hat{u}_z = -r\mathrm{D}(r\hat{w}_\theta) + \mathrm{i}mr\hat{w}_r. \tag{2.61}$$

The Λ_2 family, in its simplest form, may be obtained by setting $\hat{w}_z = 0$ for $r > a$, while allowing for the radial vorticity field to include a delta function. The resulting singular structure at $r = r_f$ is characterized by a vorticity field in the plane transverse to the rotation axis, $(\hat{w}_r, \hat{w}_\theta) \equiv [A_{r\Lambda_2}\delta(r - r_f), r_f A_{\theta\Lambda_2}\delta'(r - r_f)]$, with $r_f \geqslant a$ and $A_{r\Lambda_2} = -\mathrm{i}mA_{\theta\Lambda_2}$. Equation (2.61) takes the form

$$[r^2\mathrm{D}^2 + r\mathrm{D} - m^2 - r^2k^2]\hat{u}_z^o = A_1(r_f)\delta(r - r_f) + A_2(r_f)\delta'(r - r_f) + A_3(r_f)\delta''(r - r_f), \tag{2.62}$$

where $A_1 = (m^2 - 1)r_f A_{\theta\Lambda_2}$, $A_2 = 3r_f^2 A_{\theta\Lambda_2}$ and $A_3 = -r_f^3 A_{\theta\Lambda_2}$. For the Λ_2 modes, $\hat{u}_r$ is discontinuous at $r = r_f$, implying a delta-function singularity in $\hat{u}_z$, and thence, a localized axial jet riding on the convected singular structure. With $\hat{u}_z = \hat{u}_z^{reg} + P_1\delta(r - r_f)$, P_1 being a measure of the jet volumetric flux per unit wavelength along the azimuth, the following matching conditions result from integrating (2.62) in an infinitesimal interval around r_f:

$$r_f^2[\mathrm{D}\hat{u}_z^{reg}]_{r_f^-}^{r_f^+} - r_f[\hat{u}_z^{reg}]_{r_f^-}^{r_f^+} - P_1\{(m^2 - 1) + (kr_f)^2\} = A_1, \tag{2.63}$$

$$-r_f^2[\hat{u}_z^{reg}]_{r_f^-}^{r_f^+} + 3r_f P_1 = -A_2, \tag{2.64}$$

$$2r_f^2 P_1 = 2A_3. \tag{2.65}$$

The expressions for the velocity fields and the different regions under consideration remain identical to § 2.2.1. Enforcing the continuity of the radial and axial velocity components at $r = a$, and a little algebra, leads to the following expressions for the

https://doi.org/10.1017/jfm.2013.666 Published online by Cambridge University Press

constants characterizing the velocity fields in the different regions (see (2.43)–(2.44) and (2.45)):

$$c_1 = A_{\theta\Lambda_2}\mathrm{K}_m(kr_f)(kr_f)^2, \tag{2.66}$$

$$c_2 = f(ka)\frac{\Omega_0 a^2}{r_f} - A_{\theta\Lambda_2}\mathrm{I}_m(kr_f)(kr_f)^2, \tag{2.67}$$

$$d = \frac{(f(ka)\Omega_0 a^2/r_f)\mathrm{K}_m(ka) + A_{\theta\Lambda_2}(kr_f)^2\{\mathrm{K}_m(kr_f)\mathrm{I}_m(ka) - \mathrm{I}_m(kr_f)\mathrm{K}_m(ka)\}}{\mathrm{J}_m(\beta a)}. \tag{2.68}$$

The amplitude of the singular vortical structure at $r = r_f$ is given by

$$A_{\theta\Lambda_2}(r_f) = -f(ka)\frac{\Omega_0 a^2}{r_f}\frac{M(r_f;\, ka,\, \beta a)}{(kr_f)^2\{\mathrm{K}_m(kr_f)N(r_f;\, ka,\, \beta a) - \mathrm{I}_m(kr_f)M(r_f;\, ka,\, \beta a)\}} \tag{2.69}$$

with $P_1 = r_f A_{\theta\Lambda_2}$; a sketch of a typical Λ_2 eigenmode ($m = 3$) appears in figure 4(*d*). From (2.69), and similar to the Λ_1 modes, the singular structure again disappears for $M = 0$, the dispersion relation for the Kelvin modes. The amplitude, $A_{\theta\Lambda_2}$, also diverges at the zeros of $\mathrm{K}_m(kr_f)N - \mathrm{I}_m(kr_f)M$ with the zeros and divergences of $A_{\theta\Lambda_2}$ interlacing each other as shown in figure 6(*a*). The singularities again imply a quiescent exterior ($r > r_f$) as the singular structure at these radii screens the perturbation velocity field induced by the column oscillations. An analogy with a bounded domain problem is, however, not evident owing to the axial jet riding on the vessel walls. Finally, the vorticity field associated with a Λ_2 eigenmode is given by

$$\hat{w}_z^{\Lambda_2}(r;\, r_f) = -\frac{2dg\Omega_0\beta^2\mathrm{J}_m(\beta r)}{k\{g^2 - 4\Omega_0^2\}}\mathcal{H}(a-r) + \left[\hat{u}_\theta\right]_{r=a^-}^{r=a^+}\delta(r-a), \tag{2.70}$$

$$\hat{w}_r^{\Lambda_2}(r;\, r_f) = -\frac{2\mathrm{i}d\Omega_0}{r\{g^2 - 4\Omega_0^2\}}\left[g\beta r\mathrm{J}_m'(\beta r) + 2m\Omega_0\mathrm{J}_m(\beta r)\right]\mathcal{H}(a-r) - \mathrm{i}mA_{\theta\Lambda_2}\delta(r-r_f), \tag{2.71}$$

$$\hat{w}_\theta^{\Lambda_2}(r;\, r_f) = \frac{2d\Omega_0}{r\{g^2 - 4\Omega_0^2\}}\left[2\Omega_0\beta r\mathrm{J}_m'(\beta r) + mg\mathrm{J}_m(\beta r)\right]\mathcal{H}(a-r) + r_f A_{\theta\Lambda_2}\delta'(r-r_f), \tag{2.72}$$

where

$$\left[\hat{u}_\theta\right]_{r=a^-}^{r=a^+} = \frac{m}{ka}\left[c_1\mathrm{I}_m(ka) + c_2\mathrm{K}_m(ka)\right] - \frac{dg}{ka\{g^2 - 4\Omega_0^2\}}\left[2\Omega_0\beta a\mathrm{J}_m'(\beta a) + mg\mathrm{J}_m(\beta a)\right], \tag{2.73}$$

and c_1, c_2 and d being given by (2.66)–(2.68). As shown in figure 6(*b*), in light of the Λ_1 and Λ_2 families, the Kelvin-mode frequencies and the corresponding eigenfunctions (2.36)–(2.38) may now be regarded as degenerate in that they correspond to the zeros of both $A_1(r_f)$ and $A_{\theta\Lambda_2}(r_f)$.

2.2.3. *The modal decomposition for an arbitrary vortical initial condition*

For a fixed m ($\neq 0$) and k, an arbitrary smooth initial distribution of vorticity of the form $\boldsymbol{w}(\boldsymbol{x},\, 0) = [w_{r0}(r),\, w_{\theta 0}(r),\, (\mathrm{i}/(kr))(\mathrm{i}mw_{\theta 0}(r) + (rw_{r0}(r))')]\mathrm{e}^{\mathrm{i}(kz+m\theta)}$ may now be evolved as the following superposition of the Kelvin modes, and the Λ_1 and Λ_2

https://doi.org/10.1017/jfm.2013.666 Published online by Cambridge University Press

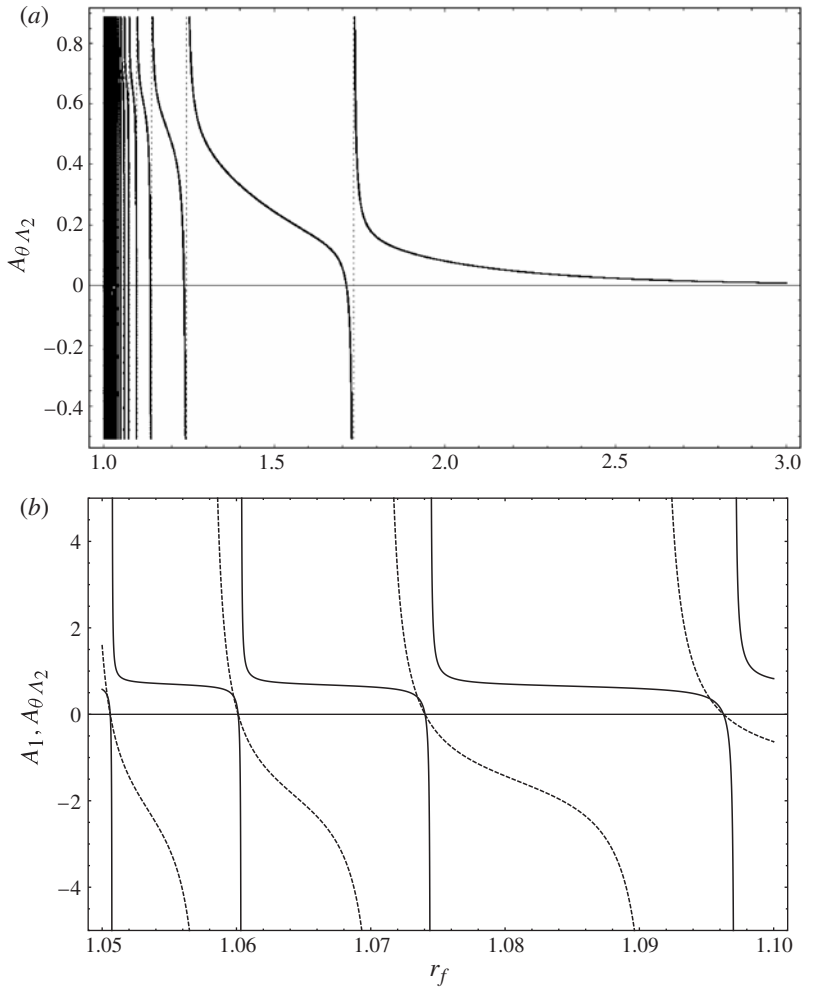

FIGURE 6. (*a*) The amplitude of the vortex sheet for Λ_2 family, $A_{\theta\Lambda_2}$, as a function of r_f, for $m=2$ and $k=2$. (*b*) A magnified view of the rapid variation near the core of the amplitudes of the singular structures for the Λ_2 (dashed) family and its comparison with its Λ_1 (continuous) counterpart. The amplitudes A_1 and $A_{\theta\Lambda_2}$ evidently have coincident zeros (which correspond to the Kelvin radii) but distinct singularities.

families:

$$\boldsymbol{w}(\boldsymbol{x},t)=\int_{a^+}^{\infty}\left[X_{\Lambda_1}(r_f)\hat{\boldsymbol{w}}^{\Lambda_1}(r;r_f)+X_{\Lambda_2}(r_f)\hat{\boldsymbol{w}}^{\Lambda_2}(r;r_f)\right]\mathrm{e}^{\mathrm{i}[kz+m(\theta-\Omega(r_f)t)]}\,\mathrm{d}r_f + \left\{\sum_{b=\pm1}\sum_{n=1}^{\infty}(C_{nb}-A_{nb})\hat{\boldsymbol{w}}_{nb}^{Kelvin}(r)\mathrm{e}^{-\mathrm{i}\omega_n^b t}\right\}\mathrm{e}^{\mathrm{i}(kz+m\theta)}, \tag{2.74}$$

where

$$X_{\Lambda_1}(r_f)=\frac{r_f}{A_1}\left[w_{\theta0}(r_f)\mathcal{H}(r_f-a)-\frac{\mathrm{i}}{m}\left(r_f w_{r0}(r_f)\mathcal{H}(r_f-a)\right)'\right], \tag{2.75}$$

$$X_{\Lambda_2}(r_f)=\frac{\mathrm{i}}{m}\frac{w_{r0}(r_f)\mathcal{H}(r_f-a)}{A_{\theta\Lambda_2}}, \tag{2.76}$$

https://doi.org/10.1017/jfm.2013.666 Published online by Cambridge University Press

and $\hat{\boldsymbol{w}}_{nb}^{Kelvin}$, $\hat{\boldsymbol{w}}^{\Lambda_1}$ and $\hat{\boldsymbol{w}}^{\Lambda_2}$ are known from (2.36)–(2.38), (2.57)–(2.59) and (2.70)–(2.72), respectively. The ω_n^b in (2.74) are the Kelvin-mode frequencies obtained from (2.35), and the C_{nb} and A_{nb} denote the corresponding modal amplitudes. The expression (2.74) has been shown to be equivalent to one obtained from a solution of the IVP (Roy 2013), and this will reported in detail elsewhere. Herein, we argue that the general form of (2.74) may be arrived at by examining the modal superposition at $t = 0$. Our choice of the CS-mode families, in particular, the absence of radial vorticity in the Λ_2 family eigenfunctions, in the irrotational exterior, allows one to construct this initial superposition in a simple sequential manner. To begin with, a superposition of Λ_2 eigenmodes alone is needed to represent the initial radial vorticity in $r > a$, the required amplitude distribution being given by (2.76). The difference between the initial and Λ_2 azimuthal vorticities, for $r > a$, may then be represented by a superposition of Λ_1 eigenmodes (the axial component is automatically determined from the solenoidal constraint) with the amplitude distribution being given by (2.75). This superposition of Λ_1 and Λ_2 eigenmodes now accounts for the entire initial vorticity outside the core. What remains is the difference between the initial vorticity inside the core (and a possible axial vortex sheet at its edge) and the additional core and edge vorticities generated by the Λ_i superposition. This vorticity distribution is equivalent to a column deformation and, therefore, using the results of Arendt *et al.* (1997), it may be expressed as a summation over Kelvin modes, and the required Kelvin-mode amplitude distributions are

$$C_{nb}(A_{nb}) = \left[\frac{g_{C(A)}(a)\mathrm{J}'_m(k\xi_{n,b}a)}{k\xi_{n,b}a\mathrm{J}_m(k\xi_{n,b}a)} - a\frac{g'_{C(A)}(a)}{(k\xi_{n,b}a)^2} + P_{C(A)}\right] B_n^b, \tag{2.77}$$

where C_{nb} and A_{nb}, respectively, correspond to the Kelvin-mode superpositions needed to represent the original initial vorticity, and that in the Λ_i superpositions. The various quantities in (2.77) are as defined below:

$$B_n^b = \frac{2\xi_{n,b}^2 b\mathrm{i}\Omega_0}{(\xi_{n,b}^2+1)^{3/2}}\left[\frac{2\mathrm{J}'_m(k\xi_{n,b}a)}{k\xi_{n,b}a\mathrm{J}_m(k\xi_{n,b}a)} + \left\{\frac{\mathrm{J}'_m(k\xi_{n,b}a)}{\mathrm{J}_m(k\xi_{n,b}a)}\right\}^2 + 1 - \frac{m^2}{(k\xi_{n,b}a)^2} + \frac{bm(\xi_{n,b}^2+2)}{\sqrt{\xi_{n,b}^2+1}(k\xi_{n,b}a)^2}\right]^{-1}, \tag{2.78}$$

$$P_{C(A)} = \frac{1}{k^2 a}\left\{\frac{2\Omega_0 w^{core}_{rC(A)}(a) + \mathrm{i}(\omega_n^b - m\Omega_0)w^{core}_{\theta C(A)}(a)}{(\omega_n^b - m\Omega_0)^2 - 4\Omega_0^2}\right\}, \tag{2.79}$$

$$g_{C(A)}(a) = \int_0^a \frac{\pi r'}{2}\left[\frac{2\Omega_0 \mathrm{i}k}{(\omega_n^b - m\Omega_0)^2}w^{core}_{zC(A)} - \frac{\mathrm{i}}{\omega_n^b - m\Omega_0}\left\{\frac{\mathrm{d}}{\mathrm{d}r'}(r' w^{core}_{\theta C(A)}) - \mathrm{i}m w^{core}_{rC(A)}\right\}\right] \times \left\{Y_m(k\xi_{n,b}a)\mathrm{J}_m(k\xi_{n,b}r') - \mathrm{J}_m(k\xi_{n,b}a)Y_m(k\xi_{n,b}r')\right\}\,\mathrm{d}r', \tag{2.80}$$

where

$$\xi_{n,b} = \frac{\beta_{n,b}}{k} = \frac{4\Omega_0^2}{g_{n,b}^2} - 1, \quad g_{n,b} = (m\Omega_0 - \omega_n^b). \tag{2.81}$$

The expressions (2.79) and (2.81) suggest singularities at the frequency values $\omega = m\Omega_0$ and $\omega = (m \pm 2)\Omega_0$, corresponding to the limits $k \to 0$ and $k \to \infty$,

https://doi.org/10.1017/jfm.2013.666 Published online by Cambridge University Press

respectively, of the Kelvin dispersion curves. It may be shown that $\omega = (m \pm 2)\Omega_0$ are apparent singularities. The core angular frequency ($\omega = m\Omega_0$), although an essential singularity of the Bessel functions in (2.78), does not contribute for any initial condition that lacks a singular w_θ projection at the edge of the core ($\propto \delta(r-a)$). Thus, equation (2.77) may be written in the following simplified form:

$$C_{nb}(A_{nb}) = -\frac{B_n^b}{g_{n,b}^2(\beta_{n,b}a)^2}\left[\int_0^a \left\{2\Omega_0 \mathrm{i}kr' w_{zC(A)}^{core} + \mathrm{i}g_{n,b}\left\{\frac{\mathrm{d}}{\mathrm{d}r'}(r' w_{\theta C(A)}^{core}) - \mathrm{i}m w_{rC(A)}^{core}\right\}\right\}\frac{\mathrm{J}_m(k\xi_{n,b}r')}{\mathrm{J}_m(k\xi_{n,b}a)}\,\mathrm{d}r' + a\left\{w_{rC(A)}^{core}(a) - \mathrm{i}g_{n,b} w_{\theta C(A)}^{core}(a)\right\}\right]. \quad (2.82)$$

Here, $\boldsymbol{w}_C^{core}(\boldsymbol{x}, t)$ is the initial vorticity in the core, namely $(w_{rC}^{core}(r), w_{\theta C}^{core}(r)) \equiv (w_{r0}(r), w_{\theta 0}(r))\mathcal{H}(a-r)\mathrm{e}^{\mathrm{i}(kz+m\theta)}$, and $\boldsymbol{w}_A^{core}(\boldsymbol{x}, t)$ is the core projection of the Λ_i modes given by

$$w_{rA}^{core}(r) = \int_{a^+}^{\infty} X_{\Lambda_2}(r_f)\hat{w}_r^{\Lambda_2}(r; r_f)\,\mathrm{d}r_f\,\mathcal{H}(a-r), \quad (2.83)$$

$$w_{\theta A}^{core}(r) = \int_{a^+}^{\infty}\left[X_{\Lambda_1}(r_f)w_\theta^{\Lambda_1}(r; r_f) + X_{\Lambda_2}(r_f)w_\theta^{\Lambda_2}(r; r_f)\right]\mathrm{d}r_f\,\mathcal{H}(a-r). \quad (2.84)$$

The modal superposition, (2.74), may now be rewritten as

$$\boldsymbol{w}(\boldsymbol{x}, t) = \int_{a^+}^{\infty}\left[X_{\Lambda_1}(r_f)\hat{\boldsymbol{w}}^{\Lambda_1}(r; r_f) + X_{\Lambda_2}(r_f)\hat{\boldsymbol{w}}^{\Lambda_2}(r; r_f)\right]\mathrm{e}^{\mathrm{i}[kz+m(\theta-\Omega(r_f)t)]}\,\mathrm{d}r_f\mathcal{H}(r-a) + \left\{\sum_{b=\pm1}\sum_{n=1}^{\infty} C_{nb}\hat{\boldsymbol{w}}_{nb}^{Kelvin}(r)\mathrm{e}^{-\mathrm{i}\omega_n^b t} - \int_{a^+}^{\infty}\sum_{b=\pm1}\sum_{n=1}^{\infty}\left[X_{\Lambda_1}(r_f)G_{nb}^{\Lambda_1} + X_{\Lambda_2}(r_f)G_{nb}^{\Lambda_2}\right] \times \hat{\boldsymbol{w}}_{nb}^{Kelvin}(r)(\mathrm{e}^{-\mathrm{i}\omega_n^b t} - \mathrm{e}^{-\mathrm{i}m\Omega(r_f)t})\,\mathrm{d}r_f\right\}\mathrm{e}^{\mathrm{i}(kz+m\theta)}, \quad (2.85)$$

with

$$G_{nb}^{\Lambda_i} = \left[\frac{g_i(a)\mathrm{J}'_m(k\xi_{n,b}a)}{k\xi_{n,b}a\mathrm{J}_m(k\xi_{n,b}a)} - a\frac{g_i'(a)}{(k\xi_{n,b}a)^2} + P_i\right]B_n^b, \quad (2.86)$$

where

$$P_i = \frac{1}{k^2 a}\left\{\frac{2\Omega_0 w_r^{\Lambda_i}(a) + \mathrm{i}(\omega_n^b - m\Omega_0)w_\theta^{\Lambda_i}(a)}{(\omega_n^b - m\Omega_0)^2 - 4\Omega_0^2}\right\}, \quad (2.87)$$

$$g_i(a) = \int_0^a \frac{\pi r'}{2}\left[\frac{2\Omega_0 \mathrm{i}k}{(\omega_n^b - m\Omega_0)^2}w_z^{\Lambda_i} - \frac{\mathrm{i}}{\omega_n^b - m\Omega_0}\left\{\frac{\mathrm{d}}{\mathrm{d}r'}(r w_\theta^{\Lambda_i}) - \mathrm{i}m w_r^{\Lambda_i}\right\}\right] \times \left\{Y_m(k\xi_{n,b}a)\mathrm{J}_m(k\xi_{n,b}r') - \mathrm{J}_m(k\xi_{n,b}a)Y_m(k\xi_{n,b}r')\right\}\mathrm{d}r', \quad (2.88)$$

and $i = 1, 2$. Using the expressions for CS-mode vorticity fields $(w_r^{\Lambda_i}, w_\theta^{\Lambda_i}, w_z^{\Lambda_i})$ from (2.57)–(2.59) and (2.70)–(2.72) one can simplify $G_{nb}^{\Lambda_i}$ to

$$G_{nb}^{\Lambda_i} = \frac{d^{\Lambda_i}}{\mathrm{i}(\omega_n^b - m\Omega)}\frac{M}{(ka)^2\mathrm{K}_m(ka)}\frac{1}{4\Omega_0^2 - g^2}B_n^b, \quad (2.89)$$

where M is defined in (2.55) ($M = 0$ being the Kelvin-mode dispersion relation).

https://doi.org/10.1017/jfm.2013.666 Published online by Cambridge University Press

For any finite t, each of the Λ_i modes in the initial superposition is convected with the local angular velocity $\Omega(r_f)$ in the irrotational exterior, leading to the first term in (2.85) that denotes exterior vorticity. The evolution of the initial core vorticity is entirely characterized by the Kelvin modes, leading to the second term in (2.85). Finally, the third term accounts for the dephasing between the core projection of the Λ_i eigenmodes that is convected with $\Omega(r_f)$, and the Kelvin-mode contributions, characterized by the ω_n^b, that cancel out this core projection at the initial instant. The amplitude coefficients in this term, A_{nb}, have a denumerably infinite sequence of singularities of at $\omega = \omega_n^b$ corresponding to the zeros of A_1 and $A_{\theta\Lambda 2}$. These singularities are the signatures of the secular growth that would occur for singular initial conditions localized at the Kelvin critical radii, and as in the two-dimensional case, may again be interpreted as resonances between the point and continuous spectra. For helical vortex-sheet-type initial conditions, localized at one or more Kelvin radii, resonant interactions between the advected sheet and the corresponding Kelvin mode(s) lead to a quadratic growth in the kinetic energy. In three dimensions, one may also have a localized initial radial vorticity field, in which case there is a further enhancement due to the tilting and stretching of the initial radial vorticity field by the shear in the irrotational exterior. A resonant interaction arises now between a Kelvin mode and a co-rotating exterior azimuthal vorticity field that grows linearly with time, and the resulting kinetic energy grows quartically with time (Roy 2013).

For a point vortex, the spectrum is purely continuous, being made up of the Λ_1 and Λ_2 families, and only the first term in (2.85) remains. Redefining the CS-mode eigenfunctions as $\tilde{\boldsymbol{w}}_{\Lambda_1} \equiv (0,\ -kr_f\delta(r - r_f),\ m\delta(r - r_f))$ and $\tilde{\boldsymbol{w}}_{\Lambda_2} \equiv (-\mathrm{i}mkr_f\delta(r - r_f), kr_f^2\delta'(r - r_f), 0)$, an arbitrary initial condition evolves as the following integral superposition of these convected modes:

$$\boldsymbol{w}(\boldsymbol{x}, t) = \int_0^\infty \left\{X^p_{\Lambda_1}(r_f)\hat{\boldsymbol{w}}_{\Lambda_1}(r; r_f) + X^p_{\Lambda_2}(r_f)\hat{\boldsymbol{w}}_{\Lambda_2}(r; r_f)\right\} \mathrm{e}^{\mathrm{i}[kz+m(\theta-\Omega(r_f)t)]}\,\mathrm{d}r_f, \quad (2.90)$$

where $X^p_{\Lambda_1}(r_f) = -(1/kr_f)(w_{\theta 0}(r_f) - (\mathrm{i}/m)(\mathrm{d}/\mathrm{d}r_f)(rw_{r0}(r_f)))$ and $X^p_{\Lambda_2}(r_f) = (\mathrm{i}/m)(w_{r0}(r_f)/kr_f)$. For an initial condition with $w_{r0} = 0$, the evolution is solely on account of differential convection, and (2.90) reduces to $\boldsymbol{w}(\boldsymbol{x}, t) = \boldsymbol{w}(\boldsymbol{x}, 0)\mathrm{e}^{\mathrm{i}[kz+m(\theta-\Omega(r)t)]}$. With radial vorticity, an integration by parts of $\delta'(r - r_f)$ naturally accounts for the (non-modal) linear growth in w_θ with t, and one obtains $\boldsymbol{w}(\boldsymbol{x}, t) = [w_{r0}(r),\ w_{\theta 0}(r) - 2\Omega(r)tw_{r0}(r),\ w_{z0}(r)]\mathrm{e}^{\mathrm{i}[kz+m(\theta-\Omega(r)t)]}$. The equivalence of (2.90) to the solution of the corresponding IVP is readily established, while that of (2.85) is shown in Roy (2013).

2.2.4. *The axisymmetric eigenmodes*

As already pointed out, axisymmetric Kelvin modes are the eigenfunctions of an ordinary differential equation that conforms to classical Sturm–Liouville theory (Ince 1956; Chandrasekhar 1961) provided only that the base state vorticity is non-zero. However, the spatial separation of the regions of strain and vorticity in the Rankine vortex means that the completeness of these oscillatory modes only extends to axisymmetric column deformations. Radial-vorticity in the region $r > a$ leads to a non-modal (secular) response. This is immediate from the governing (linearized) equation for w_θ which, for axisymmetric perturbations outside the core, takes the form $\partial w_\theta/\partial t = (w_r r)(\partial\Omega/\partial r)$ with $\Omega(r) = \Omega_0 a^2/r^2$; so, an arbitrary $w_r(r)$ for $r > a$ leads to $w_\theta(r, t) \propto t$. Although the modal representation in the earlier section, given by (2.74), was developed for a non-zero m, the evolution of an arbitrary axisymmetric

https://doi.org/10.1017/jfm.2013.666 Published online by Cambridge University Press

vorticity field at the initial instant may nevertheless be obtained by taking the limit $m \to 0$ in (2.74).

For $m = 0$, the dispersion curves for positive and negative ω are symmetric about $\omega = 0$, there no longer being a structureless branch, with the positive and negatives values of ω corresponding to waves that propagate in the downward and upward directions, respectively. We therefore reorder the modes such that $b = -1$, $n = 1$ is now the first mode for both wave families (recall that, for non-zero m, the labelling was asymmetric on account of the structureless branch). Thus, we have $\omega_n^{-1} = -\omega_n^{+1}$, $B_n^{-1} = -B_n^{+1}$, $\hat{w}^{Kelvin}_{r,n(-1)}(r) = -\hat{w}^{Kelvin}_{r,n(+1)}(r)$ and $\hat{w}^{Kelvin}_{\theta,n(-1)}(r) = \hat{w}^{Kelvin}_{\theta,n(+1)}(r)$, and the modal superposition may be expressed in terms of either family. With $\hat{w}^{Kelvin}_{r,n}(r) \equiv \hat{w}^{Kelvin}_{r,n(+1)}(r)$, $\hat{w}^{Kelvin}_{\theta,n}(r) \equiv \hat{w}^{Kelvin}_{\theta,n(+1)}(r)$, $\omega_n \equiv \omega_n^{+1}$ and $B_n \equiv B_n^{+1}$, the radial and azimuthal vorticity components at time t are given by

$$\begin{aligned} w_r(\boldsymbol{x}, t) = {} & w_{r0}(r)\mathcal{H}(r-a)\mathrm{e}^{\mathrm{i}kz} \\ & + 2\sum_{n=1}^{\infty} \frac{B_n}{\omega_n^2(\beta_{n,b}a)^2}\hat{w}^{Kelvin}_{r,n}(r)\left\{2\Omega_0\cos(\omega_n t)F_{n1} - \omega_n \sin(\omega_n t)F_{n2}\right\}\mathrm{e}^{\mathrm{i}kz} \\ & + 2\sum_{n=1}^{\infty} \frac{B_n}{\omega_n}\hat{w}^{Kelvin}_{r,n}(r)\mathrm{e}^{\mathrm{i}kz}\left\{\sin(\omega_n t)\int_a^{\infty} \frac{\mathrm{K}_0(kr')}{(ka)^2\mathrm{K}_0(ka)}\frac{\mathrm{d}}{\mathrm{d}r'}[r'w_{\theta 0}(r')]\,\mathrm{d}r'\right. \\ & \left. + \frac{\cos(\omega_n t) - 1}{\omega_n}\int_a^{\infty} \frac{\mathrm{K}_0(kr')}{(ka)^2\mathrm{K}_0(ka)} 2\Omega w_{r0}(r')\,\mathrm{d}r'\right\}, \end{aligned} \tag{2.91}$$

$$\begin{aligned} w_\theta(\boldsymbol{x}, t) = {} & \{w_{\theta 0}(r) - 2\Omega t w_{r0}(r)\}\,\mathcal{H}(r-a)\mathrm{e}^{\mathrm{i}kz} \\ & - 2\mathrm{i}\sum_{n=1}^{\infty} \frac{B_n}{\omega_n^2(\beta_{n,b}a)^2}\hat{w}^{Kelvin}_{\theta,n}(r)\left\{2\Omega_0\sin(\omega_n t)F_{n1}\right. \\ & \left. + \omega_n\cos(\omega_n t)F_{n2}\right\}\mathrm{e}^{\mathrm{i}kz} + 2\mathrm{i}\sum_{n=1}^{\infty}\frac{B_n}{\omega_n}\hat{w}^{Kelvin}_{\theta,n}(r)\mathrm{e}^{\mathrm{i}kz} \\ & \times \left\{(\cos(\omega_n t) - 1)\int_a^{\infty} \frac{\mathrm{K}_0(kr')}{(ka)^2\mathrm{K}_0(ka)}\frac{\mathrm{d}}{\mathrm{d}r'}[r'w_{\theta 0}(r')]\,\mathrm{d}r'\right. \\ & \left. + \left(t - \frac{\sin(\omega_n t)}{\omega_n}\right)\int_a^{\infty} \frac{\mathrm{K}_0(kr')}{(ka)^2\mathrm{K}_0(ka)} 2\Omega w_{r0}(r')\,\mathrm{d}r'\right\}, \end{aligned} \tag{2.92}$$

where

$$F_{n1} = \int_0^a \mathrm{i}kr' w_{z0}(r')\frac{\mathrm{J}_0(\beta_n r')}{\mathrm{J}_0(\beta_n a)}\,\mathrm{d}r' + a w_{r0}(a), \tag{2.93}$$

$$F_{n2} = \int_0^a \frac{\mathrm{d}}{\mathrm{d}r'}\left(r'w_{\theta 0}(r')\right)\frac{\mathrm{J}_0(\beta_n r')}{\mathrm{J}_0(\beta_n a)}\,\mathrm{d}r' - a w_{\theta 0}(a), \tag{2.94}$$

and the secular term in (2.92) arises due to the initial radial vorticity. With $w_{r0}(r) = 0$, $w_\theta(\boldsymbol{x}, t)$ reduces to the following simpler form:

$$\begin{aligned} w_\theta(\boldsymbol{x}, t) = {} & w_{\theta 0}(r)\mathcal{H}(r-a)\mathrm{e}^{\mathrm{i}kz} - 2\mathrm{i}\sum_{n=1}^{\infty}\frac{B_n}{\omega_n(\beta_{n,b}a)^2}\hat{w}^{Kelvin}_{\theta,n}(r)\cos(\omega_n t)F_{n2}\mathrm{e}^{\mathrm{i}kz} \\ & + 2\mathrm{i}\sum_{n=1}^{\infty}\frac{B_n^{-1}}{\omega_n}\hat{w}^{Kelvin}_{\theta,n}(r)\mathrm{e}^{\mathrm{i}kz}(\cos(\omega_n t) - 1)\int_a^{\infty}\frac{\mathrm{K}_0(kr')}{(ka)^2\mathrm{K}_0(ka)}\frac{\mathrm{d}}{\mathrm{d}r'}\left(r'w_{\theta 0}(r')\right)\mathrm{d}r', \end{aligned} \tag{2.95}$$

https://doi.org/10.1017/jfm.2013.666 Published online by Cambridge University Press

without algebraically growing terms. The response given by (2.95) may be divided into two components: the term proportional to F_{n2} denotes the initial core vorticity that evolves as a discrete summation of sausaging modes; the first and the last terms together denote the response to exterior azimuthal vorticity and involve both a superposition of sausaging modes and a steady contribution. The unsteady part arises due to the vortex column deformation induced by the exterior vorticity. Since this deformation is driven by $u_r|_{r=a} = \int_a^\infty (\mathrm{d}/\mathrm{d}r')[r' w_{\theta 0}(r')]\mathrm{K}_0(kr')\,\mathrm{d}r'$, the restriction $\int_a^\infty (\mathrm{d}/\mathrm{d}r')[r' w_{\theta 0}(r')]\mathrm{K}_0(kr')\,\mathrm{d}r' = 0$, $F_{n2} = 0$, leads to an undeformed vortex column with a quiescent core. The resulting steady vorticity field, $w_{\theta 0}(r)\mathcal{H}(r-a)\mathrm{e}^{\mathrm{i}kz}$, or the associated velocity field given by $u_z = \mathrm{e}^{\mathrm{i}kz}[\mathrm{K}_0(kr)\int_a^r \mathrm{I}_0(kr')(\mathrm{d}/\mathrm{d}r')[r' w_{\theta 0}(r')]\,\mathrm{d}r' + \mathrm{I}_0(kr)\int_r^\infty \mathrm{K}_0(kr')(\mathrm{d}/\mathrm{d}r')[r' w_{\theta 0}(r')]\,\mathrm{d}r']\mathcal{H}(r-a)$ may be regarded as the degenerate zero-frequency axisymmetric eigenmode.

Transient growth has been observed in numerical simulations for axisymmetric perturbations to a smooth (Lamb–Oseen) vorticity profile (Pradeep & Hussain 2006), and would appear to go against the notion of such growth only being associated with non-normal differential operators with an underlying CS (Trefethen *et al.* 1993; Schimd & Henningson 2001). There is no contradiction, however. The self-adjointness of the differential operator for the axisymmetric case is not in the energy norm, and the velocity eigenfunctions are by themselves not mutually orthogonal. Except for rigid-body rotation (Greenspan 1968) the energy associated with any modal superposition will therefore necessarily vary with time, albeit only in an oscillatory fashion in the inviscid limit (there are quantities such as the pseudo-momentum and the pseudo-energy that are indeed time-invariant, and point to additional weighting functions that must be included in an inner product in order to render the eigenfunctions orthogonal (Held 1985)). Physically, the presence of a shear allows for an exchange of energy between the base state and the perturbation, via a Reynolds stress contribution, but this exchange averages out to zero over a time period of oscillation for $m = 0$. For sufficiently slow oscillations, the short-time dynamics of the energy is indistinguishable from transient growth, and is governed by the same physical mechanisms.

The response of a Rankine vortex to an axisymmetric perturbation is a singular limiting case of a smooth profile. In the latter case, the perturbation vorticity field associated with the eigenfunctions extends throughout the domain, allowing for an arbitrary axisymmetric vorticity field evolve as a summation over sausaging modes alone. For a monotonically decaying base-state vorticity profile, the radial length scale of a typical vorticity eigenfunction increases with increasing r with a corresponding decrease in the eigenfunction amplitude. For sufficiently large modal indices, the vorticity eigenfunction for a smooth vortex exhibits a rapid large-amplitude oscillation in the near-field that transitions to a small-amplitude increasingly gentle waviness in the distant, nearly irrotational, exterior. If one now considers an initial distribution of radial vorticity localized in the irrotational region, the required modal superposition will involve eigenfunctions with a projection in this region having a length scale of the same order as that characterizing the initial condition. The near-field projection of each of these eigenfunctions has a much larger amplitude, and is also characterized by a much smaller radial length scale. These near-field contributions from the different eigenfunctions involved in the superposition will cancel out at the initial instant, but the gradual dephasing with time would eventually lead to a large-amplitude fine-scaled oscillatory core response (Pradeep & Hussain 2006). The approach to this large-amplitude oscillation would be via a short-time transient wherein core perturbations are driven by an exterior azimuthal vorticity field that grows linearly

https://doi.org/10.1017/jfm.2013.666 Published online by Cambridge University Press

with time. The deviation from this behaviour due to the eventual decay of the source term (w_r), on account of Coriolis forces, would occur on a much longer time scale of the order of the inverse eigenfrequency. The Rankine limit corresponds to the oscillation time period approaching infinity, leading to a true algebraic growth.

2.2.5. *The relation between the two-dimensional and three-dimensional eigenspectra*

It is easily shown that a Λ_1 mode, characterized by (2.57)–(2.59), approaches the corresponding two-dimensional singular mode given by (2.17) for $k \to 0$ and for a fixed ω (or r_f). On the other hand, a Λ_2 mode, characterized by (2.70)–(2.72), approaches an axial jet localized at the critical radius ($u_z^{\Lambda_2} \propto \delta(r - r_f)$; $u_r^{\Lambda_2}, u_\theta^{\Lambda_2} \to 0$) in the same limit, and plays no role in the evolution of an axial vorticity distribution. Of most relevance is the $k \to 0$ limit along a fixed dispersion curve (that is, with $\omega \sim O(k)$ for $k \to 0$ rather than with ω fixed). The approach of the structureless mode, in this limit, to the two-dimensional Kelvin mode given by (2.18), is well documented (see Leibovich & Ma 1983; Saffman 1992), and we consider only the structured modes with $\omega_n^b \to m\Omega_0$ for $k \to 0$. The frequency intervals between the structured modes, corresponding to the CS, become vanishingly small for $k \to 0$, and it suffices to examine the dispersion curves (discrete modes) alone. Further, consideration of the co-grade family ($b = -1$) is sufficient since the $\beta_{n,b}$ for the co-grade and retro-grade families (excluding the structureless branch, $n = 1$) equal each other in the limit $k \to 0$, and the corresponding eigenfunctions are no longer independent. The co-grade eigenfunctions are given by (2.36)–(2.38). The small k asymptotes for ω_n^b of co-grade modes are given by

$$\omega_n^{-1} = \begin{cases} \dfrac{2ka}{j_n^0}\left[1 - (1 - 2\log ka)\dfrac{(ka)^2}{2j_n^{02}}\right] + \cdots & \text{for } m = 0, \\ m\Omega_0 + \Omega_0 \dfrac{2ka}{j_n^m}\left[1 - \dfrac{(m-2)}{m}\dfrac{(ka)^2}{2j_n^{m2}}\right] + \cdots & \text{for } m \neq 0, \end{cases} \tag{2.96}$$

(see table 1) and the $\beta_{n,b}$ are readily obtained from (2.35) as

$$\lim_{k\to 0}(\beta_{n,-1}a) = j_n^m - \frac{(ka)^2}{mj_n^m}, \tag{2.97}$$

for $m \neq 0$, where j_n^m is the nth zero of $\mathrm{J}_m(x)$ (Watson 1927). The use of (2.97) in (2.36)–(2.38) leads to the following limiting expressions for the vorticity components of the co-grade modes:

$$\lim_{k\to 0} \hat{w}_{z,n(-1)}^{Kelvin} = \frac{mj_n^m}{a(ka)^2}\left[\frac{j_n^m \mathrm{J}_m(j_n^m \frac{r}{a})}{\mathrm{J}'_m(j_n^m)} + a\delta(r-a)\right], \tag{2.98}$$

$$\lim_{k\to 0} \hat{w}_{r,n(-1)}^{Kelvin} = -\frac{\mathrm{i}m^2 j_n^m}{(ka)^2}\left[\frac{\mathrm{J}_m(j_n^m \frac{r}{a})}{r\mathrm{J}'_m(j_n^m)}\right], \tag{2.99}$$

$$\lim_{k\to 0} \hat{w}_{\theta,n(-1)}^{Kelvin} = \frac{mj_n^m}{a(ka)^2}\left[\frac{j_n^m \mathrm{J}'_m(j_n^m \frac{r}{a})}{\mathrm{J}'_m(j_n^m)}\right]. \tag{2.100}$$

The above vorticity field drives an $O(1/k^2)$ flow within the core. The normalization used in the analysis is based on the exterior axial velocity field which therefore remains $O(1)$ with the exterior radial component being $O(1/k)$. Thus, the exterior becomes increasingly quiescent relative to the core for $k \to 0$, suggesting a relation

https://doi.org/10.1017/jfm.2013.666 Published online by Cambridge University Press

	Structureless (ω_d)	Structured
ω_n^b	$(m-1)\Omega_0$	$m\Omega_0 - b\Omega_0 \dfrac{2ka}{j_\eta^m}$
$g_{n,b}$	Ω_0	$b\Omega_0 \dfrac{2ka}{j_\eta^m}$
$\xi_{n,b}$	$\sqrt{3}$	$\dfrac{j_\eta^m}{ka}$
$\beta_{n,b}a$	$\sqrt{3}ka$	$j_\eta^m - \dfrac{(ka)^2}{mj_\eta^m}$
B_n^b	$\dfrac{\mathrm{i}\Omega_0}{2}\dfrac{(ka)^2}{m}$	$\dfrac{2\mathrm{i}b\Omega_0}{m^2}\dfrac{(ka)^5}{(j_\eta^m)^3}$
$\hat{w}_{z,nb}^{Kelvin}(r)$	$\dfrac{2m}{ka}\delta(r-a)$	$-\dfrac{bmj_\eta^m}{a(ka)^2}\left\{\dfrac{j_\eta^m \mathrm{J}_m\left(j_\eta^m \dfrac{r}{a}\right)}{\mathrm{J}'_m(j_\eta^m)} + a\delta(r-a)\right\}$

TABLE 1. The asymptotic forms, for $k \to 0$, of quantities related to the structureless and structured Kelvin modes. Here $\eta = n$ and $n-1$ for the co-grade and structured retrograde modes, respectively.

between the long-wavelength structured modes and the two-dimensional core eigenmodes in § 2.1. Considering the general expression, (2.19), for the latter, and expanding $g(r/a)$ as a Fourier–Bessel series, one obtains

$$\hat{w}_z^{core} = \sum_{n=1}^{\infty} a_n \left[\mathrm{J}_m\left(j_n^m \frac{r}{a}\right) - \delta(r-a) \int_0^a \left(\frac{r'}{a}\right)^{m+1} \mathrm{J}_m\left(j_n^m \frac{r'}{a}\right) \mathrm{d}r' \right], \tag{2.101}$$

where the a_n are the coefficients in the Fourier–Bessel expansion of $g(r/a)$, being defined as

$$a_n = \frac{2}{J_{m+1}^2(j_n^m)} \int_0^1 x g(x) \mathrm{J}_m(j_n^m x)\, \mathrm{d}x. \tag{2.102}$$

Using the relation $x^m = \sum_{p=1}^{\infty} (2\mathrm{J}_m(j_p^m x)/j_p^m \mathrm{J}_{m+1}(j_p^m))$ (see Watson 1927), equation (2.101) takes the form

$$\hat{w}_z^{core} = \sum_{n=1}^{\infty} a_n \left[\mathrm{J}_m\left(j_n^m \tfrac{r}{a}\right) - \delta(r-a) \sum_{p=1}^{\infty} \frac{2}{j_p^m \mathrm{J}_{m+1}(j_p^m)} \int_0^a \tfrac{r'}{a} \mathrm{J}_m\left(j_n^m \tfrac{r'}{a}\right) \mathrm{J}_m\left(j_p^m \tfrac{r'}{a}\right) \mathrm{d}r' \right]. \tag{2.103}$$

Using the orthogonality of the Bessel functions, and that $\mathrm{J}_{m+1}(j_n^m) = -\mathrm{J}'_m(j_n^m)$, the above expression simplifies to

$$\hat{w}_z^{core} = \sum_{n=1}^{\infty} a_n \left[\mathrm{J}_m\left(j_n^m \frac{r}{a}\right) + \frac{a\mathrm{J}'_m(j_n^m)}{j_n^m} \delta(r-a) \right], \tag{2.104}$$

https://doi.org/10.1017/jfm.2013.666 Published online by Cambridge University Press

which may be rewritten as

$$\hat{w}_z^{core} = \sum_{n=1}^{\infty} a'_n \lim_{k\to 0} \hat{w}_{z,n(-1)}^{Kelvin}, \tag{2.105}$$

with $a'_n = a_n(\mathrm{J}'_m(j_n^m)/m)(ka/j_n^m)^2$ and $\hat{w}_{z,n(-1)}^{Kelvin}$ being given by (2.98). Thus, a linear superposition of the axial vorticity components of the structured Kelvin modes, in the limit of vanishing axial wavenumber, maps onto the Fourier–Bessel representation of the general core eigenmode given by (2.19). It is interesting to note that the radial and azimuthal vorticity components of the structured modes are of the same order as the axial vorticity for $k \to 0$ (see (2.98) and (2.99)), but drive a purely axial flow in this limit. Thus, the original three-dimensional velocity field decouples into independent axial ($[\hat{w}_z;\ \hat{u}_r,\ \hat{u}_\theta]$ and transverse ($[\hat{w}_r,\ \hat{w}_\theta;\ \hat{u}_z]$) components in the long-wavelength limit.

The main result obtained thus far is a modal interpretation of the IVP involving a Rankine vortex. Such an interpretation leads to (2.20) and (2.74)–(2.85) for vortical initial conditions in two and three dimensions, respectively. In the final part of this section, we examine the manner in which (2.74) reduces to (2.20) for $k \to 0$, and for this purpose, we consider an initial vorticity field devoid of radial vorticity, $\boldsymbol{w}(\boldsymbol{x}, 0) = [0, -(kr/m)w_{z0}(r), w_{z0}(r)]\mathrm{e}^{\mathrm{i}(kz+m\theta)}$. This is because any additional radial vorticity will only drive an axial flow in the limit $k \to 0$, and this is, in any case, not included in (2.20). Thus, with $X_{\Lambda_1} = -(kr_f^2/mA_1)w_{z0}(r_f)\mathcal{H}(r_f - a)$, $X_{\Lambda_2} = 0$, we consider the $k \to 0$ limit of the arbitrary time expression for axial vorticity:

$$\begin{aligned} w_z(\boldsymbol{x}, t) = &\int_{a^+}^{\infty} X_{\Lambda_1}(r_f)\hat{w}_z^{\Lambda_1}(r; r_f)\mathrm{e}^{\mathrm{i}[kz+m(\theta-\Omega(r_f)t)]}\,\mathrm{d}r_f\mathcal{H}(r-a) \\ &+ \left\{ \sum_{b=\pm1}\sum_{n=1}^{\infty} C_{nb}\hat{w}_{z,nb}^{Kelvin}(r)\mathrm{e}^{-\mathrm{i}\omega_n^b t} \right. \\ &\left. - \int_{a^+}^{\infty} \sum_{b=\pm1}\sum_{n=1}^{\infty} X_{\Lambda_1}(r_f)G_{nb}^{\Lambda_1}\hat{w}_{z,nb}^{Kelvin}(r)(\mathrm{e}^{-\mathrm{i}\omega_n^b t} - \mathrm{e}^{-\mathrm{i}m\Omega(r_f)t})\,\mathrm{d}r_f \right\} \mathrm{e}^{\mathrm{i}(kz+m\theta)}. \end{aligned} \tag{2.106}$$

Further simplification results from using the expression for $G_{nb}^{\Lambda_1}$ from (2.89), and that for C_{nb} from (2.82), leading to

$$\begin{aligned} w_z(\boldsymbol{x}, t) = w_{z0}(r)\mathrm{e}^{\mathrm{i}[kz+m(\theta-\Omega(r)t)]}\mathcal{H}(r-a) + \Bigg[&-\mathrm{i}ka \sum_{b=\pm1}\sum_{n=1}^{\infty} \frac{B_n^b}{g_{n,b}^2(\beta_{n,b}a)^2}\hat{w}_{z,nb}^{Kelvin}(r) \\ &\times \int_0^a w_{z0}(r_f)\left(\frac{r_f}{a}\right)\left\{2\Omega_0\frac{\mathrm{J}_m(\beta_{n,b}r_f)}{\mathrm{J}_m(\beta_{n,b}a)} + \frac{g_{n,b}}{m}\frac{\beta_{n,b}r_f\mathrm{J}'_m(\beta_{n,b}r_f)}{\mathrm{J}_m(\beta_{n,b}a)}\right\}\mathrm{d}r_f\mathrm{e}^{-\mathrm{i}\omega_n^b t} \\ &+ \sum_{b=\pm1}\sum_{n=1}^{\infty} B_n^b\hat{w}_{z,nb}^{Kelvin}(r)\int_{a^+}^{\infty}\left(\frac{r_f}{a}\right)^2\frac{\mathrm{K}'_m(kr_f)}{\mathrm{K}_m(ka)}\frac{w_{z0}(r_f)}{m}\frac{\mathrm{e}^{-\mathrm{i}\omega_n^b t} - \mathrm{e}^{-\mathrm{i}m\Omega(r_f)t}}{\mathrm{i}(\omega_n^b - m\Omega(r_f))}\mathrm{d}r_f\Bigg] \\ &\times \mathrm{e}^{\mathrm{i}(kz+m\theta)}. \end{aligned} \tag{2.107}$$

The summations in the above expression can be split into two contributions, one from the structureless branch ($\omega_1^{+1} \to (m-1)\Omega_0$), and the other from the structured branch ($\omega_n^b \to m\Omega_0$), as $k \to 0$. Table 1 highlights the various asymptotic forms for $k \to 0$ for

https://doi.org/10.1017/jfm.2013.666 Published online by Cambridge University Press

both these cases. Use of these asymptotic results shows that, in the second summation in (2.107), only the structureless branch survives for $k \to 0$, the structured branches being $O(k^2)$ smaller. In contrast, the first summation will have contributions from both structured and structureless branches. The double summation for the structured branches can be reduced to a single summation by noting that $B_n^{-1} = -B_{n+1}^{+1}$ and $\hat{w}^{Kelvin}_{z,n(-1)}(r) = -\hat{w}^{Kelvin}_{z,n+1(+1)}(r) \equiv \hat{w}^{Kelvin}_{z,n}(r)$. On substituting the expressions from table 1, one finds

$$
\begin{aligned}
w_z(\boldsymbol{x}, t) &= w_{z0}(r)\mathrm{e}^{\mathrm{i}[m(\theta-\Omega(r)t)]}\mathcal{H}(r-a) \\
&\quad + \left[\delta(r-a)\mathrm{e}^{-\mathrm{i}\omega_d t}\int_0^a w_{z0}(r_f)\left(\frac{r_f}{a}\right)^{m+1}\mathrm{d}r_f\right. \\
&\quad + 2\sum_{n=1}^{\infty}\frac{1}{m}\left(\frac{ka}{j_n^m}\right)^2\int_0^a w_{z0}(r_f)\frac{r_f}{a}\frac{\mathrm{J}_m\left(j_n^m\frac{r_f}{a}\right)}{\mathrm{J}'_m(j_n^m)}\mathrm{d}r_f \\
&\quad \times\frac{mj_n^m}{a(ka)^2}\left\{\frac{j_n^m\mathrm{J}_m\left(j_n^m\frac{r}{a}\right)}{\mathrm{J}'_m(j_n^m)} + a\delta(r-a)\right\}\mathrm{e}^{-\mathrm{i}m\Omega_0 t} \\
&\quad \left. + \delta(r-a)\int_{a^+}^{\infty}\Omega_0\left(\frac{a}{r_f}\right)^{m-1}w_{z0}(r_f)\frac{\mathrm{e}^{-\mathrm{i}m\Omega(r_f)t}-\mathrm{e}^{-\mathrm{i}\omega_n t}}{(\omega_d - m\Omega(r_f))}\mathrm{d}r_f\right]\mathrm{e}^{\mathrm{i}m\theta}, \\
&= w_{z0}(r)\mathrm{e}^{\mathrm{i}[m(\theta-\Omega(r)t)]}\mathcal{H}(r-a) + \hat{w}_z^{core}\mathrm{e}^{\mathrm{i}m[\theta-\Omega_0 t]} \\
&\quad + \delta(r-a)\left[\mathrm{e}^{-\mathrm{i}\omega_d t}\int_0^a w_{z0}(r_f)\left(\frac{r_f}{a}\right)^{m+1}\mathrm{d}r_f\right. \\
&\quad \left. + \int_{a^+}^{\infty}\Omega_0\left(\frac{a}{r_f}\right)^{m-1}w_{z0}(r_f)\frac{\mathrm{e}^{-\mathrm{i}m\Omega(r_f)t}-\mathrm{e}^{-\mathrm{i}\omega_d t}}{(\omega_d - m\Omega(r_f))}\mathrm{d}r_f\right]\mathrm{e}^{\mathrm{i}m\theta}, \qquad (2.108)
\end{aligned}
$$

which leads to the two-dimensional modal superposition given in (2.20)–(2.21). Here, the reduction of the summation to $\hat{w}_z^{core}$ has been done using (2.104).

3. The singular eigenspectrum of a smooth vortex

The analysis for the non-axisymmetric modes in § 2 has been restricted to a Rankine vortex. The natural question is as to how the results, including the modal representations (2.20) and (2.74), generalize to a smooth vorticity profile. For two-dimensional perturbations, this is answered in § 3.1 below by adapting the analysis of Balmforth & Morrison (1995), developed originally for homogeneous nonlinear parallel flows, to the vortex case. The nature of the regular singular point in the governing linearized equations for two-dimensional perturbations remains the same in both cases, with DZ for the vortex column playing the role of U'' in a parallel flow. The Frobenius indices associated with the singular point are integers (0 and 1), and one of the radial velocity eigenfunctions must, for non-zero DZ, have a logarithmic branch point at the critical radius (r_f). As a result, the vorticity eigenfunctions of the two-dimensional CS modes associated with a smooth vortex include both a delta-function singularity and a non-local PV singularity, proportional to DZ, arising from the aforementioned logarithmic term. Physically, the latter term arises due to the radial velocity perturbation acting to convect the inhomogeneous

https://doi.org/10.1017/jfm.2013.666 Published online by Cambridge University Press

base-state vorticity field to the to the vicinity of the critical radius. This contribution is evidently absent for a Rankine vortex since DZ is zero for $r > a$.

The three-dimensional spectrum of a smooth vortex bears an analogy to stratified parallel flows, and one may indeed define a Richardson number associated with a perturbation of a given axial wavenumber involving the local vorticity and vorticity gradient (Le Dizès 2004, see also § 4). Physically, the Coriolis forces in the case of a smooth vortex play the same role as buoyancy forces in the stratified context. As a result, a rigidly rotating incompressible fluid supports transverse waves with the same dispersive characteristics as the internal gravity waves supported by an otherwise quiescent stably stratified fluid. In § 3.2, we focus on the structure of the smooth-vortex three-dimensional CS modes in the vicinity of r_f. The differences in the nature of the singularity in the three-dimensional vorticity eigenfunctions relative to those of a Rankine vortex (where both two-dimensional and three-dimensional vorticity eigenfunctions have only localized generalized function singularities), and those for two-dimensional perturbations (where the vorticity eigenfunctions have an additional non-local PV-singular term) that arise due to the singular point of the Howard–Gupta equation now having fractional Frobenius exponents are highlighted. In particular, it is shown, based on the known solution for stratified Couette flow (Engevik 1971), that the singular terms in the vorticity eigenfunctions of the three-dimensional CS modes must be interpreted in the sense of a principal finite part (Lighthill 1958; Gel'fand & Shilov 1964). This in turn implies that the forcing terms localized at the critical radius that must appear in the governing equation for the three-dimensional CS modes (that is identical in form to the Taylor–Goldstein (TG) equation in the vicinity of r_f), are not the delta function and its derivative as for the Rankine vortex (see (2.41) and (2.62) for the Λ_1 and Λ_2 families). Instead, the forcing terms correspond to genuinely non-summable singularities and are, therefore, not even generalized functions (Gel'fand & Shilov 1964). They may, symbolically, be likened to the product of a delta function and an inverse algebraic power that depends on the Frobenius exponent.

3.1. *Two-dimensional singular eigenspectrum*

With (2.1) governing the evolution of two-dimensional perturbations, the axial vorticity eigenfunction for the CS mode associated with a smooth vortex may be written as (Van Kampen 1955; Case 1959; Balmforth & Morrison 1995)

$$\hat{w}_z^{CSM}(r;\, r_f) = A_1(r_f)\delta(r - r_f) - \mathcal{P}\frac{1}{r}\frac{\mathrm{DZ}(r)\hat{\psi}^{CSM}(r;\, r_f)}{\Omega(r) - \Omega(r_f)}, \tag{3.1}$$

where the symbol $\mathcal{P}$ implies that the second term in (3.1), integrated over an interval that includes r_f, must be interpreted in the sense of a Cauchy PV. Thus, the two-dimensional CS modes associated with a smooth vortex have, in addition to a delta-function singularity, a non-local PV-singular contribution proportional to DZ. This latter singularity arises because for any DZ, however small, in a reference frame that rotates with $\Omega(r_f)$, the azimuthal convection of $\hat{w}_z$ becomes asymptotically weak close to r_f, compared with the finite rate at which the base-state vorticity field is convected towards the critical radius. The PV interpretation may be understood as a self-consistency requirement. That is, a PV interpretation of the integral in (3.1) ensures that the radial velocity induced at the critical radius remains finite despite the non-integrable singularity in the vorticity field, this being consistent with the

https://doi.org/10.1017/jfm.2013.666 Published online by Cambridge University Press

finite rate of induction in the original argument (Roy & Subramanian 2012). The perturbation streamfunction, $\hat{\psi}^{CSM}$, in (3.1) satisfies

$$\left(r\mathrm{D}^2 + \mathrm{D} - \frac{m^2}{r}\right)\hat{\psi}^{CSM}(r;\, r_f) = -r\hat{w}_z^{CSM}(r;\, r_f). \tag{3.2}$$

A normalization that is particularly convenient is one based on the total (axial) vorticity in a CS mode. As shown by Balmforth & Morrison (1995), with $\int_0^\infty \hat{w}_z^{CSM}(r';\, r_f)\,\mathrm{d}r' = 1$, equation (3.1) takes the form

$$\hat{w}_z^{CSM}(r;\, r_f) = \left\{1 + \mathcal{P}\int_0^\infty \frac{1}{r'}\frac{\mathrm{DZ}(r')\hat{\psi}^{CSM}(r';\, r_f)}{\Omega(r') - \Omega(r_f)}\,\mathrm{d}r'\right\}\delta(r - r_f)$$
$$- \mathcal{P}\frac{1}{r}\frac{\mathrm{DZ}(r)\hat{\psi}^{CSM}(r;\, r_f)}{\Omega(r) - \Omega(r_f)}. \tag{3.3}$$

The streamfunction $\hat{\psi}^{CSM}$ then satisfies an inhomogeneous Fredholm integral equation of the second kind, rather than a Cauchy integral equation with a PV-singular kernel, and is readily obtained by numerical means. Using (3.2) and (3.3), it is easily shown that

$$\hat{\psi}^{CSM}(r;\, r_f) - \int_0^\infty \mathcal{M}(r,\, r';\, r_f)\hat{\psi}^{CSM}(r';\, r_f)\,\mathrm{d}r' = -r_f\mathcal{G}(r;\, r_f), \tag{3.4}$$

where $\mathcal{G}(r;\, r_f) = -(1/2m)(r_</r_>)^m$, with $r_<$ ($r_>$) denoting the smaller (larger) of r and r_f, is the Green's function of (3.2), and the regularized kernel, $\mathcal{M}(r,\, r';\, r_f)$, is given by

$$\mathcal{M}(r,\, r';\, r_f) = \frac{\mathrm{DZ}(r')}{r'}\left\{\frac{r'\mathcal{G}(r;\, r') - r_f\mathcal{G}(r;\, r_f)}{\Omega(r') - \Omega(r_f)}\right\}. \tag{3.5}$$

An artifact of the above normalization is that the CS modes that are homogeneous solutions of (3.4) must be handled separately (see Balmforth & Morrison 1995 for details). Such solutions are expected for smooth vortices, at least those that closely approximate the Rankine profile, and correspond to the CS mode having zero net axial vorticity in $r \in [0, \infty)$ for any θ. For the Rankine vortex, this would be equivalent to the sum of the vortex sheet amplitudes at $r = a$ and $r = r_f$ being zero; using (2.15) and (2.17), this implies $m(a/r_f)^2 + (a/r_f)^{(m-1)} = (m-1)$, which has a unique solution in (a, ∞) for any $m > 1$. It must be emphasized that the homogeneous solutions of the Fredholm equation are generic CS modes and do not have any particular physical significance. However, the homogeneous solutions of the original Cauchy integral equation (that is, those with $A_1 = 0$) correspond to singular free oscillations. This is in contrast to the Kelvin mode which is the regular free oscillation of the deformed Rankine vortex. Such singular oscillations (one for each $m \geqslant 2$) are consistent with a nonlinear critical layer at the particular r_f, of a vanishingly small thickness that supports a zero phase jump across it, and are therefore the vortex analogues of the Benney–Bergeron–Davis modes for parallel flows (Benney & Bergeron 1969; Davis 1969).

The evolution of an initial axial vorticity distribution of the form $w_{z0}(r)\mathrm{e}^{\mathrm{i}m\theta}$, as an integral superposition of the two-dimensional CS modes (and the singular discrete mode), is given by

$$w_z(r,\, \theta,\, t) = \int_0^\infty \Pi(r_f)\hat{w}_z^{CSM}(r;\, r_f)\mathrm{e}^{\mathrm{i}m(\theta - \Omega(r_f)t)}\,\mathrm{d}r_f, \tag{3.6}$$

https://doi.org/10.1017/jfm.2013.666 Published online by Cambridge University Press

where the amplitude distribution of the CS modes is given by

$$\Pi(r_f) = \frac{1}{(\epsilon_R^2+\epsilon_L^2)}\left\{\epsilon_R w_{z0}(r_f) - \frac{\epsilon_L}{\pi}\frac{\Omega'(r_f)}{\hat{\psi}^{CSM}(r_f;\, r_f)}\mathcal{P}\int_0^\infty \frac{w_{z0}(r')\hat{\psi}^{CSM}(r_f;\, r')}{\Omega(r')-\Omega(r_f)}\,\mathrm{d}r'\right\}; \tag{3.7}$$

$$\epsilon_R = 1+\mathcal{P}\int_0^\infty \frac{1}{r'}\frac{\mathrm{DZ}(r')\hat{\psi}^{CSM}(r';\, r_f)}{\Omega(r')-\Omega(r_f)}\,\mathrm{d}r'; \quad \epsilon_L = \pi\frac{\mathrm{DZ}(r_f)\hat{\psi}^{CSM}(r_f;\, r_f)}{r_f\Omega'(r_f)}. \tag{3.8}$$

The above modal representation is obtained from the solution of a Riemann–Hilbert problem in the complex plane (Case 1959; Gakhov 1990), and is the required extension of (2.20) to a smooth vorticity profile. Note that the representation is only known in terms of the singular eigenfunctions, and for a general smooth vorticity profile, the latter must be obtained from the numerical solution of (3.4). The analysis leading to (3.6) closely parallels that of Balmforth & Morrison (1995) for a parallel shearing flow, and is therefore relegated to appendix B.

As pointed out in the introduction, unlike the Rankine vortex, the large-t analysis of (3.6) reveals an intermediate asymptotic regime, with an exponential decaying velocity perturbation associated with a quasi-mode, that precedes the eventual (and expected) algebraic decay for still longer times arising from the dephasing of the CS-mode superposition. For smooth vortices approaching the Rankine profile, the decay rate (Landau damping) in this exponential regime is well known (see, for instance Briggs *et al.* 1970; Schecter *et al.* 2000) and may be obtained from (3.6) by identifying the zeros of $\epsilon_R^2+\epsilon_L^2$ in the complex plane. The integration contour (over $r\epsilon[0,\infty)$) in the PV-singular integral in (3.8) is now interpreted as passing below the critical radius of the quasi-mode in the complex plane. Regarding the contour as the real axis would lead to no zeros for a monotonically decaying vorticity profile, consistent with the Rayleigh criterion. Writing $\epsilon_R^2+\epsilon_L^2 = \epsilon^+\epsilon^-$ (see appendix B), with

$$\epsilon^\pm = 1+\mathcal{P}\int_0^\infty \frac{1}{r'}\frac{\mathrm{DZ}(r')\hat{\psi}^{CSM}(r';\, r)}{\Omega(r')-\Omega(r)}\,\mathrm{d}r' \pm \pi\mathrm{i}\frac{\mathrm{DZ}(r)\hat{\psi}^{CSM}(r;\, r)}{r\Omega'(r)}, \tag{3.9}$$

and anticipating a decaying mode, the zeros must correspond to those of ϵ^-. Further, assuming the critical radius of the quasi-mode (r_Q) to be close to the real axis with the real part being r_{Qr} ($r_{Qr}\to r_{fk}$ for $\mathrm{DZ}\to -2\Omega_0\delta(r-a)$), one may write $\Omega(r_Q)\approx \Omega_{r_{Qr}} - \mathrm{i}\Omega_i$ with $\Omega_i \ll \Omega_{r_{Qr}}$ and $r_{Qi}\approx \Omega_i/\Omega'(r_{fk})$. The relation $\epsilon^-(r_Q)=0$ takes the approximate form:

$$1+\int_0^\infty \frac{1}{r'}\frac{\mathrm{DZ}(r')\hat{\psi}^{CSM}(r';\, r_{Qr})}{\Omega(r')-\Omega(r_{Qr})+\mathrm{i}\Omega_i}\,\mathrm{d}r' - \pi\mathrm{i}\frac{\mathrm{DZ}(r)\hat{\psi}^{CSM}(r_{Qr};\, r_{Qr})}{r_{Qr}\Omega'(r_{Qr})} = 0, \tag{3.10}$$

where, for non-zero Ω_i, the integral in (3.10) does not need a PV interpretation. Expanding for small Ω_i, one obtains

$$1+\mathcal{P}\int_0^\infty \frac{1}{r'}\frac{\mathrm{DZ}(r')\hat{\psi}^{CSM}(r';\, r_{Qr})}{\Omega(r')-\Omega(r_{Qr})}\,\mathrm{d}r' \approx 0, \tag{3.11}$$

from the real part with the resulting r_{Qr} determining the angular frequency of the quasi-mode. Using the approximate form, $\mathrm{DZ}\approx -2\Omega_0\delta(r-a)$, for a Rankine vortex,

https://doi.org/10.1017/jfm.2013.666 Published online by Cambridge University Press

one obtains $r_{Qr} = r_{fk}$ and $\Omega_{r_{Qr}} \approx ((m-1)/m)\,\Omega_0$. The imaginary part of (3.10) leads to

$$\Omega_i \approx -\pi \frac{\mathrm{DZ}(r_{Qr})\hat{\psi}^{CSM}(r_{Qr}; r_{Qr})}{r_{Qr}\Omega'(r_{Qr})} \left[\mathcal{P} \int_0^\infty \frac{\mathrm{DZ}(r')\mathrm{D}\hat{\psi}^{CSM}(r'; r_{Qr})}{r'\Omega'(r_{Qr})} \frac{1}{(\Omega(r') - \Omega(r_{Qr}))^2}\,\mathrm{d}r' \right.$$
$$\left. + \text{Pf.} \int_0^\infty \frac{1}{r'} \frac{\mathrm{DZ}(r')\hat{\psi}^{CSM}(r'; r_{Qr})}{(\Omega(r') - \Omega(r_{Qr}))^2}\,\mathrm{d}r' \right]^{-1}, \tag{3.12}$$

which characterizes the decay rate of the quasi-mode; here Pf. denotes the principal-finite part of the singular integral (Gel'fand & Shilov 1964). Again, using the expressions for DZ, $\hat{\psi}^{CSM}$ and $\mathrm{D}\hat{\psi}^{CSM}$ for a Rankine profile, one obtains

$$\Omega_i \approx -\frac{\pi a}{4m^2}\mathrm{DZ}(r_{Qr}) \left(\frac{m-1}{m}\right)^{m-3/2}. \tag{3.13}$$

Although the expression for the damping rate originally given by Briggs *et al.* (1970) is correct, there appears to be an error in the expressions given in Balmforth & Morrison (1995) (the analogue of (3.13) for parallel flows), and in Le Dizès (2000) which has the exponent in (3.13) as $(m-1)$ rather than $(m-3/2)$.

3.2. *Three-dimensional singular eigenspectrum*

The three-dimensional eigenvalue problem for a smooth vorticity profile is, of course, analytically intractable, and we therefore analyse the three-dimensional smooth-vortex CS modes only in the vicinity of r_f. This is the region of interest since the Rankine vortex is a singular limit, and the approach of the vorticity eigenfunctions of a smooth (Rankine-like) profile to the corresponding Rankine eigenfunctions is non-uniform, there always being an arbitrarily large difference between the two sufficiently close to r_f. The Howard–Gupta (HG) equation for $\hat{u}_r$, rather than (2.23) for $\hat{u}_z$, is suited to such a local analysis, and is given by (Howard & Gupta 1962)

$$\left(\frac{S}{r}(r\hat{u}_r)'\right)' - \hat{u}_r + \left(\frac{SZ}{r^2}\right)' \frac{mr\hat{u}_r}{\Sigma} + \frac{2k^2SZ\Omega}{\Sigma^2}\hat{u}_r = 0, \tag{3.14}$$

with $S = r^2/(m^2 + (kr)^2)$ and $\Sigma = \omega - m\Omega$. For r close to r_f, equation (3.14) reduces to

$$\hat{u}_r'' + \frac{2k^2Z(r_f)\Omega(r_f)}{[m\Omega'(r_f)]^2} \frac{\hat{u}_r}{(r - r_f)^2} = 0 \tag{3.15}$$

which is similar to the well-known TG equation that governs the inviscid evolution of infinitesimal disturbances in stratified shear flows (Turner 1973). The TG equation for stratified Couette flow, with $U(y) \propto y\mathbf{1}_x$, is given by

$$\left(\frac{\mathrm{d}^2}{\mathrm{d}y^2} - k^2\right)\hat{u}_y + Ri\frac{\hat{u}_y}{(y - y_c)^2} = 0, \tag{3.16}$$

for the normal velocity component of a single Fourier mode of the form $u_y = \hat{u}_y(y)\mathrm{e}^{\mathrm{i}k(x-ct)}$, with y_c being the critical level at which the wave speed (c) equals that of the shear flow. Here, Ri is the Richardson number, a dimensionless measure

https://doi.org/10.1017/jfm.2013.666 Published online by Cambridge University Press

of competing buoyancy and inertial forces. Notwithstanding the additional term proportional to $k^2 u_y$ which does not affect the nature of the singular point (as characterized by the Frobenius exponents; see (3.17)), the similarity between (3.15) and (3.16) is evident. One may therefore define $Ri_v = 2k^2 Z(r_f)\Omega(r_f)/[m\Omega'(r_f)]^2$ as a local Richardson number for a smooth vortex (Le Dizès 2004), and the singularity of the three-dimensional CS modes must be analogous to those of the CS modes in stratified shear flows. The solution of (3.15) in the vicinity of r_f may then be written as a generalized Frobenius expansion:

$$\begin{aligned}\hat{u}_r = {} & A_0|r-r_f|^{1/2-\nu}\{1+\alpha_1(r-r_f)+\alpha_2(r-r_f)^2\} \\ & + B_0|r-r_f|^{1/2+\nu}\{1+\beta_1(r-r_f)+\beta_2(r-r_f)^2\},\end{aligned} \tag{3.17}$$

where

$$A_0 = A_0^- H(r_f - r) + A_0^+ H(r - r_f)], \tag{3.18}$$

$$B_0 = B_0^- H(r_f - r) + B_0^+ H(r - r_f)], \tag{3.19}$$

and $\nu = \sqrt{1/4 - Ri_v}$; the series coefficients α_i and β_i may be determined in the usual manner. From (3.17), it is seen that for any finite $Ri_v(r_f)$ however small, the constraining effects of Coriolis forces become dominant at $r = r_f$, and the radial velocity associated with any three-dimensional singular mode must therefore be zero at the critical radius. An appropriate choice of the constants $A_0^{\pm}$ and $B_0^{\pm}$ should lead to the analogue of the Λ_1 and Λ_2 CS-mode families. Since the Frobenius exponents $(1/2+\nu)$ and $(1/2-\nu)$ approach 1 and 0 in the Rankine limit ($Ri_v \to 0$ due to $Z \to 0$ with k and r_f fixed, the latter at a point in the irrotational exterior). The radial velocity eigenfunctions corresponding to the Λ_1 and Λ_2 families are given by

$$\begin{aligned}\hat{u}_r^{\Lambda_1}(r;r_f) &= A_0|r-r_f|^{1/2-\nu} + B_0^-|r-r_f|^{1/2+\nu} \quad r<r_f, \\ &= A_0|r-r_f|^{1/2-\nu} + B_0^+|r-r_f|^{1/2+\nu} \quad r>r_f,\end{aligned} \tag{3.20}$$

$$\begin{aligned}\hat{u}_r^{\Lambda_2}(r;r_f) &= A_0^-|r-r_f|^{1/2-\nu} + B_0|r-r_f|^{1/2+\nu} \quad r<r_f, \\ &= A_0^+|r-r_f|^{1/2-\nu} - B_0|r-r_f|^{1/2+\nu} \quad r>r_f,\end{aligned} \tag{3.21}$$

for r close to r_f. The connection with the Λ_i families of the Rankine vortex may be seen by expanding the Frobenius forms above for small Ri_v (Maslowe & Nigam 2008), whence one obtains the corresponding forms for the homogeneous case except in a region of $O(\mathrm{e}^{-1/Ri_v})$ around r_f wherein the expansion breaks down owing to the singular nature of the Rankine limit. Consistent with the Rankine analysis in § 2.2, this outer solution has an apparent kink at $r = r_f$ for the choice of constants ($A_0^- = A_0^+ = A_0$) in (3.20) and an apparent step discontinuity for the choice ($B_0^- = -B_0^+ = B_0$) in (3.21). Using $\hat{u}_\theta = \mathrm{i}k^2 S\left(-(Z/\Sigma)u_r + (m/(kr)^2)(ru_r)'\right)$, and the continuity equation, one obtains the remaining velocity components as

$$\begin{aligned}\hat{u}_\theta^{\Lambda_i}(r;r_f) = {} & R_1^{\Lambda_i}|r-r_f|^{-1/2-\nu} + R_2^{\Lambda_i}|r-r_f|^{-1/2+\nu} + R_3^{\Lambda_i}|r-r_f|^{1/2-\nu} \\ & + R_4^{\Lambda_i}|r-r_f|^{1/2+\nu} + R_5^{\Lambda_i}|r-r_f|^{3/2-\nu} + O(|r-r_f|^{3/2+\nu}),\end{aligned} \tag{3.22}$$

$$\begin{aligned}\hat{u}_z^{\Lambda_i}(r;r_f) = {} & Q_1^{\Lambda_i}|r-r_f|^{-1/2-\nu} + Q_2^{\Lambda_i}|r-r_f|^{-1/2+\nu} + Q_3^{\Lambda_i}|r-r_f|^{1/2-\nu} \\ & + Q_4^{\Lambda_i}|r-r_f|^{1/2+\nu} + Q_5^{\Lambda_i}|r-r_f|^{3/2-\nu} + O(|r-r_f|^{3/2+\nu}),\end{aligned} \tag{3.23}$$

where the coefficients $R_1^{\Lambda_i} - R_5^{\Lambda_i}$, $Q_1^{\Lambda_i} - Q_5^{\Lambda_i}$ are listed in appendix C. In obtaining (3.22) and (3.23), we have used $|x|^\alpha \delta(x) = 0$ for any $\alpha > 0$. Strictly speaking,

https://doi.org/10.1017/jfm.2013.666 Published online by Cambridge University Press

the product of the two generalized functions $|x|^{\alpha}$ and $\delta(x)$ is not a generalized function and, thus, $x^{\alpha}\delta(x)$, for fractional α, cannot be regarded as a generalized zero. The interpretation needed is discussed below after the expressions for the vorticity eigenfunctions.

Given the local forms (3.20)–(3.23) for the Λ_1 and Λ_2 families, it is now of interest to determine the singular forcing that must appear in the HG equation in each case. Note that, in doing so, we are proceeding for the smooth vortex in a manner opposite to that for the Rankine vortex. This is because the nature of the singular structures in the latter case, a vortex sheet for the Λ_1 family (see (2.41) in § 2.2.1) and a localized axial jet for the Λ_2 family (see (2.62) in § 2.2.2), was clear from physical considerations associated with a shape-preserving inviscid normal mode. From the mathematical standpoint, the required singular forcings were the usual generalized functions. In contrast, a vortex sheet (or any derivative singular structures thereof) cannot constitute the singular forcing for a smooth vortex since such a structure leads to a non-zero radial velocity at r_f, and is thereby inconsistent with the aforementioned Frobenius forms. To arrive at the singular forcing for a smooth-vortex CS mode, we first note that the dominant contribution to the axial vorticity eigenfunction, for r close to r_f, is proportional to $\mathrm{d}^2\hat{u}_r/\mathrm{d}r^2$, implying that the vorticity eigenfunctions associated with the Λ_1 or Λ_2 analogues of a smooth vortex are, on the one hand, non-local due to the distributed 'baroclinic' source of vorticity, and on the other hand, have a non-integrable singularity at r_f. A non-integrable singularity at the critical radius is, however, inconsistent with the requirements of a modal superposition which involves an integration over the CS, with appropriately weighted amplitudes, over the entire domain. It was first shown by Engevik (1971), in the context of Couette flow with a uniform (stable) stratification, that a sensible modal superposition emerges only when the divergent integrals involving the vorticity eigenfunctions are interpreted in the sense of a Pf. part (Gel'fand & Shilov 1964). Based on the local analogy with the stratified flow CS modes, the CS modes, given by (3.20) and (3.21), must therefore be regarded as generalized functions requiring a Pf. interpretation; the Pf. interpretation also implies that the singular forcing cannot be a generalized function. The vorticity eigenfunctions corresponding to (3.20) and (3.21) may now be written as

$$\hat{w}_z^{\Lambda_1}(r;\, r_f) = \mathrm{Pf.}\frac{\mathrm{i}S_c m(B_0^- + B_0^+)}{r_f}\left\{-\epsilon|r-r_f|^{-\epsilon-1}\right\} + \cdots, \tag{3.24}$$

$$\hat{w}_r^{\Lambda_1}(r;\, r_f) = -\mathrm{Pf.}\,\frac{mA_0}{kr_f}\epsilon\,\mathrm{sgn}(r-r_f)|r-r_f|^{\epsilon-1} + \cdots, \tag{3.25}$$

$$\hat{w}_\theta^{\Lambda_1}(r;\, r_f) = -\mathrm{Pf.}\,\mathrm{i}kS_c(B_0^- + B_0^+)\left\{-\epsilon|r-r_f|^{-\epsilon-1}\right\} + \cdots, \tag{3.26}$$

and fontsize1012

$$\hat{w}_z^{\Lambda_2}(r;\, r_f) = \mathrm{Pf.}\frac{\mathrm{i}mS_c}{r_f}\left(\frac{A_0^- - A_0^+}{2}\right)\left(\alpha_1 + \frac{1}{r_f}\right)\left\{-\frac{\epsilon}{2}|r-r_f|^{-\epsilon-1} - \frac{\epsilon}{2}|r-r_f|^{\epsilon-1}\right\} + \cdots, \tag{3.27}$$

$$\hat{w}_r^{\Lambda_2}(r;\, r_f) = \mathrm{Pf.}\frac{m}{kr_f}\left(\frac{A_0^- - A_0^+}{2}\right)\epsilon|r-r_f|^{\epsilon-1} + \cdots, \tag{3.28}$$

$$\hat{w}_\theta^{\Lambda_2}(r;\, r_f) = -\mathrm{Pf.}\frac{\mathrm{i}}{k}\left(\frac{A_0^- - A_0^+}{2}\right)\epsilon\,\mathrm{sgn}(r-r_f)|r-r_f|^{\epsilon-2} + \cdots, \tag{3.29}$$

https://doi.org/10.1017/jfm.2013.666 Published online by Cambridge University Press

where we have only included the most singular contributions. From the theory of generalized functions (Lighthill 1958; Gel'fand & Shilov 1964), it is known that

$$\lim_{\lambda\to -2k-1}\frac{|x|^{\lambda}}{\Gamma\left((\lambda+1)/2\right)}=\frac{(-1)^k k!}{(2k)!}\delta^{(2k)}(x), \tag{3.30}$$

$$\lim_{\lambda\to -2k}\frac{|x|^{\lambda}\mathrm{sgn}(x)}{\Gamma\left((\lambda+2)/2\right)}=\frac{(-1)^k (k-1)!}{(2k-1)!}\delta^{(2k-1)}(x), \tag{3.31}$$

and zero otherwise. Using these, one obtains from (3.24)–(3.26), $\lim_{\nu\to 1/2}\hat{w}_z^{\Lambda_1}=\mathrm{i}S_c m(B_0^- + B_0^+)/r_f\delta(r-r_f)$, $\lim_{\nu\to 1/2}\hat{w}_r^{\Lambda_1}=0$, $\lim_{\nu\to 1/2}\hat{w}_\theta^{\Lambda_1}=-\mathrm{i}kS_c(B_0^- + B_0^+)\delta(r-r_f)$; and from (3.27)–(3.29) $\lim_{\nu\to 1/2}\hat{w}_z^{\Lambda_2}=0$, $\lim_{\nu\to 1/2}\hat{w}_r^{\Lambda_2}=m/(kr_f)(A_0^- - A_0^+)\delta(r-r_f)$, $\lim_{\nu\to 1/2}\hat{w}_\theta^{\Lambda_2}=\mathrm{i}/k(A_0^- - A_0^+)\delta'(r-r_f)$. All regular contributions, not explicitly included in (3.24)–(3.29) vanish in this limit. This then ensures consistency with the singular form of the Rankine CS modes in the irrotational exterior.

The nature of the singular forcing leading to the three-dimensional smooth-vortex CS modes is an issue that needs elaboration. For shearing flows, the discrete spectrum is almost always finite (Drazin & Reid 1981), and it is thus routinely mentioned (for instance, see Maslowe (1986)) that the additional CS modes, needed for purposes of completeness, arise from including generalized function forcings in the governing equation for linearized perturbations. This is true only for homogeneous shearing flows, and for the two-dimensional modes in the vortex case as seen in § 2.1. In these cases, the forcings are indeed proportional to the delta function and/or its derivatives. The Pf. interpretation needed for the stratified flow and the three-dimensional smooth-vortex CS modes implies, however, that the underlying singular forcing is no longer a generalized function. This may be seen from (3.15) in which such a forcing is precisely what needs to be subtracted from the baroclinic source term to remove the non-integrable singularity in the vorticity field. Loosely speaking, the Pf. interpretation implies that the source term in (3.15) not be $Ri_v u_r/(r-r_f)^2$, but instead be $Ri_v[u_r/(r-r_f)^2 - F_1\delta(r-r_f)/(r-r_f)^{1/2-\nu} - F_2\delta(r-r_f)/(r-r_f)^{1/2+\nu}]$, with the F_i being related to the coefficients of the Frobenius forms in u_r. In turn, this points to a forced HG equation of the form:

$$\left(\frac{S}{r}(r\hat{u}_r)'\right)' - \hat{u}_r + \left(\frac{SZ}{r^2}\right)'\frac{mr\hat{u}_r}{\Sigma} + \frac{2k^2SZ\Omega}{\Sigma^2}\hat{u}_r = Ri_v\left[\frac{u_r}{(r-r_f)^2} - F_1\frac{\delta(r-r_f)}{(r-r_f)^{1/2-\nu}} - F_2\frac{\delta(r-r_f)}{(r-r_f)^{1/2+\nu}}\right], \tag{3.32}$$

for the three-dimensional CS modes, with S being defined as before. Now, the mathematical theory constructs a linear space of generalized functions, and within this framework, the product of an infinitely differentiable function with a generalized function is allowed, but the product of two generalized functions does not in general have an unambiguous interpretation (Gel'fand & Shilov 1964). In other words, the terms proportional to $\delta(r-r_f)$ on the right-hand side in (3.32) are not generalized functions for non-integral $(1/2 \pm \nu)$. In the Rankine limit ($Ri_v \to 0$, $\nu \to 1/2$), however, the non-generalized function forcings become vanishingly small while the baroclinic source term on the left-hand side reduces to the generalized function forcing that led to the Λ_1 and Λ_2 families in §§ 2.2.1 and 2.2.2. This crucial difference in the nature of the singular forcing, at least as far as its mathematical interpretation is concerned, is often not recognized. This fact does not find explicit mention in the

https://doi.org/10.1017/jfm.2013.666 Published online by Cambridge University Press

early work on the CS of stratified Couette flow (see Eliassen, Hoiland & Riis 1953; Engevik 1971), and there have been cases where the forcings have been erroneously taken to be similar to those for the homogeneous case: for instance, Case (1960*b*), in extending his analysis from the homogeneous case to the stratified scenario, writes down the inhomogeneous TG equation forced with a delta function and its derivative.

The nature of the singular forcing is also relevant from the standpoint of an initial-value problem. The singular forcing in the governing equation for linearized perturbations is the initial impulsive forcing that recovers an isolated CS mode for long times. A weaker forcing will lead to a long-time algebraic decay, while a stronger forcing will lead to secular growth (even in the absence of a resonant interaction). Physically, the presence of the singular forcing implies that a CS mode is associated with perturbation vorticity generated by an extraneous (baroclinic) force distribution. Here, extraneous refers to mechanisms outside of the physics already included in the governing linearized equations. For instance, in homogeneous flows, the (regular) discrete modes arise from a rearrangement of the base state vorticity while the CS modes require the generation of a vortex sheet via a baroclinic force distribution proportional to a delta function. An example in this regard was seen in the earlier paragraph where a vanishingly small stratification, together with a localized density perturbation, can act as the vorticity generating forcing in the homogeneous case. For Couette flow, an initial gradient-directed impulsive forcing of the form $\delta(y-y_c)\mathrm{e}^{\mathrm{i}kx}$ generates precisely a single CS mode with $\omega = ky_c$. For a nonlinear flow profile, such a forcing leads to an isolated CS mode but only in the limit of long times. This is because the forcing only generates the vortex-sheet contribution and not the PV-singular contribution of a single CS mode, and the finite-time response is therefore a polychromatic one involving the entire CS spectrum (Kelbert & Sazonov 1996). For the Rankine vortex, a localized forcing of the form $\delta(r-r_f)\mathrm{e}^{\mathrm{i}(m\theta+kz)}$ must similarly lead to the corresponding (two-dimensional or three-dimensional) CS mode, together with a superposition of Kelvin modes, when r_f does not coincide with any of the Kelvin-mode critical radii. A similar forcing with $k=0$, for a smooth vortex, must again lead to a finite-time polychromatic response. For stratified shear flows, however, a delta-function extraneous forcing is weaker than the non-generalized function forcings, associated with the Pf. interpretation, that appear in (3.32). Thus, one expects a non-modal response for long times characterized by an algebraic decay ($\propto t^{-1/2\pm\nu}$), the associated exponents being precisely those appearing in the denominators of the right-hand side terms in (3.32). This has been shown for the case of Couette flow with uniform stratification (Booker & Bretherton 1967; Brown & Stewartson 1980), and a similar scenario must hold for a smooth vortex in three dimensions. Finally, one may also regard the singular forcings in the Rayleigh and TG equations (and their vortex analogues) as resulting in the limit of a vanishing viscosity for the homogeneous case, and in the limit of both vanishing viscosity and (mass or thermal) diffusivity for the stratified case. It then follows that the viscous critical-layer solution (Stewartson 1981), in the homogeneous case, must approach a generalized function forcing in the limit $Re \to \infty$ and for the critical layer thickness being asymptotically small, and that the analogous critical-layer solution in the stratified case must not exhibit this property in the limit $Re, (Re \cdot Pr) \to \infty$ (Pr is the Prandtl number and denotes the ratio of the relevant diffusivities). A small but finite viscosity and/or diffusivity may also be regarded as the extraneous physics, responsible for the appearance of a singular forcing in the relevant inviscid equation. However, this no longer allows for an arbitrary (real) phase relationship between the solutions on either side of the critical layer. These relations now involve a complex-valued phase

https://doi.org/10.1017/jfm.2013.666 Published online by Cambridge University Press

angle, and are well documented for both the homogeneous (Lin 1955) and stratified cases (Miles 1961).

3.3. *The modal decomposition for an arbitrary vortical initial condition*

Having examined the local structure of the three-dimensional CS modes, we clarify the manner in which the modal superposition for a smooth vorticity profile, corresponding to an evolving (arbitrary) three-dimensional distribution of perturbation vorticity, would approach that obtained in § 2.2.3 for the Rankine vortex. The clarification must necessarily be an indirect one, since analytical forms for the eigenmodes associated with a smooth vorticity profile do not exist. The non-trivial aspect in the comparison between the Rankine vortex and smooth Rankine-like profiles concerns the crucial difference in the structure of the three-dimensional CS modes in the vicinity of the critical radius, and the relation between the two modal superpositions may therefore be illustrated by considering the respective analogies with parallel shearing flows, the analogy being based on the structure of the CS modes. The Rankine vortex would correspond to homogeneous Couette flow, the analytically tractable analog of a smooth vorticity profile would be a Couette flow with a uniform stable stratification, and the approach to the Rankine limit involves making the stratification vanishingly small.

The modal superpositions in the parallel flow analogies evolve an arbitrary initial distribution of vorticity and density perturbations. The azimuthal vorticity (w_θ) in the vortex case corresponds to the vorticity in the stratified flow problem (w_z being the only non-zero component in this case since the perturbation field is taken to be two-dimensional), and the radial vorticity (w_r) in the vortex case corresponds to the density perturbation (ρ') in stratified flow. The remaining perturbation fields are determined from solenoidal constraints. Assuming $U(y)$ and $\rho_0(y)$ to characterize the unperturbed stratified flow, the correspondence $(w_\theta, w_r) \leftrightarrow (w_z, \rho')$, may be seen from the governing equations which, in the inviscid non-diffusive limit, are given by

$$\left(\frac{\partial}{\partial t} + \Omega(r)\frac{\partial}{\partial \theta}\right) w_\theta = Z\frac{\partial u_\theta}{\partial z} + [r\Omega'(r)]w_r, \tag{3.33}$$

$$\left(\frac{\partial}{\partial t} + \Omega(r)\frac{\partial}{\partial \theta}\right) w_r = Z\frac{\partial u_r}{\partial z}, \tag{3.34}$$

for the case of a smooth vortex, and

$$\left(\frac{\partial}{\partial t} + U(y)\frac{\partial}{\partial x}\right) w_z = -g\frac{\partial \rho'}{\partial x}, \tag{3.35}$$

$$\left(\frac{\partial}{\partial t} + U(y)\frac{\partial}{\partial x}\right) \rho' = -\frac{\mathrm{d}\rho_0}{\mathrm{d}y}u_y \tag{3.36}$$

for the stratified shear flow. The w_r and ρ' perturbations are seen to arise from a balance between the convection and induction terms: the latter term is proportional to the base-state vorticity in (3.34) and to the density gradient in (3.36). The resulting induced perturbations then act as source terms for w_θ and w_z, respectively, via (3.33) and (3.35). The changes in w_θ and w_z couple back to (3.34) and (3.36) via u_r and u_y, and the overall effect is that of buoyancy forces resisting the deformation of the horizontal isopycnal lines, and the related density perturbations. In the same manner that the Coriolis forces resist the generation of radial vorticity by endowing the (axial) vortex lines in the base state with a certain stiffness. For homogeneous Couette flow, ρ_0 is a constant, and for the Rankine vortex, $Z = 0$ (the irrotational exterior being

https://doi.org/10.1017/jfm.2013.666 Published online by Cambridge University Press

the region of interest, since the analogy is based on the structure of the CS modes in the respective problems), so ρ' and w_r behave as passive scalars in these limits. The correspondence between the vortex and stratified shear problems is not an exact one since there exists an additional source term for w_θ in the vortex case. But the contribution from this term becomes asymptotically small in the Rankine limit ($Z \to 0$). If one were to neglect this contribution in (3.33), then the resulting equation for u_r would involve a modified Richardson number that differs from Ri_v in (3.15) only by $O(Z^2)$ in the limit $Z \to 0$.

We now examine the manner in which the modal superposition for stratified Couette flow involving singular Pf. eigenfunctions, originally obtained by Engevik (1971), approaches the simpler more familiar form, involving delta functions (and their derivatives), for homogeneous Couette flow in the limit of a vanishingly small stratification. Equations (3.35) and (3.36) written in terms of the streamfunction ψ and ρ' are given by

$$(\partial_t + y\partial_x)\,\nabla^2\psi = -\frac{1}{Fr^2}\partial_x\rho', \tag{3.37}$$

$$(\partial_t + y\partial_x)\,\rho' = \frac{N^2}{N_0^2}\partial_x\psi, \tag{3.38}$$

in dimensionless form with $\nabla^2 \equiv \partial^2/\partial x^2 + \partial^2/\partial y^2$. The parameter $Fr = U_0/(N_0 L)^{1/2}$ in (3.37) is a reference Froude number with U_0/L being a characteristic inverse time scale for the base state velocity gradient. The ratio N/N_0 in (3.38) is a dimensionless measure of the base state stratification with $N^2 = -(g/\rho_m)(\mathrm{d}\rho_0/\mathrm{d}y)$ being the square of the (constant) Brunt–Väisälä frequency, $N_0 = (g/L)^{1/2}$ is again a reference inverse time scale, and ρ_m is an appropriate mean density within the Boussinesq approximation (there exists a rotational equivalent of the Brunt–Väisälä frequency, the epicyclic frequency, denoting angular momentum stratification; see Shore (1992)). The separation of the single parameter, the Richardson number ($Ri = (N^2/N_0^2)Fr^{-2}$) in the TG equation that results from combining (3.37) and (3.38), into two parameters, one in each of (3.37) and (3.38), allows one to discriminate between the cases where Ri vanishes due to the absence of gravity (N/N_0 finite, $Fr^{-1} \to 0$, leading to a decoupling of the velocity and density fields), and where Ri vanishes because of a homogeneous base state ($N/N_0 \to 0$ with Fr finite). We are interested in the latter case since this allows for density perturbations to persist and drive a flow even in the homogeneous limit.

For the simpler case of homogeneous Couette flow with $N/N_0 = 0$ in (3.38), assuming a normal mode form proportional to $\mathrm{e}^{ik(x-y_c t)}$ one obtains

$$(y - y_c)\,w_z = -\frac{1}{Fr^2}\rho', \tag{3.39}$$

$$(y - y_c)\,\rho' = 0, \tag{3.40}$$

where $w_z = (\mathrm{D}^2 - k^2)\psi$. The above system of equations supports two families of CS modes. The Case vortex-sheet modes with $w_z \propto \delta(y - y_c)$, discussed in § 2.1, arise from the homogeneous solution of (3.39), and are the analogue of the Λ_1 family for the Rankine vortex. The analog of the Λ_2 family are density sheets with a dipole singularity ($w_z \propto \delta'(y - y_c)$) corresponding to a tangential jet riding at the critical level. Thus,

$$(w_z^{\Lambda_1},\, \rho'^{\Lambda_1}) = (\delta(y - y_c),\, 0), \tag{3.41}$$

$$(w_z^{\Lambda_2},\, \rho'^{\Lambda_2}) = \left(\frac{1}{Fr^2}\delta'(y - y_c),\, \delta(y - y_c)\right). \tag{3.42}$$

https://doi.org/10.1017/jfm.2013.666 Published online by Cambridge University Press

For a bounded domain, the arbitrary-time vorticity field may then be written as the following modal superposition:

$$w_z(y,t) = \int_{-1}^{1} X_{\Lambda_1} w_z^{\Lambda_1} \mathrm{e}^{-\mathrm{i}ky_c t}\,\mathrm{d}y_c + \int_{-1}^{1} X_{\Lambda_2} w_z^{\Lambda_2} \mathrm{e}^{-\mathrm{i}ky_c t}\,\mathrm{d}y_c \tag{3.43}$$

with $X_{\Lambda_1} = w_{z0}(y_c) - (1/Fr^2)\rho_0'(y_c)$ and $X_{\Lambda_2} = \rho_0'(y_c)$. The superposition is obtained by first finding the Λ_2 superposition needed to represent the initial perturbation density field (ρ_0'), and then finding the necessary Λ_1 superposition to account for the residual vorticity field.

For stratified Couette flow, the equations in normal-mode form are

$$(y - y_c)\, w_z = -\frac{1}{Fr^2}\rho', \tag{3.44}$$

$$(y - y_c)\, \rho' = \frac{N^2}{N_0^2}\psi. \tag{3.45}$$

The TG equation obtained from combining the above pair of equations has linearly independent solutions given by $f(y) = \sqrt{\mathrm{i}k(y-y_c)}\mathrm{J}_{-\nu}[\mathrm{i}k(y-y_c)]$ and $g(y) = \sqrt{\mathrm{i}k(y-y_c)}\mathrm{J}_{\nu}[\mathrm{i}k(y-y_c)]$ with $\nu = \sqrt{1/4 - Ri}$ as before (Taylor 1931). For $y \to y_c$, these Bessel solutions reduce to the local Frobenius forms, obtained from (3.16), and that are valid for a general Ri profile. For a constant-Ri Couette flow, the spectrum is purely continuous when $0 < Ri < 1/4$ (Taylor 1931; Eliassen *et al.* 1953; Dyson 1960). There arises an additional discrete spectrum consisting of a denumerable infinity of forward- and backward-propagating sheared internal gravity (IG) waves for $Ri > 1/4$, with the spectrum becoming purely discrete for $Ri \to \infty$. It is worth noting that the degenerate coalescence of an infinity of discrete modes at $Ri = 1/4$ is specific to Couette flow with a constant stratification (Banks, Drazin & Zaturska 1976), but since our focus is on CS-mode superposition, the analysis that follows is restricted to the interval $0 < Ri < 1/4$. From the results of Engevik (1971), the arbitrary time streamfunction in this parameter regime may be written as the following integral superposition over Pf. singular eigenfunctions:

$$\begin{aligned}\psi(y,t) = \mathrm{Pf.}\int_{-1}^{y} A_1(y_c)\Psi(1-y_c, y-y_c)\mathrm{e}^{-\mathrm{i}ky_c t}\,\mathrm{d}y_c \\ + \mathrm{Pf.}\int_{y}^{1} A_2(y_c)\Psi(1+y_c, y_c-y)\mathrm{e}^{-\mathrm{i}ky_c t}\,\mathrm{d}y_c,\end{aligned} \tag{3.46}$$

where $A_1(y_c)$ and $A_2(y_c)$ are given by

$$-4\mathrm{i}kA_1(y_c)f(1-y_c)g(1-y_c)\sin\pi\nu - 2\mathrm{i}kA_2(y_c)\Delta(y_c) = B_1(y_c)\cot\pi\nu, \tag{3.47}$$

$$2\mathrm{i}kA_1(y_c)\Delta(y_c) - 4\mathrm{i}kA_2(y_c)f(1+y_c)g(1+y_c)\sin\pi\nu = B_2(y_c)\cot\pi\nu, \tag{3.48}$$

with

$$B_1(y_c) = \mathrm{Pf.}\int_{y_c}^{1}\left\{\frac{w_{z0}}{y-y_c} - \frac{Fr^{-2}\rho_0'}{(y-y_c)^2}\right\}\Psi(1-y_c, y-y_c)\,\mathrm{d}y, \tag{3.49}$$

$$B_2(y_c) = \mathrm{Pf.}\int_{-1}^{y_c}\left\{\frac{w_{z0}}{y_c-y} + \frac{Fr^{-2}\rho_0'}{(y_c-y)^2}\right\}\Psi(1+y_c, y_c-y)\,\mathrm{d}y, \tag{3.50}$$

$$\Delta(y_c) = f(1+y_c)g(1-y_c) - f(1-y_c)g(1+y_c). \tag{3.51}$$

https://doi.org/10.1017/jfm.2013.666 Published online by Cambridge University Press

In (3.46), the singular CS modes are the 'one-sided' eigenfunctions originally defined by Eliassen *et al.* (1953), and given by

$$\text{Pf.}\,\Psi(1-y_c, y-y_c) = \text{Pf.}\,\{g(1-y_c)f(y-y_c) - f(1-y_c)g(y-y_c)\} \quad \text{if } y_c < y, \tag{3.52}$$

$$= 0 \quad \text{if } y_c > y \tag{3.53}$$

$$\text{Pf.}\Psi(1+y_c, y_c-z) = \text{Pf.}\,\{g(1+y_c)f(y_c-z) - f(1+y_c)g(y_c-z)\} \quad \text{if } y_c > y. \tag{3.54}$$

$$= 0 \quad \text{if } y_c < y. \tag{3.55}$$

The modal superposition for w_z may be written in the form

$$w_z(y,t) = -\text{Pf.}\int_{-1}^{y} A_1(y_c)\frac{Ri\Psi(1-y_c, y-y_c)}{(y-y_c)^2}\mathrm{e}^{-\mathrm{i}ky_ct}\,\mathrm{d}y_c - \text{Pf.}\int_{y}^{1} A_2(y_c)\frac{Ri\Psi(1+y_c, y_c-y)}{(y-y_c)^2}\mathrm{e}^{-\mathrm{i}ky_ct}\,\mathrm{d}y_c. \tag{3.56}$$

In order to show that (3.43) arises as the limiting form of (3.56) for $(N/N_0) \to 0$, it is convenient first to consider the following linear combinations of the one-sided eigenfunctions defined above:

$$\Psi^{\Lambda_1} = g(1+y_c)\Psi(1-y_c, y-y_c)\mathcal{H}(y-y_c) + g(1-y_c)\Psi(y_c+1, y_c-y)\mathcal{H}(y_c-y), \tag{3.57}$$

$$= c_1^{\Lambda_1} f(|y-y_c|) - \left(\frac{c_2^{\Lambda_1}+c_3^{\Lambda_1}}{2}\right) g(|y-y_c|) - \left(\frac{c_2^{\Lambda_1}-c_3^{\Lambda_1}}{2}\right) g(|y-y_c|)\mathrm{sgn}(y-y_c), \tag{3.58}$$

$$\Psi^{\Lambda_2} = f(1+y_c)\Psi(1-y_c, y-y_c)\mathcal{H}(y-y_c) - f(1-y_c)\Psi(y_c+1, y_c-y)\mathcal{H}(y_c-y), \tag{3.59}$$

$$= -c_1^{\Lambda_2} g(|y-y_c|)\mathrm{sgn}(y-y_c) + \left(\frac{c_2^{\Lambda_2}-c_3^{\Lambda_2}}{2}\right) f(|y-y_c|) + \left(\frac{c_2^{\Lambda_2}+c_3^{\Lambda_2}}{2}\right) f(|y-y_c|)\mathrm{sgn}(y-y_c), \tag{3.60}$$

where $c_1^{\Lambda_1} = g(1+y_c)g(1-y_c)$, $c_1^{\Lambda_2} = f(1+y_c)f(1-y_c)$, $c_2^{\Lambda_1} = c_3^{\Lambda_2} = f(1-y_c)g(1+y_c)$ and $c_3^{\Lambda_1} = c_2^{\Lambda_2} = f(1+y_c)g(1-y_c)$. As evident from the notation, the linear combinations in (3.58) and (3.60) may be identified with the Λ_1 and Λ_2 analogs of a smooth vorticity profile with local Frobenius forms similar to those defined in (3.20) and (3.21). For $N/N_0 \to 0$, (3.58) and (3.60) will be seen below to reduce to the vortex sheets and density sheets defined in (3.41) and (3.42). Using (3.58) and (3.60), (3.56) may be rewritten as

$$w_z(y,t) = -\text{Pf.}\int_{-1}^{1}\{A_1(y_c)f(1-y_c) + A_2(y_c)f(1+y_c)\}\frac{Ri\,\Psi^{\Lambda_1}}{(y-y_c)^2W(y_c)}\mathrm{e}^{-\mathrm{i}ky_ct}\,\mathrm{d}y_c - \text{Pf.}\int_{-1}^{1}\{A_1(y_c)g(1-y_c) - A_2(y_c)g(1+y_c)\}\frac{Ri\,\Psi^{\Lambda_2}}{(y-y_c)^2W(y_c)}\mathrm{e}^{-\mathrm{i}ky_ct}\,\mathrm{d}y_c, \tag{3.61}$$

https://doi.org/10.1017/jfm.2013.666 Published online by Cambridge University Press

where $W(y_c) = f(1+y_c)g(1-y_c) + f(1-y_c)g(1+y_c)$ with (3.49) and (3.50) now being given by

$$Ri\,B_1(y_c) = \text{Pf.} \int_{-1}^{1} \left[\frac{f(1-y_c)}{W(y_c)} \left\{ w_{y0} \frac{Ri\,\Psi^{A_1}}{|y-y_c|} - Fr^{-2}\rho_0 \frac{Ri\,\Psi^{A_1}}{(y-y_c)^2} \right\} + \frac{g(1-y_c)}{W(y_c)} \left\{ w_{y0} \frac{Ri\,\Psi^{A_2}}{|y-y_c|} - Fr^{-2}\rho_0 \frac{Ri\,\Psi^{A_2}}{(y-y_c)^2} \right\} \right] \mathrm{d}y, \tag{3.62}$$

$$Ri\,B_2(y_c) = \text{Pf.} \int_{-1}^{1} \left[\frac{f(1+y_c)}{W(y_c)} \left\{ w_{y0} \frac{Ri\,\Psi^{A_1}}{|y-y_c|} + Fr^{-2}\rho_0 \frac{Ri\,\Psi^{A_1}}{(y-y_c)^2} \right\} + \frac{g(1+y_c)}{W(y_c)} \left\{ w_{y0} \frac{Ri\,\Psi^{A_2}}{|y-y_c|} + Fr^{-2}\rho_0 \frac{Ri\,\Psi^{A_2}}{(y-y_c)^2} \right\} \right] \mathrm{d}y, \tag{3.63}$$

in terms of Ψ^{A_1} and Ψ^{A_2}.

In the limit $(N/N_0) \to 0$, we have $\Delta(y_c) \sim -2\mathrm{i}\sinh 2ky_c/\pi$ and $W(y_c) \sim 2\mathrm{i}\sinh 2k/\pi$, and (3.47) and (3.48) reduce to

$$B_1(y_c)\pi\,Ri \sim \frac{4k}{\pi}\left\{A_1(y_c)\sinh 2k(1-y_c) - A_2(y_c)\sinh 2ky_c\right\}, \tag{3.64}$$

$$B_2(y_c)\pi\,Ri \sim \frac{4k}{\pi}\left\{A_1(y_c)\sinh 2ky_c + A_2(y_c)\sinh 2k(1+y_c)\right\}. \tag{3.65}$$

Further, only the limiting forms of f and g for y close to y_c, given by $f(z) \sim 2^{1/2-\epsilon}(\mathrm{i}kz)^{\epsilon}/\Gamma(1/2+\epsilon)$ and $g(z) \sim 2^{-1/2+\epsilon}(\mathrm{i}kz)^{1-\epsilon}/\Gamma(3/2-\epsilon)$ are needed in this limit, and from the theory of generalized functions, we have for these limiting forms

$$\lim_{\epsilon\to 0} \begin{cases} Ri\dfrac{f(|y-y_c|)}{|y-y_c|}(1, \operatorname{sgn}(y-y_c)) \\ Ri\dfrac{f(|y-y_c|)}{|y-y_c|^2}(1, \operatorname{sgn}(y-y_c)) \\ Ri\dfrac{g(|y-y_c|)}{|y-y_c|}(1, \operatorname{sgn}(y-y_c)) \\ Ri\dfrac{g(|y-y_c|)}{|y-y_c|^2}(1, \operatorname{sgn}(y-y_c)) \end{cases} = \begin{cases} 2\sqrt{\dfrac{2}{\pi}}(\delta(y-y_c), 0), \\ -2\sqrt{\dfrac{2}{\pi}}(0, \delta'(y-y_c)), \\ 0, \\ -2\mathrm{i}k\sqrt{\dfrac{2}{\pi}}(\delta(y-y_c), 0). \end{cases} \tag{3.66}$$

This leads to the correct expressions for the vorticity eigenfunctions for homogeneous (unstratified) Couette flow:

$$\lim_{N/N_0\to 0} -\frac{Ri\,\Psi^{A_1}}{(y-y_c)^2} = k\sinh 2k\left(\frac{2}{\pi}\right)^{3/2}\delta(y-y_c), \tag{3.67}$$

$$\lim_{N/N_0\to 0} -\frac{Ri\,\Psi^{A_2}}{(y-y_c)^2} = i\sinh 2k\left(\frac{2}{\pi}\right)^{3/2}\delta'(y-y_c). \tag{3.68}$$

Substituting (3.66) in (3.62) and (3.63) leads to the following simplified expressions:

$$Ri\,B_1(y_c) = \frac{\mathrm{i}}{\pi}\left[\operatorname{cosech} 2k\{\cosh k(3-y_c) - \cosh k(1+y_c)\}(w_{y0}(y_c) - Fr^{-2}\rho'(y_c)) - 2k\cosh k(1-y_c)Fr^{-2}\rho_0(y_c)\right], \tag{3.69}$$

$$Ri\,B_2(y_c) = \frac{2\mathrm{i}}{\pi}\left[\sinh k(1+y_c)(w_{y0}(y_c) - Fr^{-2}\rho_0'(y_c)) + k\cosh k(1+y_c)Fr^{-2}\rho_0(y_c)\right]. \tag{3.70}$$

https://doi.org/10.1017/jfm.2013.666 Published online by Cambridge University Press

Finally, on substituting the above expressions in (3.64) and (3.65), one finds

$$A_1(y_c)f(1-y_c)+A_2(y_c)f(1+y_c)=\frac{\mathrm{i}}{k}\sqrt{\frac{\pi}{2}}(w_{y0}(y_c)-Fr^{-2}\rho'(y_c)), \tag{3.71}$$

$$A_1(y_c)g(1-y_c)-A_2(y_c)g(1+y_c)=\sqrt{\frac{\pi}{2}}Fr^{-2}\rho(y_c), \tag{3.72}$$

which, on substitution in (3.61), and use of (3.67) and (3.68), leads to (3.43).

Although the analysis in this section shows the essential manner in which modal superposition for a smooth vorticity profile approaches that of a Rankine vortex, it focuses on the region in the vicinity of the critical radius. Thus, the analogy ends up ignoring the global nature of the spectrum, in particular, the discrete modes in the respective problems. As already seen, both Rankine and smooth vortices support a denumerable infinity of Kelvin modes (only co-grade in the latter case; see Leibovich & Ma (1983)). In contrast, the spectrum of homogeneous Couette flow is purely continuous (Case 1960*a*; Dikii 1960) and stratified Couette flow again exhibits only a CS when $Ri < 1/4$ (Taylor 1931). This is not a fundamental constraint, however. As shown by Roy (2013), one may indeed develop more elaborate stratified shear flow configurations that mirror both the discrete and continuous spectra of Rankine and smooth vorticity profiles, and the analysis here may readily be extended to these cases. Finally, in drawing the analogy between a smooth vorticity profile and stratified Couette flow, we have neglected the effect of the curvature of the velocity profile on the CS. This is because the additional induction term in the governing equation for the vorticity field does not alter the local Frobenius forms and, thence, the nature of the singular forcing needed at the critical level.

4. The inviscid centre modes

Smooth vorticity profiles support a class of eigenmodes generically known as centre modes. Center modes are nearly-convected modes (that is, with a vanishingly small Doppler frequency) with their structure concentrated in the vicinity of the rotation axis, and may have a viscous (*Re*-dependent growth rate) or inviscid origin (*Re*-independent growth rate for sufficiently large *Re*). They are known to play an important role in determining the inviscid stability characteristics of aircraft trailing vortices (Fabre & Le Dizès 2008), and have been extensively studied in two types of swirling flows: a swirling Poiseuille flow (Stewartson, Ng & Brown 1988) and the Batchelor vortex (Fabre 2002; Fabre & Jacquin 2004; Le Dizès & Fabre 2007; Heaton 2007*a*; Fabre & Le Dizès 2008). For the Batchelor vortex, in particular, the neutral curve is largely controlled by such modes (Fabre & Le Dizès 2008). Herein, we consider centre modes of an inviscid origin, and for a base state with only an azimuthal flow component. Our focus is on what happens to these modes as a smooth vorticity profile approaches the Rankine limit. In the absence of an axial flow, centre-mode behaviour is observed only in the limit of small axial wavenumbers (Leibovich, Brown & Patel 1986). Each of the structured modes of a smooth vortex becomes a centre mode for $k \to 0$, the corresponding co-grade eigenfunction being characterized by a vanishingly small radial length scale (the focus here is on the co-grade modes; the retrograde modes transform to inviscidly damped singular oscillations best interpreted in terms of a superposition of decaying quasi-modes).

https://doi.org/10.1017/jfm.2013.666 Published online by Cambridge University Press

The centre-mode behaviour may be seen by considering the one-parameter family of smooth vorticity profiles given by $\Omega(r) = \Omega_0 - (r^{2p}/(2p)!)\Omega_{2p}$ for small r with $\Omega_{2p} > 0$, p being a parameter characterizing the flatness of the angular velocity profile around the rotation axis. Thus, $p = 1$ corresponds to the local quadratic behaviour for a Lamb–Oseen profile, and the limit $p \to \infty$ corresponds to the Rankine vortex. Substitution in the HG equation gives

$$r\frac{\mathrm{d}}{\mathrm{d}r}\left[\frac{m^2 r}{m^2+k^2r^2}\frac{\mathrm{d}}{\mathrm{d}r}(ru_r)\right] - \left[m^2 - 4m\left\{\frac{k^2r^2\Omega_0}{m^2} + \left(p - \frac{k^2r^2}{m^2}\right)\frac{(p+1)\Omega_{2p}r^{2p}}{(2p)!}\right\}(m\Omega-\omega)^{-1} - 4k^2r^2\Omega_0^2\left\{1 - \frac{r^{2p}(p+2)}{(2p)!}\frac{\Omega_{2p}}{\Omega_0} + \frac{r^{4p}(p+1)}{(2p)!}\left(\frac{\Omega_{2p}}{\Omega_0}\right)^2\right\}\{(m\Omega-\omega)^2\}^{-1}\right] ru_r = 0, \tag{4.1}$$

for $r \to 0$. In the limit of a nearly convected mode, $\omega \approx m\Omega_0$, and for r not too close to the rotation axis, we have $(\omega - m\Omega(r)) \approx m(\Omega(0) - \Omega(r)) \approx O(r^{2p})$. This is equivalent to approximating the two regular singular points, one at the origin and the other close to it at $\Omega^{-1}(\omega)/m$, as being coincident at leading order. The coalescence of the regular singular points leads to the origin behaving as an irregular singular point. The resulting divergence of the terms involving the inverse of the Doppler frequency in (4.1), leads to an increasingly rapid oscillation of the eigenfunction as r approaches the origin, that is, a centre-mode behaviour. For a Rankine vortex, on the other hand, $\Omega = \Omega_0$ and $\omega - m\Omega \sim O(k)$ for $k \to 0$, so that the terms involving the Doppler frequency remain finite even as $r \to 0$. In order to resolve the radial oscillation of the eigenfunction for a smooth vorticity profile, we define $\omega - m\Omega_0 = -\epsilon(k)(m\Omega_{2p}/(2p)!)$ and, thence, the following rescaled boundary layer variables: $r^{2p} = \epsilon(k)s$, $ru_r(r) = U(s)$. At leading order, the rescaled HG equation takes the form

$$s^2U'' + sU' + \left[-\frac{m^2}{4p^2} - \frac{p+1}{p}\frac{s}{s+1} + \mu(\mu+1)\frac{s^{1/p}}{(s+1)^2}\right]U = 0, \tag{4.2}$$

with $\mu(\mu+1) = 4[(2p-1)!\Omega_0]^2$ and $\epsilon(k) = (k/m\Omega_{2p})^{2p/(2p-1)}$. Thus, the dispersion curve in the nearly convected limit has the asymptotic form $\omega - m\Omega_0 \sim O(k^{2p/(2p-1)})$, consistent with a vanishing group velocity for $k \to 0$, while the radial extent of the oscillatory boundary layer around the rotation axis is $O(k/m\Omega_{2p})^{1/(2p-1)}$ which determines the radial scale of the eigenmode. The case $p = 1$, for which $\epsilon(k) \sim O(k^2)$ and (4.2) reduces to the hypergeometric equation, was analysed by Leibovich *et al.* (1986). For large p, the reduction in the radial length scale ($\propto k^{1/2p}$) of the eigenfunction with decreasing k becomes increasingly gradual, and correspondingly, the transition to a centre-mode behaviour with a vanishing group velocity occurs at an increasingly small value of k. In the limit $p \to \infty$, there is no boundary layer, and consequently no centre-mode behaviour, with $\omega - m\Omega_0 \sim O(k)$ and a finite group velocity at $k = 0$. The implication is that the radial length scale that the radial length scale $(1/\beta_n)$, characterizing a given structured mode eigenfunction ($\propto \mathrm{J}_m(\beta_n r)$) of a

https://doi.org/10.1017/jfm.2013.666 Published online by Cambridge University Press

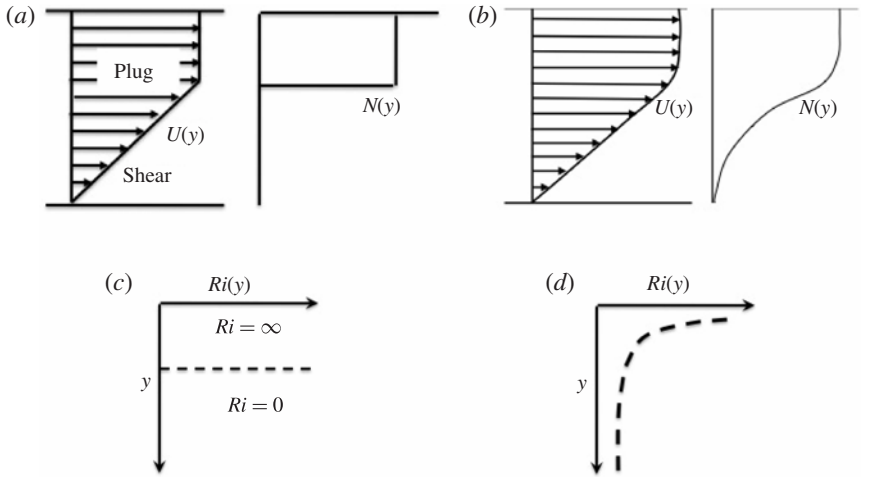

FIGURE 7. The stratified shear-flow analogues for a Rankine vortex (*a*) and a smooth vorticity profile (*b*). The corresponding *Ri*–*y* profiles are shown in (*c*) and (*d*), respectively.

Rankine vortex, remains fixed even as k goes to zero. This is seen from the analysis in § 2.2.5. The relation (2.97) shows that $1/\beta_n \approx a/j_n^m$ for $k \to 0$, and for $k \to \infty$, it is readily shown using (2.35) that $\omega_n \sim (m+2)\Omega_0 - \Omega_0(j_n^{m+1})^2/(ka)^2$, so $1/\beta_n \approx a/j_n^{m+1}$. Since $1/\beta_n$ remains finite in both limits, it is clear that the Rankine limit is a singular one from the point of view of the existence of centre modes.

The onset of centre-mode behaviour in smooth vortices may be explained in a more intuitive manner by appealing to the analogy between (stably) stratified shear flows and rotational flows. The underlying similarity between the stiffening of the vortex lines and isopycnic lines has already been exploited, in a local sense, in order to account for the structure of the CS modes in the respective problems (note again that the analogy is a qualitative one (Yih 1980); an exact mathematical correspondence only exists in two dimensions with the rotation and stratification axes being at right angles to each other (Bretherton 1967)). In the context of the centre modes, the key element is for the *Ri*–*y* profile of the stratified shear flow analog to mimic the Ri_v–*r* profile of the vorticity profile, where the Richardson (*Ri*) and the vortex Richardson (Ri_v) numbers have been defined earlier in § 3.2. Given this correspondence, the centre-mode behaviour in the stratified flow analogue may be seen by examining the characteristics of the sheared IG waves as a function of N, the characteristic scale for the Brunt–Väisälä frequency. Here, N plays the role of k in the vortex case, there also being a correspondence between the streamwise wavenumber in the stratified-flow analogue and the azimuthal wavenumber in the vortex case. The stratified shear-flow analogues for a Rankine vortex and a smooth vorticity profile, with the corresponding *Ri*–*y* profiles, are shown in figure 7.

For the Rankine vortex analog, the *Ri*–*y* profile is invariant to N with the plug-flow region always corresponding to $Ri = \infty$, and the homogeneous shear zone corresponding to $Ri = 0$. On the other hand, for the stratified flow analog of a smooth vortex, $Ri = \infty$ only for $y = 0$, and for any other y, *Ri* is finite, and will decrease with decreasing N. As already discussed in § 3.2, for the analytically soluble case of stratified Couette flow, with a constant Brunt–Väisälä frequency, and in a

https://doi.org/10.1017/jfm.2013.666 Published online by Cambridge University Press

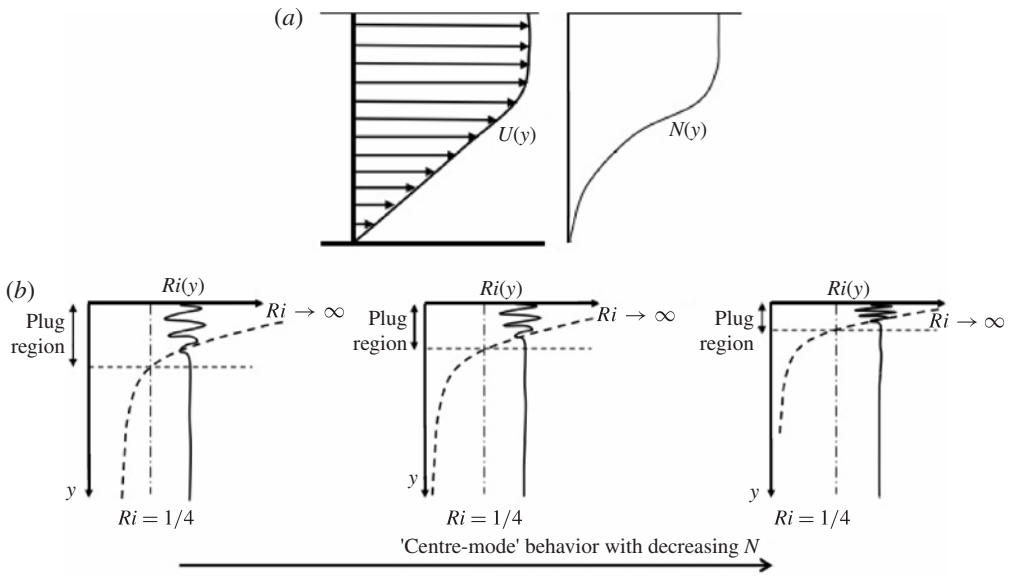

FIGURE 8. The structure of centre-modes via the stratified shear-flow analogue for a smooth vorticity profile. In (*b*) the dashed lines indicate the *Ri* profile while the continuous line is the schematic for a centre mode eigenmode that shows the oscillations getting increasingly squeezed towards a region of smaller y.

bounded domain (Taylor 1931; Eliassen *et al.* 1953), there exists a regular IG-wave spectrum only for $Ri > 1/4$. It follows that, for the smooth-vortex analogue, the plug region that sustains vorticity oscillations characteristic of IG waves may be identified with the region $Ri > 1/4$. Further, as shown in figure 8, with decreasing N for the smooth-vortex analogue, the plug region becomes progressively thinner in extent. Even within this plug, the constraint of a normal mode, that is, an invariant transverse structure, implies that the parts of the wave in higher-Ri regions must travel slower, and must therefore have a relatively fine-scaled structure (Turner 1973). This in turn implies that the length scale of the eigenfunction must decrease continuously with decreasing y, a feature characteristic of centre-mode behaviour.

Similar to the stratified-flow analogue above, the 'core' of a smooth vortex, capable of sustaining vorticity oscillations, may be identified with the region $Ri_v > Ri_v^*$ (although, Ri_v^* will not be $1/4$ since, as already indicated, the analogy is not a precise mathematical one). This core region must recede towards the axis with decreasing k. There must then be a corresponding reduction in the radial length scale of the oscillations along a given dispersion curve, and an eventual transition to centre-mode behaviour for $k \to 0$. The boundary-layer scaling obtained above is, in fact, physically equivalent to keeping Ri_v fixed even for $k \to 0$, and thereby precludes the structureless branch along which $\lim_{k\to 0} Ri_v = 0$. For smooth profiles approaching the Rankine vortex, the rate of recession of the oscillatory core region towards the rotation axis becomes increasingly insensitive to a decrease in k as the angular velocity variation assumes a flatter profile. In the Rankine limit, the size of the core region (which now corresponds to $Ri_v = \infty$) becomes independent of k, and there can be no centre-mode behaviour.

https://doi.org/10.1017/jfm.2013.666 Published online by Cambridge University Press

5. Conclusions

In this paper we have obtained the complete inviscid spectrum for a Rankine vortex (§§ 2.1 and 2.2). The well-known Kelvin modes do not form a complete set by themselves. The inclusion of the singular eigenfunctions completes the spectrum, and these eigenfunctions allow one to represent the evolution of exterior vortical disturbances. A modal superposition, involving both the discrete and the continuous spectra, is arrived at for describing evolution of an arbitrary initial vorticity field ((2.20) and (2.74)). The completeness of the modal approach, and thereby its equivalence to the solution of the IVP, will be shown in a later paper where we also examine the inviscid resonances arising due to initial conditions localized at the critical radii of the discrete modes. The analysis for the Rankine vortex is also extended to the CS modes of smooth vorticity profiles (§§ 3.1 and 3.2). In two dimensions, one may again obtain the required modal representation by solving a Riemann–Hilbert problem, even in the absence of closed-form expressions for the eigenfunctions. But, in three dimensions, the analysis is approximate. It is based on approximate forms of the eigenfunctions close to the critical radius, and an analogy with the the known solution for stratified shear flows is used to clarify the nature of the modal representation is then used to clarify the nature of the modal representation. Finally, we also rigourously demonstrate the absence of the inviscid centre modes for a Rankine vortex (§ 4).

Appendix A. The three-dimensional vessel modes

From (2.54), the amplitude of second vortex sheet for the three-dimensional CS modes of the Λ_1 family is given by

$$A_1(r_f) = \frac{M}{k\{\mathrm{K}'_m(kr_f)N - \mathrm{I}'_m(kr_f)M\}}, \tag{A 1}$$

where

$$M = g^2\beta a\mathrm{J}'_m(\beta a)\mathrm{K}_m(ka) + 2mg\Omega_0\mathrm{J}_m(\beta a)\mathrm{K}_m(ka) + (4\Omega_0^2 - g^2)\mathrm{J}_m(\beta a)ka\mathrm{K}'_m(ka), \tag{A 2}$$

$$N = g^2\beta a\mathrm{J}'_m(\beta a)\mathrm{I}_m(ka) + 2mg\Omega_0\mathrm{J}_m(\beta a)\mathrm{I}_m(ka) + (4\Omega_0^2 - g^2)\mathrm{J}_m(\beta a)ka\mathrm{I}'_m(ka). \tag{A 3}$$

As discussed in § 2.2, the zeros of M correspond to the Kelvin modes. The question arises as to what the singularities of $A_1(r_f)$ or, equivalently, the zeros of $\{\mathrm{K}'_m(kr_f)N - \mathrm{I}'_m(kr_f)M\}$ correspond to? The result for $m = 1$ in § 2.1 suggests that the divergence of the vortex-sheet amplitude must reflect the confinement of the perturbation velocity field to the region $r \leqslant r_f$, and that the zeros of $\mathrm{K}'_m(kr_f)N - \mathrm{I}'_m(kr_f)M$ must therefore correspond to the three-dimensional modes of vibration of a Rankine vortex inside a container of radius r_f. That this is indeed the case may be seen by writing down the velocity field for a Rankine vortex inside a container of radius r_f:

$$\underline{r < a}$$

$$\hat{u}_z = d\mathrm{J}_m(\beta r), \tag{A 4}$$

$$\hat{u}_r = -\frac{\mathrm{i}}{kr}\frac{gd}{g^2 - 4\Omega_0^2}\left\{2m\Omega_0\mathrm{J}_m(\beta r) + g\beta r\mathrm{J}'_m(\beta r)\right\}, \tag{A 5}$$

$$\underline{r_f > r > a}$$

$$\hat{u}_z = c_1\mathrm{K}_m(kr) + c_2\mathrm{I}_m(kr), \tag{A 6}$$

$$\hat{u}_r = -\mathrm{i}\{c_1\mathrm{K}'_m(kr) + c_2\mathrm{I}'_m(kr)\}. \tag{A 7}$$

https://doi.org/10.1017/jfm.2013.666 Published online by Cambridge University Press

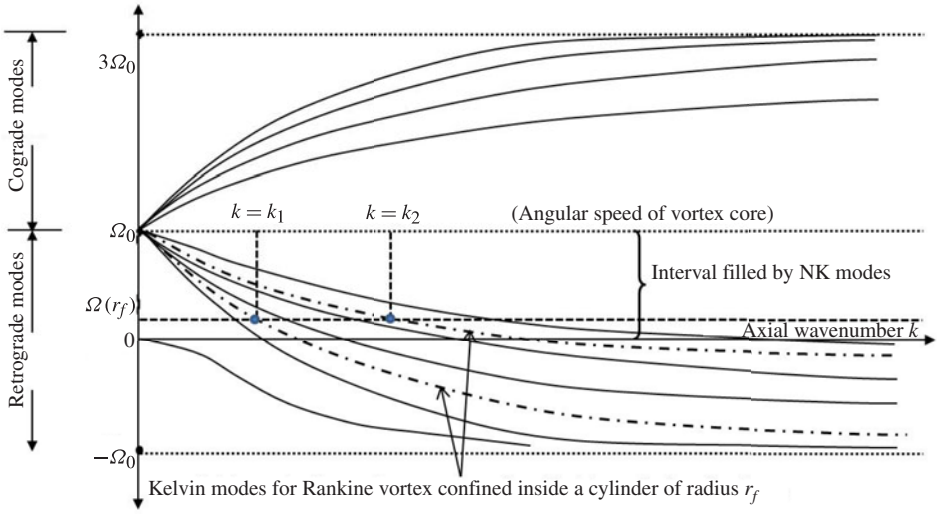

FIGURE 9. (Colour online) Schematic of dispersion curves for Rankine vortex for $m = 1$. The continuous lines represent dispersion curves for an unbounded Rankine vortex whereas the dash–dot lines are dispersion curves for a Rankine vortex confined in a container of radius r_f.

Without loss of generality, we choose $d = 1/\mathrm{J}_m(\beta a)$. Enforcing continuity of $\hat{u}_z$ across the core ($r = a$) and $\hat{u}_r(r_f) = 0$ at the cylinder wall ($r = r_f$), one obtains

$$c_1 = \frac{\mathrm{I}'_M(kr_f)}{\mathrm{K}_m(ka)\mathrm{I}'_m(kr_f) - \mathrm{I}_m(ka)\mathrm{K}'_m(kr_f)}, \tag{A 8}$$

$$c_2 = -\frac{\mathrm{K}'_M(kr_f)}{\mathrm{K}_m(ka)\mathrm{I}'_m(kr_f) - \mathrm{I}_m(ka)\mathrm{K}'_m(kr_f)}. \tag{A 9}$$

Finally, enforcing continuity of radial velocity across the vortex core leads to

$$\mathrm{K}'_m(kr_f)N - \mathrm{I}'_m(kr_f)M = 0, \tag{A 10}$$

which is the dispersion relation for three-dimensional vibrations of a vortex column confined inside a cylindrical vessel of radius r_f. Expectedly, the bounded problem too has a denumerably infinite number of discrete modes. From figure 9 one observes that the horizontal line, $\omega = m\Omega(r_f)$, corresponding to the second vortex-sheet location r_f, intersects the discrete modes of a Rankine vortex inside a cylinder of radius r_f at discrete locations in k space. Thus, for a fixed r_f, there exist a denumerably infinite set of k such that the perturbation velocity field for $r > r_f$ is identically zero. Similarly for every ordered pair (m, k) there exists a denumerably infinite number of CS modes which are also the discrete modes of a confined vortex column.

Appendix B. Riemann–Hilbert problem for a smooth vortex

To obtain the CS-mode amplitude distribution, $\Pi(r_f)$, corresponding to an initial condition of the form $w_{z0}(r)\mathrm{e}^{\mathrm{i}m\theta}$, we will follow the framework developed by Balmforth & Morrison (1995) for parallel shear flows. The integral equation that

https://doi.org/10.1017/jfm.2013.666 Published online by Cambridge University Press

needs to be solved (see (3.6) in § 3.1) is given by

$$w_{z0}(r)\mathrm{e}^{\mathrm{i}m\theta} = \int_0^\infty \Pi(r_f)\hat{w}_z^{CSM}(r;\, r_f)\mathrm{e}^{\mathrm{i}m\theta}\,\mathrm{d}r_f, \tag{B 1}$$

and, on using (3.3) for $\hat{w}_z^{CSM}(r;\, r_f)$, equation (B 1) takes the form

$$w_{z0}(r) = \left[1 + \mathcal{P}\int_0^\infty \frac{1}{r'}\frac{\mathrm{D}Z(r')\hat{\psi}^{CSM}(r';\, r)}{\Omega(r') - \Omega(r)}\,\mathrm{d}r'\right]\Pi(r) - \frac{\mathrm{D}Z(r)}{r}\mathcal{P}\int_0^\infty \frac{\hat{\psi}^{CSM}(r;\, r_f)}{\Omega(r) - \Omega(r_f)}\Pi(r')\,\mathrm{d}r'. \tag{B 2}$$

Equation (B 2) is formulated as a Riemann–Hilbert problem by defining the following two sectionally analytic functions:

$$\boldsymbol{\Phi} = \frac{1}{2\pi\mathrm{i}}\mathcal{P}\int_0^\infty \frac{1}{r'}\frac{\mathrm{D}Z(r')\hat{\psi}^{CSM}(r';\, r)}{\Omega(r') - \Omega(r)}\,\mathrm{d}r', \tag{B 3}$$

$$\boldsymbol{\Psi} = \frac{1}{2\pi\mathrm{i}}\mathcal{P}\int_0^\infty \frac{\Pi(r')\hat{\psi}^{CSM}(r';\, r)}{\Omega(r') - \Omega(r)}\,\mathrm{d}r', \tag{B 4}$$

where r is now regarded as a complex variable, and Φ and Φ are analytic except when $r\epsilon[0,\, \infty)$. From the Sokhotski–Plemelj formulae (Gakhov 1990), one has the following expressions for the limiting values of these functions for r approaching the positive real axis through complex-valued sequences with positive (+) and negative (−) imaginary parts:

$$\boldsymbol{\Phi}^{\pm} = \pm\frac{1}{2}\frac{\mathrm{D}Z(r)\hat{\psi}^{CSM}(r;\, r)}{r\Omega'(r)} + \frac{1}{2\pi\mathrm{i}}\mathcal{P}\int_0^\infty \frac{1}{r'}\frac{\mathrm{D}Z(r')\hat{\psi}^{CSM}(r';\, r)}{\Omega(r') - \Omega(r)}\,\mathrm{d}r', \tag{B 5}$$

$$\boldsymbol{\Psi}^{\pm} = \pm\frac{1}{2}\frac{\Pi(r_f)\hat{\psi}^{CSM}(r;\, r)}{\Omega'(r)} + \frac{1}{2\pi\mathrm{i}}\mathcal{P}\int_0^\infty \frac{\Pi(r')\hat{\psi}^{CSM}(r';\, r)}{\Omega(r') - \Omega(r)}\,\mathrm{d}r'. \tag{B 6}$$

Using (B 5) and (B 6), equation (B 2) may be written as

$$\frac{\hat{\psi}^{CSM}(r;\, r)w_{z0}(r)}{\Omega'(r)} = \epsilon^{+}\boldsymbol{\Psi}^{+} - \epsilon^{-}\boldsymbol{\Psi}^{-}, \tag{B 7}$$

where $\epsilon^{+} = 1 + 2\pi\mathrm{i}\boldsymbol{\Phi}^{+}$ and $\epsilon^{-} = 1 + 2\pi\mathrm{i}\boldsymbol{\Phi}^{-}$. Further, if one defines another sectionally analytic function:

$$\boldsymbol{Q} = \frac{1}{2\pi\mathrm{i}}\int_0^\infty \frac{w_{z0}(r')\hat{\psi}^{CSM}(r';\, r)}{\Omega(r') - \Omega(r)}\,\mathrm{d}r' \tag{B 8}$$

with the limiting values

$$\boldsymbol{Q}^{\pm} = \pm\frac{1}{2}\frac{\hat{\psi}^{CSM}(r;\, r)w_{z0}(r)}{\Omega'(r)} + \frac{1}{2\pi\mathrm{i}}\mathcal{P}\int_0^\infty \frac{w_{z0}(r')\hat{\psi}^{CSM}(r';\, r)}{\Omega(r') - \Omega(r)}\,\mathrm{d}r', \tag{B 9}$$

then (B 7) takes the form

$$\boldsymbol{Q}^{+} - \boldsymbol{Q}^{-} = \epsilon^{+}\boldsymbol{\Psi}^{+} - \epsilon^{-}\boldsymbol{\Psi}^{-}, \tag{B 10}$$

$$\Rightarrow \boldsymbol{Q}^{+} - \epsilon^{+}\boldsymbol{\Psi}^{+} = \boldsymbol{Q}^{-} - \epsilon^{-}\boldsymbol{\Psi}^{-}. \tag{B 11}$$

It is clear that the function $\boldsymbol{Q} - \epsilon\boldsymbol{\Psi}$ is analytic even for $r\epsilon\ (0,\, \infty)$. In the absence of regular discrete modes, as is the case for a monotonically decreasing base-state

https://doi.org/10.1017/jfm.2013.666 Published online by Cambridge University Press

vorticity profile, this function is, in fact, analytic on the entire complex plane. In accordance with Liouville's theorem, it must therefore be a constant. Moreover, since $\boldsymbol{Q}-\epsilon\boldsymbol{\Psi}\to 0$ for $|r|\to\infty$, we have $\boldsymbol{Q}=\epsilon\boldsymbol{\Psi}=0$, or $\boldsymbol{\Psi}=\boldsymbol{Q}/\epsilon$. One may now write

$$\begin{aligned}\Pi(r)&=\frac{\Omega'(r)}{\hat{\psi}^{CSM}(r;\,r)}(\boldsymbol{\Psi}^{+}-\boldsymbol{\Psi}^{-}),\\&=\frac{\Omega'(r)}{\hat{\psi}^{CSM}(r;\,r)}\left[\frac{\boldsymbol{Q}^{+}}{\epsilon^{+}}-\frac{\boldsymbol{Q}^{-}}{\epsilon^{-}}\right],\\&=\frac{\Omega'(r)}{\epsilon^{+}\epsilon^{-}\hat{\psi}^{CSM}(r;\,r)}\left[\left(\frac{\epsilon^{+}+\epsilon^{-}}{2}\right)\frac{\hat{\psi}^{CSM}(r;\,r)w_{z0}(r)}{\Omega'(r)}\right.\\&\quad\left.-\left(\frac{\epsilon^{+}-\epsilon^{-}}{2\pi\mathrm{i}}\right)\mathcal{P}\int_0^{\infty}\frac{w_{z0}(r')\hat{\psi}^{CSM}(r';\,r)}{\Omega(r')-\Omega(r)}\,\mathrm{d}r'\right],\\\Rightarrow\Pi(r)&=\frac{1}{\epsilon_R^2+\epsilon_L^2}\left\{\epsilon_R w_{z0}(r)-\frac{\epsilon_L}{\pi}\mathcal{P}\frac{\Omega'(r)}{\hat{\psi}^{CSM}(r;\,r)}\int_0^{\infty}\frac{w_{z0}(r')\hat{\psi}^{CSM}(r;\,r')}{\Omega(r')-\Omega(r)}\,\mathrm{d}r'\right\}\end{aligned}\tag{B 12}$$

where $\epsilon_R=(\epsilon^{+}+\epsilon^{-})/2$ and $\epsilon_L=(\epsilon^{+}-\epsilon^{-})/2\mathrm{i}$.

Appendix C. Constants for smooth-vortex eigenfunctions

We have

$$R_1=\mathrm{i}k^2S_cA_0\left[\frac{m}{k^2r_f}\epsilon\,\mathrm{sgn}(r-r_f)+\frac{Z_c}{m\Omega_c'}\,\mathrm{sgn}(r-r_f)\right],\tag{C 1}$$

$$R_2=\mathrm{i}k^2S_cB_0\left[\frac{m}{k^2r_f}(1-\epsilon)\,\mathrm{sgn}r-r_f)+\frac{Z_c}{m\Omega_c'}\,\mathrm{sgn}(r-r_f)\right],\tag{C 2}$$

$$\begin{aligned}R_3=\mathrm{i}k^2S_cA_0&\left[\frac{m\epsilon}{k^2r_f}\left(1-\frac{\alpha_1}{r_f}\right)+\frac{m}{k^2r_f^2}+\left(\frac{m}{k^2r_f}+\frac{Z_c}{m\Omega_c'}\right)\alpha_1+\frac{2Z_c'\Omega_c'-Z_c\Omega_c''}{2m\Omega_c'}\right]\\&+\frac{S_c'}{S_c}R_1\,\mathrm{sgn}(r-r_f),\end{aligned}\tag{C 3}$$

$$\begin{aligned}R_4=\mathrm{i}k^2S_cB_0&\left[\frac{m(1-\epsilon)}{k^2r_f}\left(\beta_1-\frac{1}{r_f}\right)+\frac{m}{k^2r_f^2}+\left(\frac{m}{k^2r_f}+\frac{Z_c}{m\Omega_c'}\right)\beta_1+\frac{2Z_c'\Omega_c'-Z_c\Omega_c''}{2m\Omega_c'}\right]\\&+\frac{S_c'}{S_c}R_2\,\mathrm{sgn}(r-r_f),\end{aligned}\tag{C 4}$$

$$\begin{aligned}R_5=\mathrm{i}S_cA_0\frac{m}{r_f}\,\mathrm{sgn}(r-r_f)&\left\{\epsilon\left(\alpha_2-\frac{\alpha_1}{r_f}+\frac{1}{r_f^2}\right)+2\left(\alpha_2-\frac{1}{r_f^2}\right)\right\}\\&+\frac{S_c'}{S_c}\left(R_3\,\mathrm{sgn}(r-r_f)-\frac{S_c'}{S_c}R_1\right)+\frac{R_1S_c''}{2S_c}\end{aligned}\tag{C 5}$$

$$Q_1=\frac{\mathrm{i}}{k}\left[\epsilon A_0\,\mathrm{sgn}(r-r_f)+\frac{\mathrm{i}m}{r_f}R_1\right],\tag{C 6}$$

$$Q_2=\frac{\mathrm{i}}{k}\left[(1-\epsilon)B_0\,\mathrm{sgn}(r-r_f)+\frac{\mathrm{i}m}{r_f}R_2\right],\tag{C 7}$$

$$Q_3=\frac{\mathrm{i}}{k}\left[(1+\epsilon)\alpha_1A_0+\frac{1}{r_f^2}\left\{r_f(A_0+\mathrm{i}mR_3)-\mathrm{i}mR_1\,\mathrm{sgn}(r-r_f)\right\}\right],\tag{C 8}$$

https://doi.org/10.1017/jfm.2013.666 Published online by Cambridge University Press

$$Q_4 = \frac{\mathrm{i}}{k}\left[(2-\epsilon)\beta_1 B_0 + \frac{1}{r_f^2}\left\{r_f(B_0 + \mathrm{i}mR_4) - \mathrm{i}mR_2\,\mathrm{sgn}(r-r_f)\right\}\right], \tag{C 9}$$

$$Q_5 = \frac{\mathrm{i}}{k}\left[(2+\epsilon)\alpha_2 A_0 + \frac{1}{r_f^3}\left\{r_f^2\left\{A_0\alpha_1\,\mathrm{sgn}(r-r_f) + \mathrm{i}m\left(R_5 + \frac{R_1 S_c''}{2S_c}\right)\right\}\right.\right.$$
$$\left.\left. - r_f\,\mathrm{sgn}(r-r_f)\left\{A_0 + \mathrm{i}mR_3\right\} + 2\mathrm{i}mR_1\right\}\right], \tag{C 10}$$

where

$$S_c = \frac{r_f^2}{m^2 + (kr_f)^2}, \quad S_c' = \frac{2m^2 r_f}{(m^2+(kr_f)^2)^2}, \quad S_c'' = \frac{2m^2(m^2 - 3(kr_f)^2)}{(m^2+(kr_f)^2)^3}. \tag{C 11}$$

REFERENCES

ANTKOWIAK, A. & BRANCHER, P. 2004 Transient growth for the Lamb–Oseen vortex. *Phys. Fluids* **16**, L1–L4.

ARENDT, S., FRITTS, D. & ANDREASSEN, Ø. 1997 The initial value problem for Kelvin vortex waves. *J. Fluid Mech.* **344**, 181–212.

BALMFORTH, N. J. & MORRISON, P. J. 1995 Singular eigenfunctions for shearing fluids I. Institute for Fusion studies, University of Texas, Austin, Report No. 692.

BALMFORTH, N. J., SMITH, S. G. L. & YOUNG, W. R. 2001 Disturbing vortices. *J. Fluid Mech.* **426**, 95–133.

BANKS, W. H. H., DRAZIN, P. G. & ZATURSKA, M. B. 1976 On the normal modes of parallel flow of inviscid stratified fluid. *J. Fluid Mech.* **75**, 149–271.

BASSOM, A. P. & GILBERT, A. D. 1998 The spiral wind-up of vorticity in an inviscid planar vortex. *J. Fluid Mech.* **371**, 109–140.

BATCHELOR, G. K. 1967 *Introduction to Fluid Dynamics*. Cambridge University Press.

BENNEY, D. J. & BERGERON, R. F. 1969 A new class of nonlinear waves in parallel flows. *Stud. Appl. Math.* **48**, 181–204.

BOOKER, J. R. & BRETHERTON, F. P. 1967 The critical layer for internal gravity waves in a shear flow. *J. Fluid Mech.* **27**, 513–539.

BRETHERTON, F. P. 1967 The time-dependent motion due to a cylinder moving in an unbounded rotating or stratified fluid. *J. Fluid Mech.* **28**, 545–570.

BRIGGS, R. J., DAUGHERTY, J. D. & LEVY, R. H. 1970 Role of Landau damping in cross-field electron beams and inviscid shear flow. *Phys. Fluids* **13**, 421–432.

BROWN, S. N. & STEWARTSON, K. D. 1980 On the algebraic decay of disturbances in a stratified linear shear flow. *J. Fluid Mech.* **100**, 811–816.

CASE, K. M. 1959 Plasma oscillations. *Ann. Phys. (NY)* **7**, 349–364.

CASE, K. M. 1960*a* Stability of inviscid plane Couette flow. *Phys. Fluids* **3**, 143–148.

CASE, K. M. 1960*b* Stability of idealized atmosphere. I. Discussion of results. *Phys. Fluids* **3**, 149–154.

CHANDRASEKHAR, S. 1961 *Hydrodynamic and Hydromagnetic Stability*. Dover.

DAVIS, R. E. 1969 On the high Reynolds number flow over a wavy boundary. *J. Fluid Mech.* **36**, 337–346.

DIKII, L. A. 1960 The stability of plane-parallel flows of an ideal fluid. *Sov. Phys. Dokl.* **135**, 1179–1182.

DRAZIN, P. G. & REID, W. H. 1981 *Hydrodynamic Stability*. Cambridge University Press.

DYSON, F. J. 1960 Stability of idealized atmosphere. II. Zeros of the confluent hypergeometric function. *Phys. Fluids* **3**, 155–157.

ELIASSEN, A., HOILAND, E. & RIIS, E. 1953 *Two-Dimensional Perturbation of a Flow with Constant Shear of a Stratified Fluid*. Inst. Weather and Climate Res., publ. no. 1.

ENGEVIK, L. 1971 A note on a stability problem in hydrodynamics. *Acta Mech.* **12**, 143–153.

https://doi.org/10.1017/jfm.2013.666 Published online by Cambridge University Press

FABRE, D. 2002 Instabilités et instationnarités dans les tourbillons: application aux sillages avions. PhD thesis, Université Paris VI.

FABRE, D. & JACQUIN, L. 2004 Viscous instabilities in trailing vortex at large swirl number. *J. Fluid Mech.* **500**, 239–262.

FABRE, D. & LE DIZÈS, S. 2008 Viscous and inviscid centre modes in the linear stability of vortices: the vicinity of the neutral curves. *J. Fluid Mech.* **603**, 1–38.

FABRE, D., SIPP, D. & JACQUIN, L. 2006 Kelvin waves and the singular modes of the Lamb Oseen vortex. *J. Fluid Mech.* **551**, 235–274.

FADEEV, L. D. 1971 On the theory of the stability of stationary plane-parallel flows of an ideal fluid. *Zapiski Nauch. Semin. Leningrad. Otdel. Matemat. Instit. Akad. Nauk SSSR* **21**, 164–172.

FARRELL, B. F. 1984 Modal and non-modal baroclinic waves. *J. Atmos. Sci.* **41**, 668–673.

FARRELL, B. F. 1989 Optimal excitation of baroclinic waves. *J. Atmos. Sci.* **46**, 1193–1206.

FARRELL, B. F. & IOANNOU, P. J. 1993*b* Stochastic forcing of the linearized Navier–Stokes equations. *Phys. Fluids* **5**, 2600–2609.

FRAENKEL, L. E. 1970 On steady vortex rings of small cross-section in an ideal fluid. *Proc. R. Soc. Lond.* **316**, 29–62.

FRIEDMAN, B. 1990 *Principles and Techniques of Applied Mathematics*. Dover.

GAKHOV, F. D. 1990 *Boundary Value Prolems*. Dover.

GEL'FAND, I. M. & SHILOV, G. E. 1964 *Generalized Functions, Vol. 1 – Properties and Operations*. Academic.

GRAHAM, M. D. 1998 Effect of axial flow on viscoelastic Taylor–Couette instability. *J. Fluid Mech.* **360**, 341–374.

GREENSPAN, H. P. 1968 *The Theory of Rotating Fluids*. Cambridge University Press.

HEATON, C. J. 2007*a* Centre modes in inviscid vortex flows, and their application to the stability of the Batchelor vortex. *J. Fluid Mech.* **576**, 325–348.

HEATON, C. J. 2007*b* Optimal growth of the Batchelor vortex viscous modes. *J. Fluid Mech.* **592**, 495–505.

HEATON, C. J. & PEAKE, N. 2006 Algebraic and exponential instability of inviscid swirling flow. *J. Fluid Mech.* **565**, 279–318.

HEATON, C. J. & PEAKE, N. 2007 Transient growth in vortices with axial flow. *J. Fluid Mech.* **587**, 271–301.

HELD, I. M. 1985 Pseudomomentum and the orthogonality of modes in shear flows. *J. Atmos. Sci.* **42**, 2280–2288.

HIROTA, M., TATSUNO, T. & YOSHIDA, Z. 2003 Degenerate continuous spectra producing localized secular instability – an example in a non-neutral plasma. *J. Plasma Phys.* **69**, 397–412.

HOWARD, L. N. & GUPTA, A. S. 1962 On the hydrodynamic and hydromagnetic stability of swirling flows. *J. Fluid Mech.* **14**, 463–476.

INCE, E. L. 1956 *Ordinary Differential Equations*. Dover.

KELBERT, M. & SAZONOV, I. 1996 *Pulses and other Wave Processes in Fluids*. Kluwer.

KELVIN, LORD 1880 Vibrations of a columnar vortex. *Phil. Mag.* **10**, 155–168.

KHORRAMI, M. R. 1991 On the viscous modes of instability of a trailing line vortex. *J. Fluid Mech.* **225**, 197–212.

KOPIEV, V. F. & CHERNYSHEV, S. A. 1997 Vortex ring eigen-oscillations as a source of sound. *J. Fluid Mech.* **341**, 19–57.

KUPFERMAN, R. 2005 On the linear stability of plane Couette flow for an Oldroyd-B fluid and its numerical approximation. *J. Non-Newton. Fluid Mech.* **127**, 169–190.

LAMB, H. 1932 *Hydrodynamics*. Dover.

LANDAHL, M. T. 1980 A note on an algebraic instability of inviscid parallel shear flows. *J. Fluid Mech.* **98**, 243–251.

LE DIZÈS, S. 2000 Non-axisymmetric vortices in two-dimensional flows. *J. Fluid Mech.* **406**, 175–198.

LE DIZÈS, S. 2004 Viscous critical-layer analysis of vortex normal modes. *Stud. Appl. Math.* **112**, 315–332.

LE DIZÈS, S. & BILLANT, P. 2009 Radiative instability in stratified vortices. *Phys. Fluids* **21**, 096602.

LE DIZÈS, S. & FABRE, D. 2007 Large-Reynolds-number asymptotic analysis of viscous centre modes in vortices. *J. Fluid Mech.* **585**, 153–180.

https://doi.org/10.1017/jfm.2013.666 Published online by Cambridge University Press

LE DIZÈS, S. & LACAZE, L. 2005 Non-axisymmetric vortices in two-dimensional flows. *J. Fluid Mech.* **542**, 69–96.

LEIBOVICH, S., BROWN, S. N. & PATEL, Y. 1986 Bending waves on inviscid columnar vortices. *J. Fluid Mech.* **173**, 595–624.

LEIBOVICH, S. & MA, H. Y. 1983 Soliton propagation on vortex cores and the Hasimoto soliton. *Phys. Fluids* **26**, 3173–3179.

LESSEN, M., SINGH, P. J. & PAILLET, F. 1974 The stability of a trailing line vortex. Part I. Inviscid theory. *J. Fluid Mech.* **63**, 753–763.

LIGHTHILL, M. J. 1958 *An Introduction to Fourier Analysis and Generalized Functions*. Cambridge University Press.

LIN, C. C. 1955 *The Theory of Hydrodynamic Stability*. Cambridge University Press.

MASLOWE, S. 1986 Critical layers in shear flows. *Annu. Rev. Fluid Mech.* **18**, 405–432.

MASLOWE, S. & NIGAM, N. 2008 The nonlinear critical layer for Kelvin modes on a vortex with a continuous velocity profile. *SIAM J. Appl. Math.* **68**, 825–843.

MAYER, E. W. & POWELL, K. G. 1992 Viscous and inviscid instabilities of a trailing vortex. *J. Fluid Mech.* **245**, 91–114.

MCWILLIAMS, J. C. 1984 The emergence of isolated coherent vortices in turbulent flow. *J. Fluid Mech.* **146**, 21–43.

MELANDER, M. V. & HUSSAIN, F. 1993 Coupling between a coherent structure and fine-scale turbulence. *Phys. Rev.* E **48**, 2669–2689.

MELANDER, M. V. & HUSSAIN, F. 1994 Core dynamics on a vortex column. *Fluid Dyn. Res.* **13**, 1–37.

MICHALKE, A. & TIMME, A. 1967 On the inviscid instability of certain two-dimensional vortex-type flows. *J. Fluid Mech.* **29**, 647–666.

MILES, J. W. 1961 On the stability of heterogeneous shear flows. *J. Fluid Mech.* **402**, 349–378.

ORR, W. MCF. 1907 Stability or instability of the steady motions of a perfect liquid and of a viscous liquid. Part I: A perfect liquid. *Proc. R. Irish. Acad.* A **27**, 9–68.

PRADEEP, D. S. & HUSSAIN, F. 2006 Transient growth of perturbations in a vortex column. *J. Fluid Mech.* **550**, 251–288.

PRADEEP, D. S. & HUSSAIN, F. 2010 Vortex dynamics of turbulence-coherent structure interaction. *Theor. Comput. Fluid Dyn.* **24**, 265–282.

RALLISON, J. M. & HINCH, E. J. 1995 Instability of a high-speed submerged elastic jet. *J. Fluid Mech.* **288**, 311–324.

ROY, A. 2013 Singular eigenfunctions in hydrodynamic stability: the roles of rotation, stratification and elasticity. PhD thesis, Jawaharlal Nehru Centre for Advanced Scientific Research.

ROY, A. & SUBRAMANIAN, G. 2012 Normal mode interpretation of 'lift-up' effect. *J. Fluid Mech.* (submitted).

SAFFMAN, P. G. 1992 *Vortex Dynamics*. Cambridge University Press.

SAZONOV, I. A. 1989 Interaction of continuous spectrum waves with each other and discrete spectrum waves. *Fluid Dyn. Res.* **4**, 586–592.

SAZONOV, I. A. 1996 Evolution of three-dimensional wave packets in the Couette flow. *Izv. Atmos. Ocean. Phys.* **32**, 21–28.

SCHECTER, D. A., DURBIN, D. H. D., CASS, A. C., DRITSCOLL, C. F., LANSKY, I. M. & O'NEIL, T. M. 2000 Inviscid damping of asymmetries on a two-dimensional vortex. *Phys. Fluids* **12**, 2397–2412.

SCHECTER, D. A. & MONTGOMERY, M. T. 2003 On the symmetrization rate of an intense geophysical vortex. *Dyn. Atmos. Oceans* **37**, 55–88.

SCHIMD, P. J. & HENNINGSON, D. S. 2001 *Stability and Transition in Fluid Flows*. Springer.

SHORE, S. N. 1992 *An Introduction to Astrophysical Hydrodynamics*. Academic.

SHRIRA, V. I. & SAZONOV, I. A. 2001 Quasi-modes in boundary-layer-type flows. Part 1. Inviscid two-dimensional spatially harmonic perturbations. *J. Fluid Mech.* **446**, 133–171.

SHRIRA, V. I. & SAZONOV, I. A. 2003 Quasi-modes in boundary-layer-type flows. Part 2. Large-time asymptotics of broadband inviscid small-amplitude two-dimensional perturbations. *J. Fluid Mech.* **488**, 245–282.

SPALART, P. R. 1998 Airplane trailing vortices. *Annu. Rev. Fluid Mech.* **30**, 107–138.

https://doi.org/10.1017/jfm.2013.666 Published online by Cambridge University Press

STEWARTSON, K. 1981 Marginally stable inviscid modes with critical layers. *IMA J. Appl. Maths* **27**, 133–176.

STEWARTSON, K., NG, T. W. & BROWN, S. 1988 Viscous centre modes in the stability of swirling Poiseuille flow. *Phil. Trans. R. Soc. Lond.* A **324**, 473–512.

TAYLOR, G. I. 1931 Effect of variation in density on the stability of superposed streams of fluid. *Proc. R. Soc.* A **132**, 499–523.

TREFETHEN, L. N., TREFETHEN, A. E., REDDY, S. C. & DRISCOLL, T. A. 1993 Hydrodynamic stability without eigenvalues. *Science* **261**, 578–583.

TURNER, J. S. 1973 *Buoyancy Effects in Fluids*. Cambridge University Press.

VAN KAMPEN, G. 1955 On the theory of stationary waves in plasmas. *Physica* **51**, 949–963.

WATSON, G. N. 1927 *Theory of Bessel Functions*. Cambridge University Press.

WIDNALL, S. 1975 The structure and dynamics of vortex filaments. *Annu. Rev. Fluid Mech.* **7**, 141–165.

YIH, C. S. 1980 *Stratified Flows*. Academic.

https://doi.org/10.1017/jfm.2013.666 Published online by Cambridge University Press